Classical versus Quantum Dynamics in Interacting Spin Systems

Dissertation (kumulativ)

Zur Erlangung des Grades eines
Doktors der Naturwissenschaften (Dr. rer. nat.)

dem Fachbereich Physik der Universität Osnabrück
vorgelegt von

Dennis Schubert, M.Sc.

Osnabrück, im April 2022

List of Publications

This cumulative dissertation is based on the publications [R1], [R2] and [R3] listed below.

Ref. [R1]

Tjark Heitmann, Jonas Richter, Dennis Schubert, Robin Steinigeweg
"Selected applications of typicality to real-time dynamics of quantum many-body systems",
Zeitschrift für Naturforschung, p. 421 – 432, Band **75**, Heft 5 (2020),
Preprint: `https://arxiv.org/abs/2001.05289`
Published version: `https://doi.org/10.1515/zna-2020-0010`

Ref. [R2]

Dennis Schubert, Jonas Richter, Fengping Jin, Kristel Michielsen, Hans De Raedt, Robin Steinigeweg,
"Quantum versus classical dynamics in spin models: Chains, ladders, and square lattices",
Physical Review B **104**, 054415 (2021),
Preprint: `https://arxiv.org/abs/2104.00472`
Published version: `https://doi.org/10.1103/PhysRevB.104.054415`

Ref. [R3]

Jonas Richter, Dennis Schubert, Robin Steinigeweg
"Decay of spin-spin correlations in disordered quantum and classical spin chains",
Physical Review Research **2**, 013130 (2020),
Preprint: `https://arxiv.org/abs/1911.09917`
Published version: `https://doi.org/10.1103/PhysRevResearch.2.013130`

Abstract

This dissertation deals with the dynamics of interacting quantum and classical spin models and the question of whether and to which degree the dynamics of these models agree with each other.
For this purpose, XXZ models are studied on different lattice geometries of finite size, ranging from one-dimensional chains and quasi-one-dimensional ladders to two-dimensional square lattices. Particular attention is paid to the high-temperature analysis of the temporal behavior of autocorrelation functions for both the local density of magnetization (spin) and energy, which are closely related to transport properties of the considered models. Due to the conservation of total energy and total magnetization, the dynamics of such densities are expected to exhibit hydrodynamic behavior for long times, which manifests itself in a power-law tail of the autocorrelation function in time. From a quantum mechanical point of view, the calculation of these autocorrelation functions requires solving the linear Schrödinger equation, while classically Hamilton's equations of motion need to be solved. An efficient numerical pure-state approach based on the concept of typicality enables circumventing the costly numerical method of exact diagonalization and to treat quantum autocorrelation functions with up to $N = 36$ lattice sites in total.
While, in full generality, a quantitative agreement between quantum and classical dynamics can not be expected, contrarily, based on large-scale numerical results, it is demonstrated that the dynamics of the quantum $S = 1/2$ and classical spins coincide, not only qualitatively, but even quantitatively, to a remarkably high level of accuracy for all considered lattice geometries. The agreement particularly is found to be best in the case of nonintegrable quantum models (quasi-one-dimensional and two-dimensional lattice), but still satisfactory in the case of integrable chains, at least if transport properties are not dominated by the extensive number of conservation laws.
Additionally, in the context of disordered spin chains, such an agreement of the dynamics is found to hold even in the presence of small values of disorder, while at strong disorder the agreement is pronounced most for larger spin quantum numbers.
Finally, it is shown that a putative many-body localization transition within the one-dimensional spin chain is shifted to stronger values of disorder with increasing spin quantum number. It is concluded that classical or semiclassical simulations might provide a meaningful strategy to investigate the quantum dynamics of strongly interacting quantum spin models, even if the spin quantum number is small and far from the classical limit.

Contents

List of Publications i

Abstract iii

I. Introduction 5

II. Theoretical Background 13

1. Basics in Classical Mechanics 15
1.1. Phase Space and Time Evolution 15
1.2. Classical Phase Space Distribution 17

2. Basics in Quantum Mechanics 19
2.1. Pure States 19
2.2. Density Matrices 22
2.3. Other Types of Representation 25
2.4. Correlation Functions 27

3. Models 29
3.1. Quantum Heisenberg Spin Model 29
3.2. Classical Heisenberg Spin Model 36
3.3. Remarks on Integrability 37

4. Linear Response Theory and Transport 41
4.1. Static Response to a Static Force 41
4.2. Dynamics of Local Densities 43
4.3. Diffusion in Lattice Systems 43
4.4. Remarks on the Kubo Formula 45

5. Disordered Systems 47
5.1. Paradigmatic Model for Many-Body Localization 47
5.2. Remarks on Equilibration and Thermalization 49
5.3. Transport of Densities 52

6. Numerical Approaches to Quantum Many-Body Systems 54
6.1. Exact Diagonalization 54
6.2. Dynamical Quantum Typicality 57
6.3. Pure-State Propagation 58
6.4. Numerical Linked Cluster Expansion 62

III. Guide to Publications **64**

7. Publications **65**
A. Applications of Quantum Typicality 65
B. Quantum versus Classical Spin Dynamics 70
C. Quantum versus Classical Dynamics in Disordered Spin Chains 74

IV. Conclusion **79**

8. Summary and Outlook **81**

Acknowledgements **85**

Bibliography **86**

Part I.

Introduction

Introduction

Understanding and investigating the behavior of systems consisting of many degrees of freedom is a notoriously difficult task. While, today, (quantum and classical) many-body systems in (thermal) equilibrium are well understood according to the laws of textbook *statistical mechanics* [4, 5], many-body systems out of equilibrium present a challenge in modern experimental and theoretical physics.

From an experimental point of view, studies on nonequilibrium dynamics of quantum many-body systems have recently experienced progress in the fields of ultracold quantum gases (see, e.g., Refs. [6–10] and references therein), optical lattices [7, 11–14], and trapped ions [15, 16]. Since ultracold quantum gases can be almost perfectly isolated from their surroundings, they have become a tremendous and well-established experimental tool to probe questions regarding, for example, condensed matter physics and allow for studying these systems for comparatively long coherence times [17]. One the one hand, due to the high degree of controllability and the development of sophisticated measurement techniques, these systems present new opportunities to realize certain quantum many-body systems experimentally, such as Heisenberg (spin) Hamiltonians [18–20]. On the other hand, they enable the study of fermionic and bosonic gases [21–23] and, in particular, the analysis of special states of matter such as Bose-Einstein condensates (see, e.g., Refs. [24, 25] and references therein).

In addition, low-dimensional interacting quantum systems have been the subject of many studies since these systems capture and explain magnetism of certain compounds in nature on a microscopic level [26]. A notable class of materials that provide realizations of low-dimensional quantum magnets are systems known as copper oxides (cuprates) [27–29], which can essentially act as lattices consisting of spin-1/2 degrees of freedom in terms of Cu^{2+}-ions. In essence, such materials provide physical realizations of archetypical low-dimensional spin-S systems. These include $S = 1/2$ [27–30] and $S = 1$ Heisenberg chains as well as the two-leg ladders [29, 31], which can be realized by couplings between separate $S = 1/2$ Heisenberg chains. Although the origin of magnetic properties of certain materials is deeply rooted in quantum mechanical principles, even *classical spin* models have attracted attention for the understanding of magnetism in spin systems [32–34]. In this context, the notion of "classical spins" has to be understood as the classical limit of a quantum spin model, characterized by simultaneously taking the limit of Planck's constant to zero ($\hbar \to 0$) and the spin quantum number to infinity ($S \to \infty$) while keeping the product $\hbar\sqrt{S(S+1)}$ constant [35].

Also inspired by the latest developments and advances in the field of experimental physics, the interest of theoretical physics in understanding the dynamics of quantum many-body systems being out of equilibrium has been extensively renewed and invigorated [cf. Refs. [20, 36–40] and references therein]. This is because quantum spin systems represent an appropriate platform for testing intriguing theoretical concepts and providing access to the investigation of long-standing questions of quantum thermalization [38, 41–44], which is theoretically related to the eigenstate thermalization hypothesis (ETH) [42, 43, 45], and phenomena in the context of many-body localization (MBL) [46–50]. Within these

concepts, the notion of *integrability* in both the classical and quantum realm plays a significant role.

For classical systems, whose constituents evolve in time according to differential equations known as Hamilton's equations of motion, the concept of integrability is unambiguously defined in terms of Liouville integrability [51]. In the spirit of Liouville integrability, a classical system consisting of s degrees of freedom (i.e. the system possesses a $2s$-dimensional phase space) is considered *integrable* if it possesses s independent first integrals of motion in involution [51]. As a result, the Hamilton's equations of motion are explicitly solvable by exploiting action-angle variables [51] while the solutions exhibit periodic motions on invariant tori in phase space [52, 53]. In this case, the concept of ergodicity [54, 55], which states that phase-space trajectories, in principle, can get arbitrarily close to any point of the phase space for long times, is lacking [56]. The dynamics of such classical systems is strongly restricted due to the presence of several conservation laws and cannot traverse the full phase space. In this sense, integrable systems are referred to as nonergodic [54], while the trajectories of more generic, nonintegrable classical systems can exhibit chaotic behavior [57, 58] and the phase space is densely covered. In the context of classical chaos, one diagnostic tool to detect it is related to deterministic randomness [57] and the notion of Lyapunov exponents [57, 59], which measure the exponential distance between two phase space points in the course of time.

For quantum systems, whose dynamics are described by the Schrödinger equation, a commonly accepted definition of integrability is more delicate and remains a subject of debate [56]. Due to the lack of a reasonable notion of phase space trajectories in the quantum realm, a straightforward transfer of ergodicity is not possible [38, 48, 60]. Nevertheless, despite the lack of a well-defined notion of integrability, one way to delineate integrability can be summarized by so-called Bethe ansatz-integrable models (see Refs. [61] for introductory references, or, for a more comprehensive discussion, see [62, 63]).

In principle, Bethe ansatz-based techniques provide a strategy to obtain exact eigenstates (and eigenvalues) of a certain class of one-dimensional quantum models by solving nonlinear equations, known as Bethe ansatz equations [62–65]. Prototypical one-dimensional integrable models which have been solved exactly by means of Bethe ansatz methods include the isotropic [61] and anisotropic spin-1/2 Heisenberg model [66]. The Fermi-Hubbard chain [62] has been solved as well. Beyond the originally formulated coordinate Bethe ansatz [61, 67], ample literature has been published on advanced Bethe ansatz-like methods such as the algebraic Bethe ansatz [68] and the quantum inverse scattering method [69, 70]. Within the quantum inverse scattering method, the so-called Young-Baxter equation [71, 72] has been found to define integrability for one-dimensional quantum systems. Therefore, these quantum models are integrable if a so-called scattering matrix ($\mathcal{R}$-matrix), which is related to the model, obeys the Yang-Baxter equation [69, 71, 72]. Since integrable models, in principle, provide analytical results (exact eigenstates and eigenvalues), they serve as theoretical cross-checking reference systems to ensure the correctness and validity of approximate approaches.

A potential crossover from integrable to nonintegrable (chaotic, generic) quantum systems is often described by means of the statistical properties of *energy levels* [73] of a quantum system, specifically the spacing of consecutive energy levels of nonintegrable systems follow a Wigner-Dyson distribution [74], while the energy levels of integrable systems obey a Poissonian distribution [74]. Nonintegrable models, which are considered in this thesis, mainly arise through examining (*i*) higher spin quantum numbers ($S > 1/2$) or (*ii*) higher spatial dimensions ($d > 1$) or by (*iii*) adding some additional perturbations

to the system, which are expected to break all (nontrivial) conservation laws, such as additional disorder terms.

Studies over recent decades have provided valuable information on transport properties of certain physical models. On the one hand, integrable models play a decisive role due to the fact that integrability can strongly impact their dynamics. Integrable models are characterized by an extensive number of conservation laws which can lead to anomalous thermalization [75, 76] and nondecaying currents, that is, ballistic transport (i.e. ideal transport) [77–80]. Conversely, this means that diffusion generally cannot be expected within these models. Moreover, due to an extensive number of conserved quantities, complete decay of correlation functions can be slowed or prevented [77, 78]. For generic interacting many-body systems in the high-temperature limit, a signature of diffusive transport is manifested in a characteristic long-time decay of the autocorrelation function [81]

$$\langle \varrho_i(t)\varrho_i(0)\rangle \propto t^{-d/2},$$

where d denotes spatial lattice dimensions and ϱ_i represents a local density. In the context of the anisotropic one-dimensional Heisenberg spin-1/2 chain (XXZ model), at formally infinite temperature, and independent of the anisotropy parameter Δ, energy transport is purely ballistic and the energy current conserved [82]. In contrast, spin transport depends on the actual value of Δ [83–86]. For $\Delta = 1$ and $S = 1/2$, the correlation function $\langle S_i^z(t)S_i^z(0)\rangle \propto t^{-\alpha}$ decays with an exponent $\alpha \approx 2/3$ for long times, which suggests *superdiffuisve* spin transport within the Kardar-Parisi-Zhang (KPZ) universality class [86–91]. For nonintegrable chains with $S > 1/2$, the situation is less clear. While it has been suggested that superdiffusion might persist despite the absence of integrability [92, 93], it has also been argued that α will eventually approach its diffusive value $\alpha = 1/2$ asymptotically for larger system sizes and longer timescales [94]. Even for the classical Heisenberg spin chain, the unambiguous detection of diffusion is known to be a delicate problem [95–103]. Due to the lack of integrability, normal diffusion is said to be maintained for both spin and energy [96, 100, 104–106]. However, there are also suggestions that the dynamics are anomalous [95, 107, 108].

The clarification of this question is not only vital from a theoretical point of view but also experimentally. Commonly performed experiments on, for example , nuclear magnetic resonance (NMR) [109, 110] or muon spin resonance (μSR) strive to measure relaxation rates. Those relaxation rates can be described by certain spin autocorrelation functions [81, 111, 112]. Moreover, superdiffusive spin dynamics (consistent with the Kardar-Parisi-Zhang universality class) have been observed in experiments with $KCuF_3$ in the high-temperature regime [113]. In the field of NMR, it is well known that the dynamics of classical spins commonly reproduces the behavior of systems with quantum spins, including spin-1/2 [114]. Furthermore, ultracold atomic gases provide another opportunity to investigate transport properties of many-body systems experimentally. In particular, both the Fermi- and Bose-Hubbard model have been realized in optical lattices [10, 14]. In addition, the XXZ model has been imitated in the context of ultracold quantum gases [20], where spin transport has been observed to be superdiffusive for $0 < \Delta < 1$, diffusive for $\Delta = 1$, and subdiffusive for $\Delta > 1$.

Novel experimental developments have also restored interest in the issue of thermalization (or lack of thereof) in the context of isolated quantum systems. In the classical domain, the notion of thermalization can be understood in terms of chaotic dynamics and the ergodicity hypothesis [41]. The question of thermalization in classical systems can be

traced back to numerical investigations by Fermi, Pasta, Ulam, and Tsingou [115, 116]. In the quantum domain, the understanding of thermalization is largely based on the eigenstate thermalization hypothesis [42, 43], which enables an explanation of thermalization on a microscopic level. Roughly speaking, ETH implies that the expectation values of local observables in isolated quantum systems, which are initially prepared in an out-of-equilibrium state, relax to long-time values that can be described using textbook statistical mechanics ensembles [42–44]. Although a rigorous mathematical proof of the eigenstate thermalization hypothesis is still lacking, it has been confirmed numerically for a variety of systems [38, 44, 117].

There are well-known classes of quantum systems that are expected to violate the ETH, namely (*i*) integrable systems [38] and (*ii*) many-body localized systems [48, 118]. While the well-understood concept of Anderson localization [47, 119] states that noninteracting particles are localized, even at arbitrarily small values of disorder, the concept of many-body localization (MBL) serves as a "generalization" of Anderson localization by allowing interactions in the model. The absence of thermalization within the many-body localized phase has been attributed to the existence of an extensive number of locally conserved quantities, so-called local integrals of motion [48, 120, 121]. Based on seminal works and numerous subsequent works [122–128], many-body localization is today believed to be a generic property of one-dimensional short-range lattice models with sufficiently strong randomness [48, 50].

For generic one-dimensional disordered quantum models, at least two phases are expected: (*i*) an ergodic phase at weak disorder strength where all eigenstates obey the ETH and (*ii*) a localized phase at strong disorder where ETH is fully violated. Essentially, the MBL phase is characterized by the fact that autocorrelation functions of local operators retain memory of their initial states at long times [50] and nonequilibrium initial states will never relax [125, 129]. In addition, great efforts have recently been made to put the phenomenon of MBL into a broader perspective and to understand the dynamics of models which might not be strictly localized but exhibit anomalously small relaxation rates and considerably long equilibrium times [130]. While the occurrence of genuine MBL is not expected for classical spin models, strong disorder has been demonstrated to cause a drastic reduction of transport coefficients and anomalously slow relaxation [104, 131].

While analytical (exact) solutions for integrable quantum models are (in principle) possible (Bethe ansatz), particularly the study of nonintegrable models requires the use of mostly numerical techniques. Consequently, the development of efficient numerical algorithms for these types of systems poses one of the most critical challenges within the field of theoretical physics. Thanks to a number of eminent and efficient numerical algorithms in recent decades, large-scale numerical studies have become possible for certain classes of quantum lattice models. Apart from exact diagonalization techniques (see, e.g., Ref. [132], which enable evaluation of the entire spectrum and all eigenstates of certain models, variational methods such as density functional theory [133] and matrix product state techniques and relatives [134, 135] have proven to be successful for ground state problems. Furthermore, the development of novel theoretical concepts, such as *typicality* [136–140], leads to the numerical approach of dynamical quantum typicality (DQT) (see Ref. [141] for a comprehensive review) and further extended numerical techniques, for example numerical linked-cluster expansions (see Refs. [142, 143] for comprehensive reviews).

By comparing the dynamics of quantum and classical spin systems to each other, likely substantial differences will appear at very low temperatures, where quantum effects become dominant. Nevertheless, a quantitative agreement between the dynamics of classical and

quantum spin models cannot be expected in general, even at high temperatures, as dealing with the high-temperature limit does not necessarily imply that all quantum behavior is lost. On the one hand, the integrability of certain $S = 1/2$ quantum models is essentially manifested in their dynamical behavior, even in the high-temperature limit. On the other hand, the classical chain might lack integrability and, therefore, exhibit significantly different dynamical behavior. Moreover, the lack of a classical counterpart in the context of a potential onset of the phenomenon of many-body localization in strongly disordered quantum models leads to the agreement between quantum and classical dynamics becoming unlikely, since the onset of many-body localization represents a pure quantum effect. Although various studies on the dynamics of classical and quantum spin lattices (particularly on the XXZ Heisenberg model) have a long history [95–97, 100, 102, 104, 144, 145], less attention has been paid to a comparison of the dynamics in classical and quantum spin lattice models both qualitatively and quantitatively [146–149]. While it seems likely that quantum and classical systems grow more similar as the spin quantum number increases, that is, starting with the most quantum case ($S = 1/2$) up to the classical limit ($S \to \infty$), it remains a nontrivial question whether and to what level the dynamics of both the quantum and classical spin system coincide.

The present dissertation explores the question of quantum versus classical dynamics in spin models on different geometries by studying time-dependent autocorrelation functions of local densities, which are intimately related to the transport properties of these models.

Thesis Outline

To provide a clear structure, this cumulative thesis is divided into *four* parts. The current part (Pt.) has been dedicated to the introduction of this thesis. Afterwards, Pt. II introduces the main theoretical concepts needed in the course of this thesis. To this end, section (Sec.) 1 provides a brief overview of the basic concepts of classical mechanics, while Sec. 2 deals with the basics of quantum mechanics. The subsequent section (Sec. 3) describes the models considered in this thesis. In Sec. 3.1, the anisotropic quantum-S Heisenberg model (XXZ model) is introduced on three different lattice geometries, ranging from (*i*) one-dimensional chains and (*ii*) quasi-one-dimensional ladders to (*iii*) two-dimensional square lattices. Furthermore, the relevant observables are described in the subsequent section. Moreover, certain global symmetries of the XXZ chain are highlighted. After turning to the classical XXZ model, the third section closes with remarks on the notion of integrability in both the classical and quantum realm. Sec. 4 is dedicated to describing aspects of the theory of linear response as a commonly used approach to study transport processes in many-body systems. In this context, diffusion in many-body systems is described in greater detail. The section concludes with remarks on dynamical linear response functions and the Kubo formula. While the previous sections have exclusively considered disorder-free models, Sec. 5 discusses the disordered XXZ model. The phenomena of many-body localization and equilibration (thermalization) in many-body systems are explained, while, especially in the context of thermalization, the eigenstate thermalization hypothesis is considered. To close the section, in Sec. 5.3, transport properties of local densities in the presence of disorder are discussed. As the final section of the second part, Sec. 6 provides an overview of certain numerical approaches in the context of many-body systems. In particular, Sec. 6.1 deals with the numerical technique of exact diagonalization followed by a description of the concept of dynamical quantum typicality in Sec. 6.2. In this context, Sec. 6.3 deals with the propagation of

pure states, while the section closes with the numerical approach of numerical linked cluster expansion in Sec. 6.4. Based on the publications Refs. [R1–R3], the third part (Pt. III) of this thesis provides a survey of the publications, which are (*i*) "*Selected applications of typicality to real-time dynamics of quantum many-body systems*" ([R1]), (*ii*) "*Quantum versus classical dynamics in spin models: Chains, ladders, and square lattices*" ([R2]), and (*iii*) "*Decay of spin-spin correlations in disordered quantum and classical spin chains*" ([R3]). The fourth part (Pt. IV) provides a brief summary of this thesis and gives an outlook on future work beyond this thesis.

Part II.

Theoretical Background

1. Basics in Classical Mechanics

This section is concerned with the basic framework of classical mechanics according to Hamilton's formulation of classical mechanics. First, in Sec. 1.1 the concept of a phase space is briefly described and in this context the notion of generalized coordinates and momenta is outlined. To describe the time evolution of classical (many-body) systems, Hamilton's equations of motion are presented, which leads to the notion of Poisson brackets. Subsequently, in Sec. 1.2 a probability-based description of statistical mechanics is highlighted. In this context, the notion of phase space distribution functions as well as their temporal evolution is presented. Finally, the ensemble expectation value of a classical observable is pointed out. It is worth noting that this section is based on the Refs. [51, 52].

1.1. Phase Space and Time Evolution

Consider a classical system that consists of N identical (classical) pointlike particles. These can be described according to the standard three-dimensional Euclidean space. A classical *microstate* of the system is specified by s generalized (spatial) coordinates, denoted by $\mathbf{q}(t) = (q_1(t), q_2(t), \ldots, q_s(t))$, and their associated s conjugated momenta $\mathbf{p}(t) = (p_1(t), p_2(t), \ldots, p_s(t))$, which are both s-dimensional vectors. It is worth mentioning that if the classical particles can move independently from each other in space, the system has exactly $s = 3N$ degrees of freedom. Nevertheless, in this thesis the more general case of $s \neq 3N$ degrees of freedom is considered.

To proceed, the generalized coordinates $\mathbf{q}(t)$ and momenta $\mathbf{p}(t)$ span the $2s$-dimensional *phase space* Γ. Since the generalized coordinates and momenta are independent variables, both can be summarized as a phase space vector $\boldsymbol{\pi}_\Gamma(t)$ according to

$$\begin{aligned}\boldsymbol{\pi}_\Gamma(t) &= (\pi_1(t), \pi_2(t), \ldots, \pi_{2s}(t)) \\ &= (q_1(t), q_2(t), \ldots, q_s(t), p_1(t), p_2(t), \ldots, p_s(t))\,. \end{aligned} \tag{1.1}$$

As becomes apparent, every classical microstate corresponds to a certain point in phase space Γ and, therefore, the state of the classical system is entirely determined by the phase space vector (1.1). The set of phase space points, $\boldsymbol{\pi}_\Gamma(t) = (\mathbf{q}(t), \mathbf{p}(t))$, the system can occupy over time, is called the *phase space trajectory*. For some given initial conditions, namely

$$\boldsymbol{\pi}_\Gamma(0) = (\mathbf{q}(0), \mathbf{p}(0))\,, \tag{1.2}$$

the time evolution of the phase space vector $\boldsymbol{\pi}_\Gamma(t)$ is unambiguously given in terms of the *Hamilton's equations of motion*. These are explicitly given by

$$\frac{\mathrm{d}q_i(t)}{\mathrm{d}t} = \frac{\partial H(\mathbf{q}(t), \mathbf{p}(t))}{\partial p_i} \quad \text{and} \quad \frac{\mathrm{d}p_i(t)}{\mathrm{d}t} = -\frac{\partial H(\mathbf{q}(t), \mathbf{p}(t))}{\partial q_i}\,, \quad i = 1, \ldots, s\,, \tag{1.3}$$

where $H(\mathbf{q}(t), \mathbf{p}(t))$ denotes the *Hamilton function*. In particular, for an isolated classical

system the Hamilton function cannot explicitly depend on time (i.e. $\partial H/\partial t = 0$) and, for some constraints, $H(\mathbf{q}, \mathbf{p})$ is identical to the total energy E of the system, that is, $H(\mathbf{q}, \mathbf{p}) = E$. It is worth noting that Hamilton's equations of motion (1.3) consist of a set of $2s$ first-order differential equations for the s generalized coordinates and associated momenta. As a result, Hamilton's equations of motion depict the unique temporal evolution of the coordinates and momenta, depending on a set of initial conditions. Therefore, the phase space trajectory never intersects or represents a simply closed curve on phase space. Furthermore, the phase space trajectory is bounded by the $(2s-1)$-dimensional hypersurface (energy surface) of the phase space, defined by means of the constraint $H(\mathbf{q}, \mathbf{p}) = E$.

Apart from the Hamilton function, any other classical quantity can be written as a function on phase space. To this end, an arbitrary classical quantity O is given by

$$O(\boldsymbol{\pi}_\Gamma(t), t) = O(\mathbf{q}(t), \mathbf{p}(t), t)\,, \tag{1.4}$$

and evolves in time as

$$\frac{\mathrm{d}O}{\mathrm{d}t} = \sum_i \left(\frac{\partial O}{\partial q_i}\frac{\mathrm{d}q_i}{\mathrm{d}t} + \frac{\partial O}{\partial p_i}\frac{\mathrm{d}p_i}{\mathrm{d}t} \right) + \frac{\partial O}{\partial t}\,. \tag{1.5}$$

Substituting Hamilton's equations of motion (1.3) into the preceding equation, Eq. (1.5) can be rewritten as

$$\frac{\mathrm{d}O}{\mathrm{d}t} = \sum_i \left(\frac{\partial O}{\partial q_i}\frac{\partial H}{\partial p_i} - \frac{\partial O}{\partial p_i}\frac{\partial H}{\partial q_i} \right) + \frac{\partial O}{\partial t} = \{O, H\} + \frac{\partial O}{\partial t}\,, \tag{1.6}$$

where each of the functions have to be evaluated at the same point $(\mathbf{q}(t), \mathbf{p}(t), t)$ in phase space. Moreover, in the last step the *Poisson bracket* $\{\bullet, \bullet\}$ have been used. To briefly explain the notion of Poisson brackets, consider two arbitrary phase space functions $f = f(\mathbf{q}(t), \mathbf{p}(t))$ and $g = g(\mathbf{q}(t), \mathbf{p}(t))$. The Poisson bracket for f and g is defined as follows,

$$\{f, g\} \equiv \sum_i \left(\frac{\partial f}{\partial q_i}\frac{\partial g}{\partial p_i} - \frac{\partial f}{\partial p_i}\frac{\partial g}{\partial q_i} \right)\,. \tag{1.7}$$

Without giving proofs, note that the Poisson bracket contains the mathematical properties of bilinearity, that is, $\{\mu f_1 + \nu f_2, g\} = \mu\{f_1, g\} + \nu\{f_2, g\}$ for some real numbers μ and ν and phase space functions f_1, f_2 and g. Moreover, the Poisson bracket obeys the antisymmetry condition, that is, $\{f, g\} = -\{g, f\}$. In particular, due to mutual independence of the phase space coordinates, the so-called *fundamental Poisson brackets* are given by the following identities

$$\{q_j, q_k\} = \{p_j, p_k\} = 0 \quad \text{and} \quad \{q_j, p_k\} = \delta_{jk}\,, \tag{1.8}$$

where δ_{jk} denotes the Kronecker delta defined as

$$\delta_{jk} = \begin{cases} 1\,, & \text{if } j = k \\ 0\,, & \text{if } j \neq k \end{cases}\,. \tag{1.9}$$

The properties of the fundamental Poisson brackets (1.8) can explicitly be shown by using

Eq. (1.7). Finally, Hamilton's equations of motion (1.3) can be rewritten by means of the Poisson bracket (1.7) as,

$$\frac{\mathrm{d}q_i}{\mathrm{d}t} = \{q_i, H\} \quad \text{and} \quad \frac{\mathrm{d}p_i}{\mathrm{d}t} = \{p_i, H\}\,, \quad i = 1, \ldots, s\,, \tag{1.10}$$

where, the arguments of the phase space variables have been omitted for the sake of clarity.

For practical reasons, solving the equations of motion (1.3) strictly is in general not possible for macroscopic systems, which consist of a large number of degrees of freedom s. Although in an isolated system, the classical quantity O will not explicitly depend on time, the state will change its position in phase space in the course of time, which implies a change in the values of O. As a consequence, the idea of a pure deterministic microscopic description of classical many-body systems has to be abandoned. Instead, it is usual to turn to a macroscopic description, based on the probability of finding a system in a respective microscopic state.

1.2. Classical Phase Space Distribution

Since in a classical many-body system the exact microstate at a time t is not "known" exactly, a probability distribution on phase space, the *phase space distribution function* $\rho_\Gamma(\mathbf{q}, \mathbf{p}, t)$, is introduced. This distribution function depends on the generalized coordinates $\mathbf{q} = (q_1, q_2, \ldots, q_s)$ and generalized momenta $\mathbf{p} = (p_1, p_2, \ldots, p_s)$ (and for nonequilibrium situations additionally on time t). By definition, the phase space distribution function $\rho_\Gamma(\mathbf{q}, \mathbf{p}, t)$ is strictly nonnegative and normalized to unity, that is,

$$\rho_\Gamma(\mathbf{q}, \mathbf{p}, t) \geq 0\,, \tag{1.11a}$$

$$\int_\Gamma \rho_\Gamma(\mathbf{q}, \mathbf{p}, t)\, \mathrm{d}^{(2s)} V_\Gamma = 1\,, \tag{1.11b}$$

where the term $\rho_\Gamma(\mathbf{q}, \mathbf{p}, t)\, \mathrm{d}^{(2s)} V_\Gamma$ represents the probability of finding a microstate of the system at time t in an infinitesimally small "volume" element $\mathrm{d}^{(2s)} V_\Gamma$ around a point $(\mathbf{q}, \mathbf{p})$ in phase space Γ. Moreover, the integral in Eq. (1.11b) has to be performed over the complete phase space and the phase space "volume" element $\mathrm{d}^{(2s)} V_\Gamma$ has to be understood as a decomposition of infinitesimal small phase space volume elements according to

$$\mathrm{d}^{(2s)} V_\Gamma \equiv \mathrm{d}q_1\, \mathrm{d}q_2\, \ldots\, \mathrm{d}q_s\, \mathrm{d}p_1\, \mathrm{d}p_2\, \ldots\, \mathrm{d}p_s = \prod_i \mathrm{d}q_i\, \mathrm{d}p_i\,, \tag{1.12}$$

which is usually equipped with a normalization constant, but without loss of generality, this constant is set to unity.

A central concept of statistical mechanics can be traced back to Gibbs and states that describing a many-body system in a given macrostate refers to a large number of identical systems that are in different microscopic states but share common macroscopic properties. The total number of systems then forms a *statistical ensemble*.

It is worth pointing out that the time evolution of the phase space density $\rho_\Gamma(\mathbf{q}, \mathbf{p}, t)$ is given by the so-called *Liouville equation*,

$$\frac{\mathrm{d}}{\mathrm{d}t}\rho_\Gamma = \frac{\partial \rho_\Gamma}{\partial t} + \{\rho_\Gamma, H\} = 0\,, \tag{1.13}$$

where Eq. (1.6) has been exploited and $\{\bullet, \bullet\}$ denotes the Poisson bracket given in Eq. (1.7). A precise derivation of the Liouville equation is not provided here. Nevertheless, it is worth noting that this equation can be derived by exploiting both (*i*) the s-dimensional divergence theorem and (*ii*) assuming that the phase space probability density $\rho_\Gamma(\mathbf{q}, \mathbf{p}, t)$ obeys a s-dimensional continuity equation. As becomes apparent, the space phase density vanishes along a phase space trajectory. This statement is known as the *Liouville theorem*. It is worth to briefly comment on the Liouville equation (1.13). By means of the so-called *classical Liouville operator* $\imath\mathcal{L}_{\mathrm{cm}}$, Eq. (1.13) is rewritten as

$$\frac{\partial \rho_\Gamma}{\partial t} + \imath\mathcal{L}_{\mathrm{cm}}[\rho_\Gamma] = 0\,, \tag{1.14}$$

where $\imath\mathcal{L}_{\mathrm{cm}}$ is defined as

$$\imath\mathcal{L}_{\mathrm{cm}}[\bullet] \equiv \sum_i \left(\frac{\partial H}{\partial p_i} \frac{\partial\,[\bullet]}{\partial q_i} - \frac{\partial H}{\partial q_i} \frac{\partial\,[\bullet]}{\partial p_i} \right) = \{\bullet, H\}\,. \tag{1.15}$$

For an isolated classical system, the classical Liouville operator is time independent (similar to the Hamilton function). Thus, Eq. (1.13) can be formally integrated, yielding the following solution:

$$\rho_\Gamma(\mathbf{q}, \mathbf{p}, t) = \mathrm{e}^{-\imath\mathcal{L}_{\mathrm{cm}} t} \rho_\Gamma(\mathbf{q}, \mathbf{p}, t = 0)\,, \tag{1.16}$$

with the initial phase space density $\rho_\Gamma(\mathbf{q}, \mathbf{p}, 0)$ at $t = 0$. With the previously mentioned considerations, the ensemble expectation value of any classical observable $O(t) = O(\mathbf{q}(t), \mathbf{p}(t))$ can be expressed in terms of the phase space distribution function $\rho_\Gamma(\mathbf{q}, \mathbf{p}, t)$ according to

$$\langle O(t) \rangle = \frac{\displaystyle\int_\Gamma O(\mathbf{q}(t), \mathbf{p}(t))\, \rho_\Gamma(\mathbf{q}(t), \mathbf{p}(t), t)\, \mathrm{d}^{(2s)} V_\Gamma}{\displaystyle\int_\Gamma \rho_\Gamma(\mathbf{q}(t), \mathbf{p}(t), t)\, \mathrm{d}^{(2s)} V_\Gamma}\,, \tag{1.17}$$

which leads to

$$\langle O(t) \rangle = \int_\Gamma O(\mathbf{q}(t), \mathbf{p}(t))\, \rho_\Gamma(\mathbf{q}(t), \mathbf{p}(t), t)\, \mathrm{d}^{(2s)} V_\Gamma\,, \tag{1.18}$$

by using the normalization condition given in (1.11b). Moreover, the variance can be defined in terms of Eq. (1.18) as

$$\sigma_O^2(t) = \langle O(t)^2 \rangle - \langle O(t) \rangle^2\,. \tag{1.19}$$

It is worth pointing out that in particular, by choosing $O = H$, the conservation of energy is essentially recovered due to the vanishing of the Poisson bracket (i.e. $\{H, H\} = 0$). On a more general level, conserved quantities are described in greater detail in the context of (classical) integrability (see Sec. 3.3.1). In the course of this thesis, the description of classical many-body systems will play an important role. In the context of classical spin systems (see Sec. 3.2), Hamilton's equations of motion [cf. Eq. (1.3)] will govern the dynamics of classical spin variables. Moreover, in the context of classical integrability (see Sec. 3.3.1), the Poisson bracket [cf. Eq. (1.7)] will provide integrals of motion.

2. Basics in Quantum Mechanics

This section is referred to the basic framework of quantum mechanics. Sec. 2.1 briefly explains the notion of pure states and their time evolution governed by the Schrödinger equation, which is subsequently solved by the unitary time-evolution operator. In this context, the time evolution of expectation values is described. For later purposes, the time evolution of pure states and expectation values is also presented in the energy eigenbasis of some Hamiltonian. Moreover, Sec. 2.2 deals with the concept of density matrices, which enables the description of pure and mixed states. In this context, Sec. 2.2.1 is dedicated to the von-Neumann equation. Furthermore, the canonical ensemble is described. While the quantities given in Sec. 2.1 are exclusively formulated according to the Schrödinger representation of quantum mechanics, the following sections refer to additional types of representations, namely the (*i*) Heisenberg and (*ii*) interaction representation. The section concludes with correlation functions, which provide one possibility to study dynamical properties of many-body systems.
It is worth noting that this section is based on the Refs. [150, 151].

2.1. Pure States

According to the *Schrödinger representation* of quantum mechanics, a pure quantum state is represented by a time-dependent state vector $|\psi(t)\rangle$, which is an element of a potentially high-dimensional Hilbert space $\mathscr{H}$. Observables are represented by Hermitian operators $\mathcal{O}$ acting on $\mathscr{H}$ and, unlike the states, the operators are constant in time. The notion of a pure state means that the quantum system under consideration is in a precisely defined state, i.e. the system is found with a probability of $w = 1$ in the state $|\psi\rangle$.

2.1.1. Schrödinger Equation

The time evolution of a pure state $|\psi(t)\rangle$ is fully determined in terms of the *Schrödinger equation*,

$$\imath \frac{\mathrm{d}}{\mathrm{d}t} |\psi(t)\rangle = \mathcal{H} |\psi(t)\rangle \ , \tag{2.1}$$

where $\imath$ denotes the imaginary unit and $\mathcal{H}$ represents a time-independent Hamiltonian of the quantum system. Usually, Eq. (2.1) contains the Planck constant $\hbar$, but from this point on and for the rest of this thesis the Planck constant is set to unity, that is, $\hbar \equiv 1$.

For a time-independent Hamiltonian $\mathcal{H}$, the Schrödinger equation (2.1) is a linear differential equation of first order with constant coefficients. The Schrödinger equation is formally solved in terms of the so-called *unitary time-evolution operator* $\mathcal{U}(t, t_0)$, which maps the state $|\psi(t_0)\rangle$, at some initial time t_0, linearly to the state $|\psi(t)\rangle$, evaluated at some later time $t > t_0$,

$$|\psi(t)\rangle = \mathcal{U}(t, t_0) |\psi(t_0)\rangle \ , \tag{2.2}$$

with $\mathcal{U}(t_0, t_0) = \mathbb{1}_{\mathcal{D}}$ for $t \to t_0$ and $\mathbb{1}_{\mathcal{D}}$ has to be understood as the identity operator with regard to some $\mathcal{D}$-dimensional Hilbert space $\mathscr{H}$. To respect the linearity of quantum mechanics, the time-evolution operator has to be linear for each reference point in time, which is reflected by the property of transitivity,

$$\mathcal{U}(t_2, t_1)\,\mathcal{U}(t_1, t_0) = \mathcal{U}(t_2, t_0)\,, \tag{2.3}$$

for some points in time t_0, t_1 and t_2. The notion of unitarity can be traced back to the fact that the norm of the states remains invariant under time evolution which can formally be expressed as

$$\mathcal{U}^{\dagger}(t, t_0)\,\mathcal{U}(t, t_0) = \mathcal{U}(t, t_0)\,\mathcal{U}^{\dagger}(t, t_0) = \mathbb{1}_{\mathcal{D}}\,, \tag{2.4}$$

where $\mathcal{U}^{\dagger}(t, t_0)$ represents the Hermitian conjugated operator of $\mathcal{U}\,(t, t_0)$. Substituting the state $|\psi(t)\rangle$ in Eq. (2.2) into the Schrödinger equation (2.1), leads to an equation for the unitary time-evolution operator of the following form:

$$\imath \frac{\partial}{\partial t} \mathcal{U}\,(t, t_0) = \mathcal{H}\,\mathcal{U}\,(t, t_0)\ . \tag{2.5}$$

Since the Hamiltonian is assumed to be time-independent, the preceding operator equation (2.5) is solved by explicit integration, which leads to

$$\mathcal{U}\,(t, t_0) = \mathrm{e}^{-\imath \mathcal{H}(t - t_0)}\,. \tag{2.6}$$

As becomes apparent, the full time evolution of the state $|\psi(t)\rangle$ can be absorbed into an exponential operator. It should be mentioned that if the Hamiltonian becomes time-dependent, that is, $\mathcal{H} \to \mathcal{H}(t)$, the time-evolution operator $\mathcal{U}(t, t_0)$ is given by the *Dyson series* [152]

$$\mathcal{U}(t, t_0) = \mathbb{1} - \imath \int_{t_0}^{t} \mathcal{H}(t_1)\,\mathrm{d}t_1 + (-\imath)^2 \int_{t_0}^{t} \left[\int_{t_0}^{t_1} \mathcal{H}(t_1)\,\mathcal{H}(t_2)\,\mathrm{d}t_2 \right] \mathrm{d}t_1 + \cdots\,. \tag{2.7}$$

By means of the *time-ordering operator* $\mathcal{T}$, which orders each product of Hamiltonians in the Dyson series expansion (2.7) with increasing time arguments from right to left, Eq. (2.7) can be rewritten as

$$\mathcal{U}\,(t, t_0) = \mathcal{T} \left[\exp\left(-\imath \int_{t_0}^{t} \mathcal{H}(v)\,\mathrm{d}v \right) \right]\,, \tag{2.8}$$

for $t \geq t_0$. Considering an operator $\mathcal{O}$ (conjugated to an observable) according to the Schrödinger representation, the expectation value $\langle \mathcal{O}(t) \rangle$ of $\mathcal{O}$ is defined by the state vector $|\psi(t)\rangle$ as follows:

$$\langle \mathcal{O}(t) \rangle \equiv \langle \psi(t) | \mathcal{O} | \psi(t) \rangle\,. \tag{2.9}$$

The time derivative of Eq. (2.9) can explicitly be derived by means of Eq. (2.1), which leads to the expression

$$\imath \frac{\mathrm{d}}{\mathrm{d}t} \langle \psi(t) | \mathcal{O} | \psi(t) \rangle = \langle \psi(t) |\, [\mathcal{O}, \mathcal{H}]\, | \psi(t) \rangle\,, \tag{2.10}$$

where the brackets $[\bullet, \bullet]$ indicate the *commutator*, which is defined for two general operators, say $\mathcal{O}$ and $\mathcal{O}'$, as

$$[\mathcal{O}, \mathcal{O}'] \equiv \mathcal{O}\mathcal{O}' - \mathcal{O}'\mathcal{O} \,. \tag{2.11}$$

It is worth mentioning that if the operator $\mathcal{O}$ explicitly depends on time, $\mathcal{O} \to \mathcal{O}(t)$, then Eq. (2.10) would require an additional term of the form $\langle\psi(t)|\partial\mathcal{O}(t)/\partial t|\psi(t)\rangle$. Moreover, a natural implication of Eq. (2.10) is that if the operator $\mathcal{O}$ commutes with the Hamiltonian $\mathcal{H}$, the right hand side strictly vanishes and hence the expectation value turns out to be time-independent. In other words, Eq. (2.10) states that the expectation values of observables, which commute with the Hamiltonian, are *constants of motion* of the quantum system under consideration.

2.1.2. Time Evolution in Energy Eigenbasis

The time evolution of the state $|\psi(t)\rangle$ in the Schrödinger representation takes on a rather simple form in the so-called *energy eigenbasis*. To this end, the state $|\psi(t)\rangle$ is decomposed in terms of the system's energy eigenstates, denoted by $\{|n\rangle\}$, and the associated (potentially degenerated) energy eigenvalues $\{E_n\}$. The eigenvalues and eigenstates are obtained by solving the eigenvalue equation

$$\mathcal{H}\,|n\rangle = E_n\,|n\rangle \;, \tag{2.12}$$

which is the stationary Schrödinger equation. An initial state $|\psi(t_0)\rangle$ evolves in time according to

$$|\psi(t)\rangle = \mathcal{U}(t, t_0)\,|\psi(t_0)\rangle = \sum_n c_n(t_0)\,\mathrm{e}^{-\imath(t-t_0)E_n}\;|n\rangle \;. \tag{2.13}$$

The complex expansion coefficients are given by $c_n(t_0) = \langle n|\psi(t_0)\rangle$ and represent the overlap between the initial state $|\psi(t_0)\rangle$ and the eigenstates $|n\rangle$. Regarding Eq. (2.13), the probability, denoted by w_n, of finding the quantum system in an energy eigenstate $|n\rangle$ is given by the square value of the coefficients (i.e. $w_n = |c_n|^2$), and remains constant over time. As a consequence, the probability of encountering a quantum system in a certain eigenstate depends entirely on the initial conditions. Moreover, the expectation value in the Schrödinger representation from (2.9) can also be represented in terms of the energy eigenbasis. Thus, by using Eq. (2.13), the expectation value can be written as

$$\langle\mathcal{O}(t)\rangle = \langle\psi(t)|\mathcal{O}|\psi(t)\rangle = \sum_{n,m} c_m^*(t_0)\,c_n(t_0)\,\mathrm{e}^{\imath(E_m-E_n)(t-t_0)}\,\mathcal{O}_{mn}\,, \tag{2.14}$$

where $\mathcal{O}_{mn} \equiv \langle m|\mathcal{O}|n\rangle$ are the matrix elements of $\mathcal{O}$ in the eigenbasis of the Hamiltonian $\mathcal{H}$ and the asterisk of $c_m^*(t_0)$ represents the complex conjugated coefficients of $c_m(t_0)$. To shorten notion, the arguments of the coefficients are omitted in the following. Without loss of generality, the preceding equation (2.14) can further be decomposed into two independent parts, namely the diagonal and off-diagonal part,

$$\langle\mathcal{O}(t)\rangle = \sum_n |c_n|^2\,\mathcal{O}_{nn} + \sum_{m\neq n} c_m^*\,c_n\,\mathrm{e}^{\imath(E_m-E_n)(t-t_0)}\,\mathcal{O}_{mn}\,. \tag{2.15}$$

While the diagonal part $\sum_n |c_n|^2 \mathcal{O}_{nn}$ remains time-independent, the off-diagonal part carries the time dependence in the case of nondegenerate energy eigenvalues. If, however, all energy eigenvalues are degenerate, the off-diagonal part contains time-independent contributions.

The formulation of quantum states and expectation values of operators in terms of the energy eigenbasis [cf. Eq. (2.15)], will particularly be useful in the context of the concepts of equilibration and thermalization (see Sec. 5.2) as well as in the framework of numerical approaches such as exact diagonalization (see Sec. 6.1) in the course of this thesis.

2.2. Density Matrices

The concept of *density matrices* allows to describe quantum systems that are in a precisely defined state, but also quantum systems whose state is only known statistically, and, therefore, provides the possibility to explain physical situations with both mixed and pure states.

The so-called *mixed states* can be considered as a collection of pure states $|\psi_1\rangle, \ldots, |\psi_n\rangle$, which are independently prepared and weighted by the respective probability $w_1, \ldots, w_n$. The density matrix ρ for such a statistical mixture is given by

$$\rho = \sum_n w_n \mathcal{P}_n = \sum_n w_n \, |\psi_n\rangle \langle\psi_n| \quad \text{with} \quad w_n \geq 0 \quad \text{and} \quad \sum_n w_n = 1 \,, \tag{2.16}$$

where the states $|\psi_n\rangle$ are normalized to unity, but do not necessarily have to be orthogonal to each other. Moreover, the term $\mathcal{P}_n = |\psi_n\rangle \langle\psi_n|$ denotes a projection operator, which projects an arbitrary state on the n-th state. The entire information of the system is included in the density matrix. If the matrix elements of ρ are written as $\rho_{mn} = \langle\varphi_m|\rho|\varphi_n\rangle$ for an arbitrary orthonormal basis $\{|\varphi_n\rangle\}$ of a Hilbert space, then on the one hand the off-diagonal matrix elements, ρ_{mn} with $m \neq n$, denote the so-called *coherences* and give information about quantum correlations between the states $|\varphi_n\rangle$ and $|\varphi_m\rangle$. On the other hand the diagonal matrix elements, ρ_{nn}, are referred to *populations* and provide information about the probability to find the system in state $|\varphi_n\rangle$.

Similar to classical statistical mechanics, where the expectation value of a classical observable O has been defined as the integral over the phase space attached by an associated density function (see Sec. 1.2), the expectation value of a quantum mechanical observable $\mathcal{O}$ is given by the weighted sum of the expectation values in terms of pure states:

$$\begin{aligned} \mathrm{tr}\,[\rho\,\mathcal{O}] &= \sum_m \langle\varphi_m|\rho\,\mathcal{O}|\varphi_m\rangle = \sum_{m,n} w_n \, \langle\psi_n|\mathcal{O}|\varphi_m\rangle\langle\varphi_m|\psi_n\rangle \\ &= \sum_n w_n \, \langle\psi_n|\mathcal{O}|\psi_n\rangle = \langle\mathcal{O}\rangle \,, \end{aligned} \tag{2.17}$$

where the closure relation, $\sum_m |\varphi_m\rangle \langle\varphi_m| = \mathbb{1}_{\mathcal{D}}$ for a set of orthonormal basis states $\{|\varphi_m\rangle\}$ of a Hilbert space $\mathscr{H}$, has been used and $\mathbb{1}_{\mathcal{D}}$ again denotes the identity operator related to a $\mathcal{D}$-dimensional Hilbert space $\mathscr{H}$. Moreover, the *trace* of an operator $\mathcal{O}'$ is generally defined by

$$\mathrm{tr}\,[\mathcal{O}'] = \sum_m \langle\varphi_m|\mathcal{O}'|\varphi_m\rangle \,, \tag{2.18}$$

with respect to some complete set of orthonormal states $\{|\varphi_m\rangle\}$ of a Hilbert space. Due to

the representation-independence of the trace, any complete set of basis states can be used to evaluate the expectation value (2.17). To obtain physical reasonable density matrices, that is, real-valued and nonnegative probabilities, the density matrix ρ has to be both, Hermitian ($\rho = \rho^\dagger$) and positive ($\rho \geq 0$). The density matrix ρ is normalized to

$$\mathrm{tr}\left[\rho\right] = \sum_{m,n} w_n \left\langle \varphi_m | \psi_n \right\rangle \left\langle \psi_n | \varphi_m \right\rangle = \sum_n w_n \left\langle \psi_n | \psi_n \right\rangle = 1 \,, \tag{2.19}$$

which follows from Eq. (2.16). For reasons of completeness, a pure quantum state (i.e. $w_n = 1$) is captured by the density matrix formalism by

$$\rho = \left| \psi \right\rangle \left\langle \psi \right| \,. \tag{2.20}$$

To conclude the properties of a density matrix, pure and mixed quantum states can be distinguished by means of the inequality

$$\mathrm{tr}\left[\rho^2\right] \leq 1 \,, \tag{2.21}$$

where equality is fulfilled if and only if the density matrix ρ describes a pure quantum state. Conversely, for a statistical mixture of several quantum states the inequality (2.21) yields, $\mathrm{tr}\left[\rho^2\right] < 1$.

2.2.1. Von-Neumann Equation

If the considered system is in a mixed state and this state depends on time, the corresponding density matrix $\rho(t)$ can be written, similar to Eq. (2.16), as

$$\rho(t) = \sum_n w_n \left| \psi_n(t) \right\rangle \left\langle \psi_n(t) \right| \,, \tag{2.22}$$

where the time evolution of each individual pure state $|\psi_n(t)\rangle$ of the statistical mixture of states contributes to the time evolution of the entire density matrix. Since each pure state $|\psi_n(t)\rangle$ evolves unitarily in time according to the Schrödinger equation (2.1), the density matrix $\rho(t)$ evolves in time according to

$$\begin{aligned} \frac{\mathrm{d}}{\mathrm{d}t}\rho(t) &= -\imath \sum_n w_n \Big[\left(\mathcal{H} \left| \psi_n(t) \right\rangle \right) \left\langle \psi_n(t) \right| - \left| \psi_n(t) \right\rangle \left(\left\langle \psi_n(t) \right| \mathcal{H} \right) \Big] \\ &= -\imath \left[\mathcal{H}, \rho(t) \right] \,. \end{aligned} \tag{2.23}$$

This equation is known as the *von-Neumann equation* and can be deduced by inserting the complex conjugated Schrödinger equation and using the fact that the probabilities w_n are constant in time. It is worth pointing out that $\rho(t)$ in Eq. (2.23) represents the density matrix in the Schrödinger representation, and for the case of pure states (i.e. $\rho(t) = |\psi(t)\rangle \langle\psi(t)|$), the von-Neumann equation (2.23) reduces to the Schrödinger equation (2.1). Owing to the fact that the von-Neumann equation is a first order differential equation, a formal solution is given in terms of the time-evolution operator $\mathcal{U}(t, t_0)$ [cf. Eq. (2.6)] and some initial condition $\rho(t_0)$ according to

$$\rho(t) = \mathcal{U}(t, t_0)\, \rho(t_0)\, \mathcal{U}^\dagger(t, t_0) = \mathrm{e}^{-\imath \mathcal{H}(t-t_0)}\, \rho(t_0)\, \mathrm{e}^{\imath \mathcal{H}(t-t_0)} \,. \tag{2.24}$$

To emphasize the resemblance of the von-Neumann equation and the classical Liouville equation [cf. Eq. (1.13)], the von-Neumann equation can be written analogously in terms of the so-called *quantum Liouville superoperator* $\imath\mathcal{L}_{\mathrm{qm}}$:

$$\frac{\mathrm{d}}{\mathrm{d}t}\rho(t) = -\imath\mathcal{L}_{\mathrm{qm}}\left[\rho(t)\right] , \tag{2.25}$$

with $\imath\mathcal{L}_{\mathrm{qm}}[\bullet] \equiv -\imath\left[\bullet, \mathcal{H}\right]$. The notion of a superoperator is intended to illustrate that the action of $\mathcal{L}_{\mathrm{qm}}$ on an operator generates another operator. Finally, in terms of the quantum Liouville superoperator, a solution of Eq. (2.25) can formally be written as

$$\rho(t) = \exp\left(-\imath(t-t_0)\mathcal{L}_{\mathrm{qm}}\right)\,\rho(t_0)\,, \tag{2.26}$$

for some initial condition $\rho(t_0)$.

2.2.2. Time Evolution in Energy Eigenbasis

Similar to Sec. 2.1.2, where the time evolution of the state vector $|\psi(t)\rangle$ in terms of energy eigenstates has been shown, the time evolution of the density matrix $\rho(t)$ can also be decomposed in terms of energy eigenstates. The density matrix in (2.24) with the matrix elements $\rho_{mn}(t) = \langle m|\rho(t)|n\rangle$ yields

$$\rho_{nn}(t) = \rho_{nn}(t_0) \quad \text{and} \quad \rho_{mn}(t) = \rho_{mn}(t_0)\,\mathrm{e}^{-\imath(E_m - E_n)(t-t_0)} \quad \text{for } m \neq n\,. \tag{2.27}$$

The preceding expression shows that the populations in the energy eigenbasis are constant in time, while the coherences of the system oscillate.

2.2.3. Canonical Ensemble

The *quantum canonical ensemble* illustrates the behavior of a quantum system which is in thermal contact with a heat bath. For the canonical ensemble, the density matrix ρ_β is given by

$$\rho_\beta = \frac{1}{\mathcal{Z}_\beta}\,\mathrm{e}^{-\beta\mathcal{H}} = \frac{\mathrm{e}^{-\beta\mathcal{H}}}{\mathrm{tr}\left[\mathrm{e}^{-\beta\mathcal{H}}\right]}\,, \tag{2.28}$$

where the normalization factor $\mathcal{Z}_\beta$ denotes the *canonical partition function* at inverse temperature $\beta = 1/T$ and the Boltzmann constant k_{B} is set to unity, that is, $k_{\mathrm{B}} \equiv 1$ for the rest of this thesis. For (quantum) ensembles at equilibrium, the von-Neumann equation (2.23) implies that the density matrix is time-independent. Additionally, the density matrix ρ_β can be expanded in terms of a complete set of eigenstates $\{|n\rangle\}$ and associated eigenvalues $\{E_n\}$ of the Hamiltonian $\mathcal{H}$ according to

$$\rho_\beta = \frac{1}{\mathcal{Z}_\beta}\sum_n \mathrm{e}^{-\beta E_n}\,|n\rangle\,\langle n|\,, \tag{2.29}$$

where the partition function $\mathcal{Z}_\beta$ can analogously expanded as

$$\mathcal{Z}_\beta = \mathrm{tr}\left[\mathrm{e}^{-\beta\mathcal{H}}\right] = \sum_n \langle n|\mathrm{e}^{-\beta\mathcal{H}}|n\rangle = \sum_n \mathrm{e}^{-\beta E_n}\,. \tag{2.30}$$

Eventually, the canonical expectation value $\langle \mathcal{O} \rangle$ of some observable $\mathcal{O}$ can be written for the density matrix given in (2.28) as

$$\langle \mathcal{O} \rangle = \mathrm{tr}\left[\rho_\beta \, \mathcal{O}\right] = \frac{1}{\mathcal{Z}_\beta} \mathrm{tr}\left[\mathrm{e}^{-\beta \mathcal{H}} \, \mathcal{O}\right] = \frac{1}{\mathcal{Z}_\beta} \sum_n \mathrm{e}^{-\beta E_n} \langle n | \mathcal{O} | n \rangle \,, \tag{2.31}$$

by exploiting both, the definition of the trace from Eq. (2.18) and the canonical density matrix ρ_β from (2.28).

In particular, the canonical ensemble plays a major role in the context of correlation functions in the further course of this thesis. Within the framework of linear response theory, time-dependent correlation functions occur and are evaluated at canonical equilibrium according to the density matrix (2.28).

2.3. Other Types of Representation

While in the previous sections quantities have been treated exclusively within the Schrödinger representation, the following two sections refer to both, (*i*) the Heisenberg and (*ii*) the interaction representation.

2.3.1. Heisenberg Representation

In contrast to the Schrödinger representation, where the time evolution of the density matrix (pure states) is governed by the von-Neumann equation (Schrödinger equation), the so-called *Heisenberg representation* provides a different yet equivalent description of the dynamics of quantum mechanics.

According to the Heisenberg representation, the time dependence of the density matrix is transferred to the operators. For some initial time t_0, it is supposed that the density matrices in both the Schrödinger and Heisenberg representation agree with each other (i.e. $\rho(t_0) = \rho_\mathrm{H}(t_0)$). Note that in order to distinguish between the different representations, the density matrices and operators with respect to the Heisenberg representation are labelled by the subscript "H".

A relation between operators in the Schrödinger representation $\mathcal{O}$ and those in the Heisenberg representation $\mathcal{O}_\mathrm{H}(t)$ is given by the transformation

$$\mathcal{O}_\mathrm{H}(t) = \mathcal{U}^\dagger(t, t_0) \, \mathcal{O} \, \mathcal{U}(t, t_0) \,. \tag{2.32}$$

As becomes apparent from Eq. (2.32), by exploiting the properties of the unitary time-evolution operator (see Sec. 2.1), Schrödinger and Heisenberg representation coincide in the limit $t \to t_0$. The expectation values for both representations have to coincide, which implies

$$\langle \mathcal{O}(t) \rangle = \mathrm{tr}\left[\rho(t) \, \mathcal{O}\right] = \mathrm{tr}\left[\rho_\mathrm{H}(t_0) \, \mathcal{O}_\mathrm{H}(t)\right] \,. \tag{2.33}$$

For a given operator in the Heisenberg representation, the time evolution is governed by *Heisenberg's equation of motion*

$$\frac{\mathrm{d}}{\mathrm{d}t} \mathcal{O}_\mathrm{H}(t) = \imath \left[\mathcal{H}_\mathrm{H}, \mathcal{O}_\mathrm{H}(t)\right] \,, \tag{2.34}$$

which can be derived from Eq. (2.32) by taking the time derivative of both sides. The operator $\mathcal{O}_{\mathrm{H}}(t)$ has to be understood as stated in Eq. (2.32). It is worth considering limiting cases: If the Schrödinger operator $\mathcal{O}$ depends explicitly on time and if the system under consideration is isolated, the Heisenberg's equation of motion (2.34) adds an additional term, $(\partial\mathcal{O}(t)/\partial t)_{\mathrm{H}}$, which has to be understood according to the transformation (2.32).

2.3.2. Interaction Representation

It should be emphasized that operators with respect to the interaction representation are labelled by the subscript "I".

Within the *interaction representation*, the Hamiltonian of a quantum system is divided into an unperturbed part $\mathcal{H}_0$ and a perturbation part $\mathcal{H}'$. The total Hamiltonian $\mathcal{H}$ thus reads

$$\mathcal{H} = \mathcal{H}_0 + \mathcal{H}' \,, \tag{2.35}$$

where the exact form of the parts $\mathcal{H}_0$ and $\mathcal{H}'$ depends on the underlying physical problem. It is instructive to define two different unitary time-evolution operators for the evolution of operators and states, respectively:

$$\mathcal{U}_0(t,t_0) = \mathrm{e}^{-\imath\mathcal{H}_0(t-t_0)} \,, \tag{2.36}$$

and

$$\mathcal{U}_{\mathrm{I}}(t,t_0) \equiv \mathcal{U}_0^\dagger(t,t_0)\,\mathcal{U}(t,t_0) \,, \tag{2.37}$$

where $\mathcal{U}(t,t_0)$ evolves the total Hamiltonian $\mathcal{H}$ [cf. Eq. (2.6)]. An operator according to the interaction representation is defined by

$$\mathcal{O}_{\mathrm{I}}(t) \equiv \mathcal{U}_0^\dagger(t,t_0)\,\mathcal{O}\,\mathcal{U}_0(t,t_0) \,, \tag{2.38}$$

where $\mathcal{O}$ is an operator within the Schrödinger representation. Similarly, the density matrix within the interaction representation is given by

$$\rho_{\mathrm{I}}(t) \equiv \mathcal{U}_{\mathrm{I}}(t,t_0)\,\rho(t_0)\,\mathcal{U}_{\mathrm{I}}^\dagger(t,t_0) \,. \tag{2.39}$$

Then, according to Eq. (2.33), the expectation value can be written as

$$\begin{aligned}\langle\mathcal{O}(t)\rangle &= \mathrm{tr}\left[\mathcal{O}\,\rho(t)\right] = \mathrm{tr}\left[\mathcal{U}_0^\dagger(t,t_0)\,\mathcal{O}\,\mathcal{U}_0(t,t_0)\,\mathcal{U}_{\mathrm{I}}(t,t_0)\rho(t_0)\,\mathcal{U}_{\mathrm{I}}^\dagger(t,t_0)\right] \\ &= \mathrm{tr}\left[\mathcal{O}_{\mathrm{I}}(t)\,\rho_{\mathrm{I}}(t)\right] \,.\end{aligned} \tag{2.40}$$

Again, it is worth considering limiting cases. On the one hand, for $\mathcal{H}_0 = 0$, the Schrödinger representation is recovered, since the total Hamiltonian coincides with the perturbation part. This implies the equivalence of $\mathcal{U}_{\mathrm{I}}(t,t_0)$ and $\mathcal{U}\,(t,t_0)$. On the other hand, for a vanishing perturbation term (i.e. $\mathcal{H}' = 0$), the unitary time-evolution operator of $\mathcal{H}_0$ equals $\mathcal{U}\,(t,t_0)$ and thus $\mathcal{U}_{\mathrm{I}}(t,t_0) = \mathbb{1}_{\mathcal{D}}$.

Apart from many applications of the Heisenberg and interaction representation, in this thesis both are mainly used within *linear response theory* (LRT) which considers the response of a physical system to an additional perturbation within a Hamiltonian.

2.4. Correlation Functions

2.4.1. Two-Point Correlation Functions

The *time-dependent correlation function* between two observables, say $\mathcal{O}(t)$ and $\mathcal{O}'(t')$, evaluated at times t and t', is defined by

$$C^{\beta}_{\mathcal{O}\mathcal{O}'}(t,t') \equiv \langle \mathcal{O}(t)\, \mathcal{O}'(t') \rangle = \mathrm{tr}\left[\rho_\beta\, \mathcal{O}(t)\, \mathcal{O}'(t')\right] , \tag{2.41}$$

where the (canonical) density matrix is denoted by $\rho_\beta = \exp\left(-\beta \mathcal{H}\right) / \mathcal{Z}_\beta$ and $\mathcal{Z}_\beta$ represents the (canonical) partition function at inverse temperature $\beta = 1/T$ (see Sec. 2.2.3). Notably, the time dependence of the operators $\mathcal{O}(t)$ and $\mathcal{O}'(t')$ has to be understood with respect to the Heisenberg representation. In particular, for $\mathcal{O} = \mathcal{O}'$, Eq. (2.41) turns into

$$C^{\beta}_{\mathcal{O}\mathcal{O}}(t,t') = \langle \mathcal{O}(t)\, \mathcal{O}(t') \rangle = \mathrm{tr}\left[\rho_\beta\, \mathcal{O}(t)\, \mathcal{O}(t')\right] , \tag{2.42}$$

and is known as the *autocorrelation function*. A special case arises by taking the limit of formally infinite temperatures (i.e. $\beta \to 0$). In that case the autocorrelation function takes on the form

$$C(t,t') \equiv \lim_{\beta\to 0} C^{\beta}_{\mathcal{O}\mathcal{O}}(t,t') = \frac{\mathrm{tr}\left[\mathcal{O}(t)\, \mathcal{O}(t')\right]}{\mathcal{D}} , \tag{2.43}$$

where $\mathcal{D} = \dim(\mathscr{H})$ denotes the dimension of the Hilbert space $\mathscr{H}$. The preceding expression follows from $\exp\left(-\beta\mathcal{H}\right)/\mathcal{Z}_\beta \to \mathbb{1}/\mathcal{D}$ in the limit $\beta \to 0$.

In the course of this thesis, the operators $\mathcal{O}(t)$ and $\mathcal{O}'(t')$ are identified as operators of *local densities* $\varrho_{\boldsymbol{r}}$ and $\varrho_{\boldsymbol{r}'}$, acting on different (local) lattice sites $\boldsymbol{r}$ and $\boldsymbol{r}'$. In this context, the corresponding time-dependent *density-density correlation function* is denoted by

$$C^{\beta}_{\boldsymbol{r},\boldsymbol{r}'}(t,t') \equiv \langle \varrho_{\boldsymbol{r}}(t)\, \varrho_{\boldsymbol{r}'}(t') \rangle = \mathrm{tr}\left[\rho_\beta\, \varrho_{\boldsymbol{r}}(t)\, \varrho_{\boldsymbol{r}'}(t')\right] , \tag{2.44}$$

or in the limiting case of formally infinite temperature [cf. Eq. (2.43)] as

$$C_{\boldsymbol{r},\boldsymbol{r}'}(t,t') = \lim_{\beta\to 0} C^{\beta}_{\boldsymbol{r},\boldsymbol{r}'}(t,t') . \tag{2.45}$$

2.4.2. Time Evolution in Energy Eigenbasis

The two-point correlation function given in (2.41) can be written in terms of the system's energy eigenbasis by inserting complete sets of eigenstates $\{|m\rangle\}$ and $\{|n\rangle\}$ according to

$$\langle \mathcal{O}(t)\mathcal{O}' \rangle = \sum_{n,m} \frac{\mathrm{e}^{-\beta E_n}}{\mathcal{Z}_\beta}\, \mathrm{e}^{\imath (E_n - E_m) t}\, \langle m|\mathcal{O}|n\rangle\langle n|\mathcal{O}'|m\rangle . \tag{2.46}$$

In the preceding equation both $t' = 0$ and $\mathcal{O}' \equiv \mathcal{O}'(0)$ have been chosen. If the observables are equal (i.e. $\mathcal{O}' = \mathcal{O}$), Eq. (2.46) turns into

$$\langle \mathcal{O}(t)\mathcal{O} \rangle = \sum_{n,m} \frac{\mathrm{e}^{-\beta E_n}}{\mathcal{Z}_\beta}\, \mathrm{e}^{\imath (E_n - E_m) t}\, |\langle n|\mathcal{O}|m\rangle|^2 . \tag{2.47}$$

A decomposition into an energy eigenbasis, as given in Eq. (2.47), is useful in the context of certain numerical methods, such as exact diagonalization. Once all eigenvalues and

eigenstates have been found, the correlation function can in principle be calculated for arbitrarily long times. Exact diagonalization will be discussed in more detail in the course of this thesis (see Sec. 6).

3. Models

Sec. 3 is dedicated to present the models under consideration. To this end, Sec. 3.1 describes the anisotropic quantum Heisenberg model (XXZ model). The considered observables are explained in Sec. 3.1.1. While Sec. 3.1.2 deals with the one-dimensional case in greater detail, in Sec. 3.2 the classical counterpart of the quantum Heisenberg model is presented. Sec. 3 closes with remarks on both classical and quantum integrability.

3.1. Quantum Heisenberg Spin Model

One of the most studied models within a variety of low-dimensional quantum lattice models is the *anisotropic Heisenberg spin-S model*. While in the course of this thesis the spin quantum number S takes on specific values (see e.g., Pt. III), first, S is kept general.

The anisotropic Heisenberg spin-S model is here formulated on a subclass of rectangular lattices, which consist of $N = L_x \times L_y$ lattice sites in total, where L_x and L_y are the lattice extension in x and y direction, respectively. Then, the exact lattice geometry depends on the specific choice of L_x and L_y. This thesis is mainly focussed on three different lattice geometries, namely the (*i*) *one-dimensional chain* ($N = L_x \times 1$), the (*ii*) *quasi-one-dimensional two-leg ladder* ($N = L_x \times 2$) and the (*iii*) *two-dimensional square lattice* ($N = L_x \times L_y$ with $L_x = L_y$). It is worth noting that periodic boundary conditions (PBC) are imposed on each of the considered models within this thesis. In Fig. 3.1 (*a*) - (*c*), the different lattice geometries are illustrated.

To proceed, the Hamiltonian of the anisotropic Heisenberg spin-S model can be written as

$$\mathcal{H}_{\mathrm{XXZ}} = \sum_{\langle \boldsymbol{r},\boldsymbol{r}'\rangle} J_{\boldsymbol{r},\boldsymbol{r}'}\, h_{\boldsymbol{r},\boldsymbol{r}'}\,, \tag{3.1}$$

where the sum runs over all bonds $\langle \boldsymbol{r},\boldsymbol{r}'\rangle$ of nearest-neighboring sites $\boldsymbol{r} = (i,j)$ and $\boldsymbol{r}' = (i',j')$. The exchange couplings $J_{\boldsymbol{r},\boldsymbol{r}'}$ act between the lattice sites $\boldsymbol{r}$ and $\boldsymbol{r}'$ and set the energy scale. Moreover, the couplings can be considered as either antiferromagnetic ($J_{\boldsymbol{r},\boldsymbol{r}'} > 0$) or ferromagnetic ($J_{\boldsymbol{r},\boldsymbol{r}'} < 0$). Unless otherwise stated, the exchange coupling is set antiferromagnetic and constant ($J_{\boldsymbol{r},\boldsymbol{r}'} = 1$) throughout this thesis.

The local term $h_{\boldsymbol{r},\boldsymbol{r}'}$ within the Hamiltonian (3.1) explicitly reads

$$h_{\boldsymbol{r},\boldsymbol{r}'} = \left(S^x_{\boldsymbol{r}} S^x_{\boldsymbol{r}'} + S^y_{\boldsymbol{r}} S^y_{\boldsymbol{r}'} + \Delta S^z_{\boldsymbol{r}} S^z_{\boldsymbol{r}'}\right)\,, \tag{3.2}$$

where Δ parametrizes the anisotropy in z direction and the components $S^\mu_{\boldsymbol{r}}$ with $\mu = \{x,y,z\}$ describe three-dimensional spin-S operators acting locally at lattice site $\boldsymbol{r}$. In addition, they obey the fundamental $SU(2)$-algebra commutation relation [153] given by

$$[S^\mu_{\boldsymbol{r}}, S^\nu_{\boldsymbol{r}'}] = \imath\, \delta_{\boldsymbol{r}\boldsymbol{r}'}\, \varepsilon_{\mu\nu\lambda}\, S^\lambda_{\boldsymbol{r}}\,, \tag{3.3}$$

where $\delta_{\boldsymbol{r}\boldsymbol{r}'}$ again is the Kronecker delta [cf. Eq. (1.9)] and $\varepsilon_{\mu\nu\lambda}$ denotes the totally antisym-

metric Levi-Civita tensor. This tensor is defined as

$$\varepsilon_{\mu\nu\lambda} = \begin{cases} +1, & \text{if } (\mu,\nu,\lambda) \text{ is an even permutation of } (1,2,3) \\ -1, & \text{if } (\mu,\nu,\lambda) \text{ is an odd permutation of } (1,2,3) \\ 0, & \text{otherwise} \end{cases} . \tag{3.4}$$

Notably, the Einstein summation convention, that is, over indices that occur twice is summed, is used throughout this thesis.

3.1.1. Observables

This thesis focusses on the dynamics of time-dependent *local densities* $\varrho_{\boldsymbol{r}}(t)$ at lattice site $\boldsymbol{r} = (i,j)$, which can be either magnetization or energy. To study the dynamics of such local densities, time-dependent *density-density correlation functions* $C^{\beta}_{\boldsymbol{r},\boldsymbol{r}'}(t)$ are considered (see Sec. 2.4.1). Unless otherwise stated, the term $\varrho_{\boldsymbol{r}}(t)$ refers to both local densities.

Recall from Sec. 2.4 that the correlation functions $C^{\beta}_{\boldsymbol{r},\boldsymbol{r}'}(t)$ for some local density $\varrho_{\boldsymbol{r}}$ are defined as

$$C^{\beta}_{\boldsymbol{r},\boldsymbol{r}'}(t) = \langle \varrho_{\boldsymbol{r}}(t)\, \varrho_{\boldsymbol{r}'} \rangle = \frac{\operatorname{tr}\left[\mathrm{e}^{-\beta \mathcal{H}_{\mathrm{XXZ}}}\, \varrho_{\boldsymbol{r}}(t)\, \varrho_{\boldsymbol{r}'}\right]}{\mathcal{Z}_{\beta}} . \tag{3.5}$$

The time argument of $\varrho_{\boldsymbol{r}}(t)$ has to be understood according to the Heisenberg representation (see Sec. 2.3.1) and $\varrho_{\boldsymbol{r}} = \varrho_{\boldsymbol{r}}(t=0)$. As this thesis mainly considers the specific case of formally infinite temperature (i.e. $\beta \to 0$), the correlation function (3.5) turns into

$$C_{\boldsymbol{r},\boldsymbol{r}'}(t) = \frac{\operatorname{tr}\left[\varrho_{\boldsymbol{r}}(t)\, \varrho_{\boldsymbol{r}'}\right]}{\mathcal{D}} , \tag{3.6}$$

where $\mathcal{D} = (2S+1)^N$ again denotes the Hilbert-space dimension, for example, $\mathcal{D} = 2^N$ for $S = 1/2$. To proceed, it is instructive to define the local densities for the lattice geometries (*i*) - (*iii*), whose specific definition depends on the lattice geometry. First, consider the local density of magnetization $\varrho^{(\mathrm{M})}_{\boldsymbol{r}} = \varrho^{(\mathrm{M})}_{i,j}$. While such a definition is not unique and depends on the chosen unit cell, a natural definition of $\varrho^{(\mathrm{M})}_{i,j}$ can be given by

$$\varrho^{(\mathrm{M})}_{i,j} = \begin{cases} S^z_{i,1} , & \text{for } L_x \times 1 \\ S^z_{i,1} + S^z_{i,2} , & \text{for } L_x \times 2 \\ S^z_{i,j} , & \text{for } L_x \times L_y \end{cases} . \tag{3.7}$$

In addition, consider the local density of energy $\varrho^{(\mathrm{E})}_{\boldsymbol{r}} = \varrho^{(\mathrm{E})}_{i,j}$. For a one-dimensional chain ($N = L_x \times 1$), the local density of energy is defined on a single bond according to

$$\varrho^{(\mathrm{E})}_{i,j} = J h_{(i,1),(i+1,1)} . \tag{3.8}$$

For the quasi-one-dimensional two-leg ladder ($N = L_x \times 2$), this is defined on a plaquette which consists of one bond for each leg and two rungs,

$$\varrho^{(\mathrm{E})}_{i,j} = J \left[h_{(i,1),(i+1,1)} + h_{(i,2),(i+1,2)}\right] + \frac{J}{2}\left[h_{(i,1),(i,2)} + h_{(i+1,1),(i+1,2)}\right] . \tag{3.9}$$

Finally, for the two-dimensional square lattice ($N = L_x \times L_y$ with $L_x = L_y$), the local energy reads

$$\begin{aligned} \varrho_{i,j}^{(\mathrm{E})} &= \frac{J}{2}\left[h_{(i-1,j),(i,j)} + h_{(i,j),(i+1,j)}\right] \\ &+ \frac{J}{2}\left[h_{(i,j-1),(i,j)} + h_{(i,j),(i,j+1)}\right] . \end{aligned} \tag{3.10}$$

Although in general the couplings can be labelled differently, namely $J_\perp$ for the coupling on the rungs and $J_{||}$ for the coupling along the legs, throughout this thesis $J \equiv J_\perp = J_{||}$ holds. To illustrate the definitions of the previously mentioned local densities, see Fig. 3.1 (d) - (i).

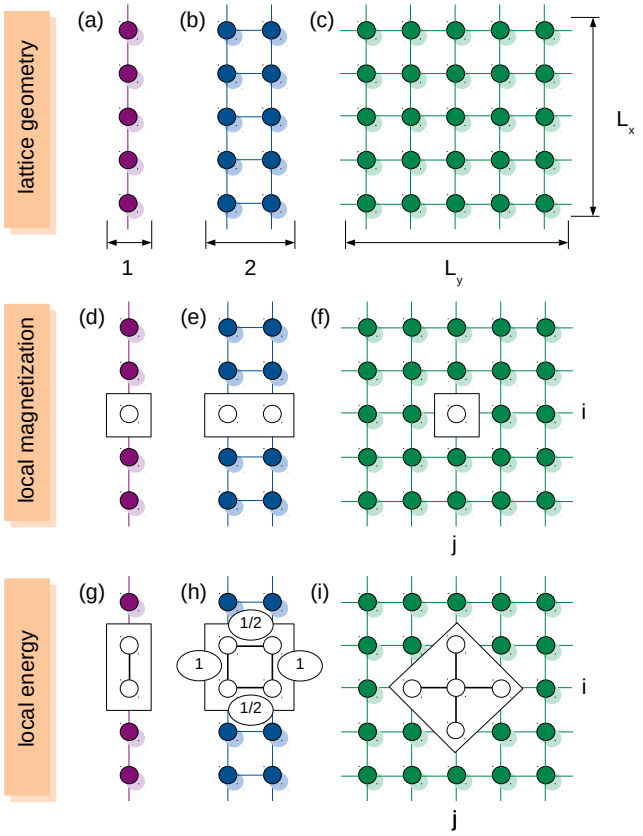

Figure 3.1.: Overview of the different models and observables. Top row (geometries): (a) One-dimensional chain, (b) quasi-one-dimensional two-leg ladder and (c) two-dimensional square lattice. Middle row: local magnetizations $(d) - (f)$ and bottom row: local energies $(g) - (i)$.

The study of (density-density) correlation functions $C_{\boldsymbol{r},\boldsymbol{r}'}(t)$ can provide information on certain transport properties. In the course of this thesis, the dynamics of such correlation functions is addressed in greater detail (see e.g., Sec. 4.2). Apart from studying correlation functions of local densities, another approach to analyze transport properties is related to the study of current-current correlation functions, briefly discussed in Sec. 4.4. For more details the reader is referred to Ref. [81].

3.1.2. One-dimensional Heisenberg Spin Model

Geometrically, the anisotropic one-dimensional spin-S Heisenberg model (XXZ model) is recovered from (3.1) by setting $L_y = 1$. The $(L_x \times L_y)$ lattice is therefore reduced to a one-dimensional chain and the Hamiltonian (3.1) simplifies to

$$\mathcal{H}_{\mathrm{XXZ}}^{(1\mathrm{d})} = J \sum_i \left(S_i^x S_{i+1}^x + S_i^y S_{i+1}^y + \Delta S_i^z S_{i+1}^z \right) , \tag{3.11}$$

where the parameters, that is, the coupling constant J and the anisotropy parameter Δ are the same as stated in Sec. 3.1. The lattice geometry is essentially transferred to a ring of N lattice sites due to imposing periodic boundary conditions (i.e. $S_1^\mu = S_{N+1}^\mu$). For the sake of illustration, within this section, spin-1/2 degrees of freedom are considered. Especially in this case, the components of the spin-1/2 operator S_i^μ can be expressed in terms of the *Pauli matrices*, $S_i^\mu = \sigma_i^\mu/2$, which are explicitly given by the following set of (2×2) matrices

$$\sigma_i^x = \begin{pmatrix} 0 & 1 \\ 1 & 0 \end{pmatrix} , \quad \sigma_i^y = \begin{pmatrix} 0 & -\imath \\ \imath & 0 \end{pmatrix} , \quad \sigma_i^z = \begin{pmatrix} 1 & 0 \\ 0 & -1 \end{pmatrix} . \tag{3.12}$$

These matrices satisfy the following commutation relations in the spirit of Eq. (3.3):

$$\left[\sigma_i^\mu, \sigma_j^\nu \right] = 2\imath \, \delta_{ij} \, \varepsilon_{\mu\nu\lambda} \, \sigma_i^\lambda . \tag{3.13}$$

Conventionally, by defining the raising- and lowering spin-operators $S_i^\pm \equiv S_i^x \pm \imath S_i^y$, which formally satisfy the commutation relations

$$\left[S_i^z, S_j^\pm \right] = \pm \delta_{ij} S_j^\pm , \quad \left[S_i^+, S_j^- \right] = 2\delta_{ij} S_j^z , \quad \left[S_i^\pm, S_j^\pm \right] = 0 , \tag{3.14}$$

the Hamiltonian (3.11) can be rewritten in terms of raising and lowering operators as

$$\mathcal{H}_{\mathrm{XXZ}}^{(1\mathrm{d})} = J \sum_i \left[\frac{1}{2} \left(S_i^+ S_{i+1}^- + S_i^- S_{i+1}^+ \right) + \Delta S_i^z S_{i+1}^z \right] . \tag{3.15}$$

To proceed, formally each lattice site is associated with a local two-dimensional complex Hilbert space $\mathscr{H}_i = \mathbb{C}^2$, $i = 1, 2, \ldots, N$. As a consequence the global Hilbert space $\mathscr{H}$ is given by the tensor product over all local complex Hilbert spaces according to

$$\mathscr{H} = \bigotimes_i \mathscr{H}_i = \mathscr{H}_1 \otimes \mathscr{H}_2 \otimes \cdots \otimes \mathscr{H}_N . \tag{3.16}$$

Bearing in mind that the local Hilbert space is two-dimensional, the global Hilbert space is 2^N-dimensional for $S = 1/2$. For a spin-S quantum number, the dimension of the total Hilbert space is $\mathcal{D} = (2S+1)^N$. Accordingly, a basis for the local vector space is essentially written in terms of basis states corresponding to the eigenstates of S_i^z, which only can take the eigenvalues $\pm 1/2$, with the corresponding eigenstates $|\cdots \uparrow_i \cdots\rangle$ (spin up) and $|\cdots \downarrow_i \cdots\rangle$ (spin down) at lattice site i. These eigenstates can be represented by two-dimensional orthogonal real vectors

$$|\uparrow_i\rangle = \begin{pmatrix} 1 \\ 0 \end{pmatrix}_i \quad \text{and} \quad |\downarrow_i\rangle = \begin{pmatrix} 0 \\ 1 \end{pmatrix}_i . \tag{3.17}$$

As a consequence, the raising and lowering operators $S_i^{\pm}$ act on a state with an up or down spin at lattice site i as follows:

$$S_i^+ \left|\cdots\downarrow_i\cdots\right\rangle = \left|\cdots\uparrow_i\cdots\right\rangle, \qquad S_i^+ \left|\cdots\uparrow_i\cdots\right\rangle = 0, \tag{3.18a}$$

$$S_i^- \left|\cdots\uparrow_i\cdots\right\rangle = \left|\cdots\downarrow_i\cdots\right\rangle, \qquad S_i^- \left|\cdots\downarrow_i\cdots\right\rangle = 0\,. \tag{3.18b}$$

The operators S_i^z act on these states according to,

$$S_i^z \left|\cdots\downarrow_i\cdots\right\rangle = -\frac{1}{2}\left|\cdots\downarrow_i\cdots\right\rangle, \quad S_i^z \left|\cdots\uparrow_i\cdots\right\rangle = \frac{1}{2}\left|\cdots\uparrow_i\cdots\right\rangle. \tag{3.18c}$$

A basis of the global Hilbert space is generated by using the product states in terms of these eigenstates:

$$\left|S_1^z\, S_2^z \cdots S_N^z\right\rangle = \bigotimes_i \left|S_i^z\right\rangle = \left|S_1^z\right\rangle \otimes \left|S_2^z\right\rangle \otimes \cdots \otimes \left|S_N^z\right\rangle \quad \text{with} \quad S_i^z \in \left\{\left|\uparrow_i\right\rangle, \left|\downarrow_i\right\rangle\right\}. \tag{3.19}$$

In the spirit of Eq. (3.16), the spin-1/2 operators act nontrivially on the i-th Hilbert space,

$$S_i^\mu = \underbrace{\mathbb{1}_2 \otimes \mathbb{1}_2 \otimes \cdots}_{i-1} \otimes \frac{1}{2}\sigma^\mu \otimes \underbrace{\mathbb{1}_2 \otimes \cdots \otimes \mathbb{1}_2}_{N-i}, \tag{3.20}$$

where $\mathbb{1}_2$ represents a (2×2)-dimensional identity matrix. In the case of $S = 1/2$ degrees of freedom, there exists a mapping from the spin-1/2 operators to fermionic creation and annihilation operators, accomplished by the Jordan-Wigner transformation (see Sec. 3.1.4).

3.1.3. Symmetries of the XXZ Chain

Operators $\mathcal{O}$ that *commute* with the Hamiltonian $\mathcal{H}$ of a respective quantum model feature essentially two significant properties: (*i*) these operators represent physically *conserved quantities* (see Sec. 2.1.1) and (*ii*) common eigenstates of the system's Hamiltonian $\mathcal{H}$ and $\mathcal{O}$ can be found [81, 154]. From a more general perspective, symmetries of a system are related to conserved quantities by the *Noether theorem* [155]. For more details the reader is referred to Refs. [154, 156].

The one-dimensional XXZ spin-1/2 model conserves the total magnetization in z direction, that is, the Hamiltonian (3.11) is invariant under rotations around the z-axis. The operator of total magnetization S^z is defined as the sum of local magnetization operators S_i^z at lattice site i,

$$S^z = \sum_i S_i^z\,. \tag{3.21}$$

Exploiting the commutation relations (3.14), it can be straightforwardly shown that the commutator of the Hamiltonian (3.15) (or alternatively Hamiltonian (3.11)) and the total magnetization operator (3.21) vanishes. This symmetry is also referred to $U(1)$ symmetry [153]. As a result, the conservation of total magnetization in z direction implies that the system's Hamiltonian matrix can be decomposed into $(N+1)$ independent subspaces (blocks). Each of the subspaces corresponds to a number M, with $0 \leq M \leq N$

of up-spins [154]. The dimension of a single subspace $\mathcal{D}_{\text{subsp.}}$ is determined by

$$\mathcal{D}_{\text{subsp.}} = \binom{N}{M} = \frac{N!}{M!(N-M)!} \,. \tag{3.22}$$

Furthermore, it is worth mentioning that in the isotropic case ($\Delta = 1$), the total spin $\mathcal{S} \equiv \sum_i \boldsymbol{S}_i$, where $\boldsymbol{S}_i = (S_i^x, S_i^y, S_i^z)$, is conserved, since the Hamiltonian (3.15) commutes with $\mathcal{S}^2$. This symmetry is also known as $SU(2)$ symmetry [153].

Since the considered model is imposed by PBC, the Hamiltonian remains invariant under translations in space. This symmetry implies the conservation of momentum. The translation symmetry is conveyed by an unitary operator, the so-called *translation operator* $\mathscr{T}$ [157]. This operator formally shifts the spin cyclically one lattice site to the "right" according to

$$\mathscr{T} \left| S_1^z, S_2^z, \ldots, S_{N-1}^z, S_N^z \right\rangle = \left| S_N^z, S_1^z, S_2^z, \ldots, S_{N-1}^z \right\rangle \,. \tag{3.23}$$

By applying the translation operator N times, the original state is returned, which leads to the condition $\mathscr{T}^N = \mathbb{1}$. The eigenstates $|\varphi(k)\rangle$ of $\mathscr{T}$ can be constructed by [157]

$$|\varphi(k)\rangle = \frac{1}{\sqrt{N}} \sum_i \mathrm{e}^{-\imath k i} \mathscr{T}^i \, |\varphi\rangle \,, \tag{3.24}$$

for an arbitrary state $|\varphi\rangle$, that is,

$$\mathscr{T} \, |\varphi(k)\rangle = \mathrm{e}^{\imath k} \, |\varphi(k)\rangle \,, \tag{3.25}$$

where $\mathrm{e}^{\imath k}$ are the eigenvalues of the translation operator $\mathscr{T}$ and the momenta k must satisfy $k = 2\pi n/N$ and $n = 0, 1, 2, \ldots, (N-1)$. Using these states, the Hamiltonian $\mathcal{H}$ decomposes into smaller matrix blocks that can be further diagonalized. For more details on translational invariance, the reader is referred to Ref. [157].

In addition to the symmetries mentioned previously, it is worth emphasizing that the XXZ Hamiltonian respects further symmetries, for example, the Hamiltonian is invariant under reflection [154]. Further symmetries will not be considered in detail in this thesis. Instead, the reader is referred to Refs. [154, 156, 157].

Exploiting certain symmetries plays a decisive role in the context of numerical techniques, such as exact diagonalization (see Sec. 6.1). Due to exploiting symmetries, the full Hilbert space can be decomposed into a direct sum of subspaces, which have a fixed quantum number. This subsequently leads to the reduction of required computational resources. For a more detailed explanation of exact diagonalization, the reader is referred to Sec. 6.1. Additionally, by taking local symmetries into account, the model can be investigated with respect to integrability or nonintegrability (see Sec. 3.3).

3.1.4. Jordan-Wigner Transformation

The *Jordan-Wigner transformation* states that there exists a mapping between the spin-1/2 degrees of freedom and those of spinless fermions. To be more precise, the spin-1/2 operators and their algebraic properties can be mapped onto fermionic creation and annihilation operators and their algebra [158]. To begin with, the set of spin-1/2 lowering and raising

operators (i.e. $S_i^{\pm}$) and S_i^z can expressed in terms of the Pauli matrices [cf. Eq. (3.12)] as

$$\sigma_i^{\pm} = \frac{1}{2}(\sigma_i^x \pm \imath\sigma_i^y)\,, \tag{3.26}$$

which obey commutation relations at different lattice sites i and j [cf. Eq. (3.14)]. Moreover, these operators satisfy anticommutation relations on the same lattice site i, that is,

$$\{\sigma_i^+, \sigma_i^-\} = 1\,. \tag{3.27}$$

The correct fermionic commutation relations have to be satisfied at all lattice sites. This can be achieved by the following transformation, known as the Jordan-Wigner transformation [158]:

$$\sigma_i^- \to c_i\, \mathrm{e}^{-\imath\phi_i}\,, \tag{3.28a}$$
$$\sigma_i^+ \to c_i^\dagger\, \mathrm{e}^{\imath\phi_i}\,, \tag{3.28b}$$
$$\sigma_i^z \to 2n_i - 1 \quad \text{with} \quad n_i = c_i^\dagger c_i\,, \tag{3.28c}$$

where the *phase factor* ϕ_i [158] essentially counts the number of spin-up operators to the left of lattice site i and is defined according to

$$\phi_i \equiv \pi \sum_{k<i} n_k = \pi \sum_{k<i} c_k^\dagger c_k\,. \tag{3.29}$$

By means of the phase factor, the fermionic operators $c_i^\dagger$ and c_i fulfil anticommutation relations

$$\{c_i^\dagger, c_j\} = \delta_{ij}\,. \tag{3.30}$$

Since these operators do not contain genuine spin degrees of freedom, they are known as *spinless fermionic operators*. In particular, the operator $c_i^\dagger$ creates a spinless fermion at lattice site i while c_i annihilates a spinless fermion at lattice site i. Finally, based on the transformations given above, the Hamiltonian from (3.11) can be rewritten as

$$\mathcal{H}_{\mathrm{JW}}^{(1\mathrm{d})} = J \sum_i \left[\frac{1}{2}\left(c_i^\dagger c_{i+1} + c_{i+1}^\dagger c_i\right) + \Delta\left(n_i - \frac{1}{2}\right)\left(n_{i+1} - \frac{1}{2}\right)\right]\,, \tag{3.31}$$

where the first term denotes the nearest-neighbor hopping of spinless fermions, while the second term represents nearest-neighbor interaction with an overall strength Δ. The expression in (3.31) therefore shows the correspondence of the one-dimensional anisotropic Heisenberg model to spinless fermions on a one-dimensional lattice.

While on the one hand the spin operators are transformed into spinless fermions by the Jordan-Wigner transformation, the Holstein-Primakoff transformation [159] on the other hand enables a fully bosonic perspective by replacing the spin operators by bosonic creation and annihilation operators.

3.2. Classical Heisenberg Spin Model

The classical XXZ model can be acquired from the quantum XXZ model by taking the limit of both, the Planck constant $\hbar \to 0$ and the spin quantum number $S \to \infty$, subjected to the constraint that $\hbar\sqrt{S(S+1)}$ is kept constant [160]. Based on these limits, the dynamics of the classical spin XXZ model is generated by the Hamilton function (see Sec. 1), which serves as the classical counterpart to the quantum Hamiltonian (3.11). The Hamiltonian changes to

$$\mathcal{H}_{\mathrm{XXZ}} \to H_{\mathrm{XXZ}}\,. \tag{3.32}$$

In the classical limit, the quantum spin-S operators turn into classical three-dimensional real *spin-vectors* $\mathbf{S}_{\boldsymbol{r}}$ subjected to unit norm (i.e. $||\mathbf{S}_{\boldsymbol{r}}|| = 1$). To determine the dynamics of the classical spin variables $\mathbf{S}_{\boldsymbol{r}}(t)$, first it is instructive to define a Poisson bracket (see Sec. 1.1) on the corresponding phase space Γ_{S}, which is given by the set of all possible classical states for each considered model. The Poisson bracket [51] reads as

$$\{S^{\mu}_{\boldsymbol{r}}, S^{\nu}_{\boldsymbol{r}'}\} = \delta_{\boldsymbol{r}\boldsymbol{r}'}\,\varepsilon_{\mu\nu\lambda}\,S^{\lambda}_{\boldsymbol{r}}\,, \tag{3.33}$$

and acts as a natural counterpart of the quantum mechanical commutation relations in Eq. (3.3). According to textbook classical mechanics and by means of Eq. (1.3), the time evolution of the spin vectors $\mathbf{S}_{\boldsymbol{r}}$ is governed by *Hamilton's equations of motion*,

$$\frac{\mathrm{d}}{\mathrm{d}t}\mathbf{S}_{\boldsymbol{r}} = \frac{\partial H_{\mathrm{XXZ}}}{\partial \mathbf{S}_{\boldsymbol{r}}} \times \mathbf{S}_{\boldsymbol{r}}\,, \tag{3.34}$$

which form a set of coupled differential equations and describe the precession of a spin around a local magnetic field resulting from the interaction with the neighboring spins. For a detailed derivation of Eq. (3.34), see, e.g., Refs. [117, 145]. Importantly, it is worth noting that the norm is preserved over the time evolution of the classical spin vectors.

Notably, there exists an equivalent formulation of classical spins according to canonical coordinates. For the sake of simplification, consider the one-dimensional case here. Due to the fact that the norm of the classical spin vectors is conserved in time, the associated classical phase space Γ_{S} is restricted to the surface of a sphere with unit radius [161]. As a consequence, the classical spins $\mathbf{S}_i$ can be parametrized by spherical coordinates,

$$(S^x_i, S^y_i, S^z_i) \to ||\mathbf{S}_i||\,(\sin(\theta_i)\cos(\phi_i),\, \sin(\theta_i)\sin(\phi_i),\, \cos(\theta_i))\,. \tag{3.35}$$

Accordingly, canonical coordinates are given by

$$(q_i, p_i) = (\omega_i, z_i) = (\phi_i,\, \cos(\theta_i))\,, \tag{3.36}$$

where $\omega_i \in [0, 2\pi]$ and $z_i \in [-1, 1]$ [144, 162]. In terms of the canonical coordinates, the three-dimensional spin vectors can be written as

$$\mathbf{S}_i = \begin{pmatrix} \sqrt{1-z_i^2}\,\cos(\omega_i) \\ \sqrt{1-z_i^2}\,\sin(\omega_i) \\ z_i \end{pmatrix}\,. \tag{3.37}$$

Since the choice of these coordinates is not unique, other types can be found in, e.g.,

Refs. [161, 163]. In terms of the set of canonical coordinates, the canonical equations of motion are given by [162]

$$\frac{\mathrm{d}}{\mathrm{d}t} z_i = \left\{ z_i, H^{(1\mathrm{d})}_{\mathrm{xxz}}(\omega, z) \right\} = -\frac{\partial}{\partial \omega_i} H^{(1\mathrm{d})}_{\mathrm{xxz}} \,, \tag{3.38a}$$

$$\frac{\mathrm{d}}{\mathrm{d}t} \omega_i = \left\{ \omega_i, H^{(1\mathrm{d})}_{\mathrm{xxz}}(\omega, z) \right\} = \frac{\partial}{\partial z_i} H^{(1\mathrm{d})}_{\mathrm{xxz}} \,. \tag{3.38b}$$

To close this section, it is worth emphasizing that the symmetries described in Sec. 3.1.3 remain valid also in the domain of classical spins. Moreover, the infinite-temperature density-density correlation function can be obtained in the classical case by taking $\langle \bullet \rangle$ from the quantum domain [cf. Eq. (3.5)] as an average over classical trajectories in phase space,

$$C(t) \approx \frac{1}{R} \sum_r \varrho_r(t)\, \varrho_r(0) \,, \tag{3.39}$$

where the initial configuration $\varrho_r(0)$ is drawn randomly for each realization and R is chosen large (i.e. $R \gg 1$), to reduce statistical fluctuations.

3.3. Remarks on Integrability

This section is dedicated as a brief overview of *integrability* in both, the classical and quantum domain. It is worth pointing out that this section should not be understood as an all-encompassing introduction to integrability, instead this section remarks on some aspects of integrability in both domains.

3.3.1. Classical Integrability

In the context of classical mechanics, integrability is described in terms of so-called *Liouville integrability* [51]. Following Liouville integrability, a classical Hamiltonian system is considered *integrable* if it has as many independent conserved quantities (integrals of motion), $\boldsymbol{Q} = (Q_1, Q_2, \ldots, Q_s)$, in involution, as degrees of freedom s,

$$\{Q_i, Q_j\} = \{Q_i, H\} = 0 \,, \quad \text{for} \quad i, j = 1, \ldots, s \,, \tag{3.40}$$

where $H = H(\mathbf{q}, \mathbf{p})$ denotes the Hamilton function depending on the generalized coordinates $\mathbf{q} = (q_1, q_2, \ldots, q_s)$ and momenta $\mathbf{p} = (p_1, p_2, \ldots, p_s)$ (see Sec. 1). As a result, the Liouville-Arnold theorem [51] implies that Hamilton's equations of motion [cf. Eq. (1.3)] are solvable by *quadratures*, which refers to the fact that the resulting differential equations can be solved explicitly by exploiting action-angle variables [51]. The solutions of the corresponding differential equations therefore exhibit (quasi-) periodic windings on so-called *invariant tori* [51, 58], embedded into the $2s$-dimensional phase space Γ [51]. Based on that, *integrable* classical models are often known to exhibit *nonchaotic (regular)* dynamics [38, 79]. Contrasted to integrable systems are so-called *nonintegrable* systems, which can exhibit *chaotic* dynamics. In this context, a diagnostic tool to identify classical chaos refers to the *exponential sensitivity* of phase space trajectories to infinitesimal perturbations on some initial conditions of the system. In other words, chaotic dynamics can occur if phase space trajectories that are initially close to each other, diverge exponentially

fast from each other in the course of time [57]. A quantity that reflects the sensitivity of phase space trajectories is the so-called *Lyapunov exponent* Λ [57, 164]. This exponent essentially evaluates the (exponential) distance of two points in time and enables to identify (most likely) chaotic dynamics [162, 165]. Classical systems that retain a strictly positive Lyapunov exponent ($\Lambda > 0$), are known as *chaotic* systems. In this sense, Lyapunov exponents serve as a quantity to distinguish between integrable and nonintegrable systems.

In the context of the classical XXZ spin chain, generalized coordinates (and momenta) have been established in Sec. 3.2. Furthermore, Hamilton's equations of motion, governing the time evolution of classical spin variables, have been presented in Eq. (3.34), and form a set of coupled differential equations, which are *nonintegrable* by means of the Liouville-Arnold theorem [51, 165]. Therefore, only for trivial initial conditions analytical solutions are possible [145]. Thus, the one-dimensional classical XXZ chain exhibits chaotic dynamics [164].

3.3.2. Bethe Ansatz methods

While in the classical domain integrability is defined precisely according to the Liouville integrability (as previously explained), a commonly accepted definition of integrability in the quantum domain is absent and still a subject of debates nowadays [56]. Reasons for that are manifold but can essentially be traced back to the fact that both the Liouville-Arnold theorem and the notion of chaos, as used to define integrability in the classical domain, cannot straightforwardly be transferred to the quantum domain. This is caused by the linearity of the Schrödinger equation, which implies that exponentially deviating trajectories for the wave functions can not occur [38]. Thus, the tools to distinguish integrable (nonchaotic) from nonintegrable (chaotic) classical systems, such as Lyapunov exponents become somehow meaningless in the quantum domain [38, 166].

To begin with, in the thermodynamic limit, for any quantum system described by a Hamiltonian $\mathcal{H}$, an infinite set of mutually commuting operators can be found, which additionally commute with the Hamiltonian [167] (for example consider projection operators $\mathcal{P} \equiv |n\rangle \langle n|$ on individual eigenstates $|n\rangle$ of the Hamiltonian). This definition alone is not sufficient. There is still an infinite number of conserved quantities required that are "nontrivial".

A commonly used notion of quantum integrable models is related to the *"exact solvability"* of quantum models. In this sense, a specific subclass of quantum integrable models is related to quantum models that are solvable in terms of so-called *Bethe ansatz techniques* [61, 63, 168]. Although the study of Bethe ansatz methods is not a central element of this thesis, it is worth commenting briefly on such techniques.

Bethe ansatz techniques do not have to resort to perturbation methods to determine physical properties of, for example, strongly interacting quantum systems. Instead, for the application of Bethe ansatz methods, no further approximations or assumptions are needed. Physical properties can be computed exactly.

In essence, the main idea of Bethe ansatz techniques is that the exact energy eigenstates can essentially be written in terms of scattering states of quasi-particles [63], that is, the eigenstates can be characterized by a set of quantum numbers corresponding to quasi-particles, which represent fundamental excitations of the model under consideration. This gives direct access to the energy spectrum of the respective model and, in addition, its thermodynamic properties [81]. Within the so-called *coordinate Bethe ansatz* [61, 69, 169] the many-body wave function can be constructed, and the problem of determining the

spectrum of the model's Hamiltonian $\mathcal{H}$ is reduced to solve a set of nonlinear coupled algebraic equations [62]. These equations are known as the *Bethe ansatz equations* and give rise to complex numbers $\{\lambda_i\}$, parametrizing the eigenstates. This leads to a substantial reduction of the problem's complexity. To be more precise, the complexity is mitigated from exponential to polynomial [62].

Another, more modern approach of Bethe ansatz techniques is related to the so-called *algebraic Bethe ansatz* [67], which is part of the *quantum inverse scattering method* [69]. This method essentially combines Bethe ansatz techniques and classical inverse scattering transforms [170], which is related to solving classical integrable partial differential equations [171]. In this context, systems are considered integrable if they fulfil the so-called *Yang-Baxter equation* [71, 72], which provides direct access to conservation laws and certain correlation functions [69] based on transfer- and $\mathcal{R}$-matrix-methods [81].

Paradigmatic one-dimensional lattice quantum models, which have been solved exactly by Bethe ansatz methods are both, the XXX chain [61] and the XXZ chain for arbitrary Δ [66], as well as the Fermi-Hubbard chain [62].

3.3.3. Energy Level Statistics

A widely used diagnostic to identify integrability is based on spectral properties, namely the statistics of *energy level spacings* [122, 172, 173]. To be more precise, the quantity of interest is the probability distribution $P(s)$ of energy level spacings $s = E_{m+1} - E_m$ (normalized to the average level spacing) of consecutive energy eigenvalues E_{m+1} and E_m for an ordered set of eigenvalues $E_1 < E_2 \cdots < E_{\mathcal{D}}$. These distributions exhibit distinct shapes, where the exact shape essentially depends on the integrability or nonintegrability of the model.

In essence, the energy levels of *integrable* quantum systems are expected to be independent from each other, and follow the so-called *Poissonian distribution* [73, 74, 166] given by

$$P_{\mathrm{P}}(s) = \mathrm{e}^{-s}\,. \tag{3.41}$$

In contrast, for *nonintegrable (chaotic)* quantum systems (obeying time-reversal property), the energy levels follow a *Wigner-Dyson distribution* $P_{\mathrm{WD}}(s)$, as predicted by the theory of random matrices [172–174]. This distribution is given by

$$P_{\mathrm{WD}}(s) = \frac{\pi s}{2}\mathrm{e}^{-\pi s^2/4}\,. \tag{3.42}$$

A crucial difference between the two distributions (3.41) and (3.42) mentioned above is rooted in the different behavior in the limit $s \to 0$. On the one hand the eigenvalues of nonintegrable (chaotic) systems have the characteristic of *level repulsion*, i.e. $P_{\mathrm{WD}}(s) \to 0$ for $s \to 0$. On the other hand in the case of integrable systems, level repulsion does not exist and crossings are not prohibited. This can be further used as an a diagnostic of quantum nonintegrable (chaotic) systems.

With regard to the (integrable) one-dimensional quantum XXZ spin-1/2 model, it has been shown that the level distribution $P(s)$ follows a Poisson distribution. By adding an additional integrability-breaking term (for example an additional anisotropy parameter $\Delta' \neq 0$), the model has been shown to cross over to a Wigner-Dyson distribution [166, 175].

Apart from investigating the probability distribution itself, a further (dimensionless) quantity to analyze the distribution is given by the *mean ratio of adjacent level spacings* [122, 123],

$$\langle r \rangle = \left\langle \frac{\min\{s_m, s_{m+1}\}}{\max\{s_m, s_{m+1}\}} \right\rangle = \frac{1}{K} \sum_m \frac{\min\{s_m, s_{m+1}\}}{\max\{s_m, s_{m+1}\}} \,, \tag{3.43}$$

where the average is examined over a subspace of the Hilbert space, with $K \approx \mathcal{D}$. On the one hand, Wigner-Dyson distributions exhibit a value of $\langle r \rangle_{\mathrm{WD}} \approx 0.53$, while on the other hand, a Poissonian distribution displays a value of $\langle r \rangle_{\mathrm{P}} \approx 0.39$ [122, 123]. In the context of disordered models (see Sec. 5), this quantity is revisited again.

4. Linear Response Theory and Transport

Sec. 4 deals with linear response theory (LRT), which can be used for spatially inhomogeneous nonequilibrium densities, based on Sec. 4.1. In addition, in Sec. 4.2, the dynamics of local densities are discussed for a specific nonequilibrium state. In this context, diffusion on one-dimensional lattices is described in Sec. 4.3. This section concludes with some remarks on dynamical response functions and the associated Kubo formula in Sec. 4.4.

4.1. Static Response to a Static Force

LRT can be regarded as a perturbative expansion of an equilibrium state of a physical system [5, 176]. While this Sec. is focussed on static responses for quantum systems, it is worth noting that the framework can be applied to classical systems as well.

As a kind of standard situation, a physical system is considered in a thermal equilibrium state. The aim is to evaluate the response of the system to an external perturbation. This perturbation can be static (i.e. constant in time) or dynamical (i.e. time dependent). Importantly, the perturbation is assumed to be small, such that it is reasonable to consider only terms being *linear* in the perturbation expansion.

Considering an unperturbed quantum system described by a Hamiltonian $\mathcal{H}_0$, which is affected by a perturbation (external force) $\mathcal{V}$, the Hamiltonian $\mathcal{H}_0$ is consequently extended by a perturbation-dependent part such that the total Hamiltonian $\mathcal{H}$ takes the form

$$\mathcal{H} = \mathcal{H}_0 + \lambda \mathcal{V} \,, \tag{4.1}$$

where λ is a constant and denotes the overall strength of the perturbation. Further, another operator $\mathcal{O}$ and its expectation value in response to the applied perturbation is considered. Following LRT [5, 177], a linear relation between the small external perturbation and the subsequent response of the system results in the expectation value $\langle \Delta \mathcal{O} \rangle$. The difference is denoted by

$$\langle \Delta \mathcal{O} \rangle = \langle \mathcal{O} \rangle_\lambda - \langle \mathcal{O} \rangle_0 \,, \tag{4.2}$$

with the expectation values

$$\langle \mathcal{O} \rangle_\lambda = \mathrm{tr}\left[\rho_\lambda \mathcal{O}\right] \quad \text{and} \quad \langle \mathcal{O} \rangle_0 = \mathrm{tr}\left[\rho_0 \mathcal{O}\right] \,, \tag{4.3}$$

where $\langle \mathcal{O} \rangle_\lambda$ ($\langle \mathcal{O} \rangle_0$) denotes the expectation value of the operator $\mathcal{O}$ in the presence (absence) of the applied external field in Eq. (4.1). The corresponding density matrices,

ρ_λ and ρ_0, read

$$\rho_0 = \frac{\mathrm{e}^{-\beta\mathcal{H}_0}}{\mathrm{tr}\left[\mathrm{e}^{-\beta\mathcal{H}_0}\right]}\,, \tag{4.4a}$$

$$\rho_\lambda = \frac{\mathrm{e}^{-\beta\mathcal{H}}}{\mathrm{tr}\left[\mathrm{e}^{-\beta\mathcal{H}}\right]} = \frac{\mathrm{e}^{-\beta(\mathcal{H}_0+\lambda\mathcal{V})}}{\mathrm{tr}\left[\mathrm{e}^{-\beta(\mathcal{H}_0+\lambda\mathcal{V})}\right]}\,, \tag{4.4b}$$

where ρ_λ refers to the total Hamiltonian $\mathcal{H}$ given in Eq. (4.1), while ρ_0 refers to the unperturbed part $\mathcal{H}_0$. To evaluate the expression given in (4.2), a useful formula for exponentiating two arbitrary noncommuting operators $\mathcal{A}$ and $\mathcal{B}$ is given by [5]

$$\mathrm{e}^{-\beta(\mathcal{A}+\mathcal{B})} = \mathrm{e}^{-\beta\,\mathcal{A}}\left[\mathbb{1} - \int_0^\beta \mathrm{e}^{\eta\mathcal{A}}\,\mathcal{B}\,\mathrm{e}^{-\eta(\mathcal{A}+\mathcal{B})}\,\mathrm{d}\eta\right]\,, \tag{4.5}$$

which can be shown by multiplying both sides by $\exp\left(-\beta\,\mathcal{A}\right)$ and subsequently taking the derivative with respect to β. Assuming $\mathcal{B}$ to be small, the exponential term $\exp\left(-\eta(\mathcal{A}+\mathcal{B})\right)$ in Eq. (4.5) can be replaced by $\exp\left(-\eta\mathcal{A}\right)$ within the integral. As a result, the density matrix ρ_λ in Eq. (4.4b) is written in linear order of λ as

$$\frac{\mathrm{e}^{-\beta(\mathcal{H}_0+\lambda\mathcal{V})}}{\mathrm{tr}\left[\mathrm{e}^{-\beta(\mathcal{H}_0+\lambda\mathcal{V})}\right]} = \rho_0\left[\mathbb{1} - \lambda\int_0^\beta \mathrm{d}\eta\,\mathrm{e}^{\eta\mathcal{H}_0}\,\Delta\mathcal{V}\,\mathrm{e}^{-\eta\mathcal{H}_0} + \lambda^2\ldots\right]\,, \tag{4.6}$$

with $\Delta\mathcal{V} = \mathcal{V} - \langle\mathcal{V}\rangle_0$ and by exploiting Eq. (4.5). To proceed, bearing in mind that the perturbation is assumed to be small, the expectation value $\langle\Delta\mathcal{O}\rangle$ depends linearly on the perturbation. As a consequence, the difference according to the expectation value reads

$$\langle\Delta\mathcal{O}\rangle = \langle\mathcal{O}\rangle_\lambda - \langle\mathcal{O}\rangle_0 \equiv \chi\,\lambda\,, \tag{4.7}$$

where the linear response constant χ denotes the static isothermal susceptibility [5, 81]. The difference in Eq. (4.7) can further be rewritten in terms of the *Kubo correlation function* [5, 178], which is defined for two operators $\mathcal{A}'$ and $\mathcal{B}'$ as

$$\mathcal{K}_{\mathcal{A}'\mathcal{B}'}(t) \equiv \frac{1}{\beta}\int_0^\beta \langle\mathcal{A}'\,\mathcal{B}'(t+\imath\eta)\rangle\,\mathrm{d}\eta\,. \tag{4.8}$$

where the brackets $\langle\bullet\rangle$ represent the canonical ensemble average $\langle\bullet\rangle = \mathrm{tr}\left[\rho_\beta\,\bullet\right]$, with $\rho_\beta = \exp\left(-\beta\mathcal{H}\right)/\mathcal{Z}_\beta$. Notably, in the case of formally infinite temperature (i.e. $\beta \to 0$), the Kubo correlation function turns into a standard correlation function [5, 81],

$$\mathcal{K}_{\mathcal{A}'\mathcal{B}'}(t) \to \langle\mathcal{A}'\,\mathcal{B}'(t)\rangle\,. \tag{4.9}$$

According to the Kubo correlation function, the static isothermal susceptibility χ can be rewritten as

$$\chi = \beta\,\mathcal{K}_{\Delta\mathcal{O}\Delta\mathcal{V}}(0)\,, \tag{4.10}$$

where $\mathcal{K}_{\Delta\mathcal{O}\Delta\mathcal{V}}(0)$ denotes the Kubo correlation function (4.8) at $t = 0$.

4.2. Dynamics of Local Densities

The dynamics of local densities can result in response to a static force, as previously explained. To this end, the dynamics of time-dependent expectation values at lattice site i can be studied. A common approach to studying transport is to investigate the dynamics of local densities. To this end, an initial state can be prepared as a *nonequilibrium state* $\rho \neq \rho_{\mathrm{eq}}$. Subsequently, the dynamics of the expectation values of such local densities are investigated [81]. To be more precise, consider the deviation of the local densities ϱ_i from their average at equilibrium $\langle \varrho_i \rangle_{\mathrm{eq}}$, that is,

$$\Delta \varrho_i = \varrho_i - \langle \varrho_i \rangle_{\mathrm{eq}} \,, \tag{4.11}$$

and examine the dynamics of expectation values [81, 179]

$$\langle \Delta \varrho_i(t) \rangle = \mathrm{tr}\left[\rho(t)\, \Delta \varrho_i\right] \,, \tag{4.12}$$

where the density matrix $\rho(t)$ evolves unitarily in time according to $\rho(t) = \mathrm{e}^{-\imath \mathcal{H} t}\, \rho(0)\, \mathrm{e}^{\imath \mathcal{H} t}$ (see Sec. 2.2.1). To relate LRT to the dynamics of local densities, the system is affected by a static force, in correspondence to Sec. 4.1. To proceed, consider the following initial state ρ, which is sufficiently close to the equilibrium state ρ_{eq} [81],

$$\rho = \frac{\mathrm{e}^{-\beta\left(\mathcal{H}_0 - \lambda \sum_i f_i\, \varrho_i\right)}}{\mathcal{Z}_\lambda} \,, \tag{4.13}$$

where, again, the overall strength of the static perturbation is denoted by λ and the operator $\mathcal{V}$ has been replaced by $\sum_i f_i\, \varrho_i$. Moreover, the partition function is denoted by $\mathcal{Z}_\lambda = \mathrm{tr}\left[\exp\left(-\beta(\mathcal{H}_0 - \lambda \sum_i f_i\, \varrho_i)\right)\right]$. Following Eq. (4.6), the density matrix (4.13) can be expanded in λ as

$$\rho = \rho_{\mathrm{eq}} \left(\mathbb{1} + \lambda \int_0^\beta \mathrm{d}\eta \sum_i f_i\, \mathrm{e}^{\eta \mathcal{H}_0}\, \Delta \varrho_i\, \mathrm{e}^{-\eta \mathcal{H}_0} + \lambda^2 \cdots \right) . \tag{4.14}$$

Given the assumption that the parameter λ is small, the expansion can be truncated to linear order. Thus, the expectation values $\langle \Delta \varrho_i(t) \rangle$ can be written as

$$\langle \Delta \varrho_i(t) \rangle = \lambda\, \beta \sum_j f_j\, \mathcal{K}_{\Delta \varrho_j \Delta \varrho_i}(t) \,, \tag{4.15}$$

with $\mathcal{K}_{\Delta \varrho_j \Delta \varrho_i}(t)$ being the Kubo correlation function, given in Eq. (4.8).

4.3. Diffusion in Lattice Systems

Possible types of transport can range from no transport at all (insulator) to ballistic transport which corresponds to ideal conduction. In between there may exist diffusion as well as anomalous diffusion, that is, subdiffusion and superdiffusion.

On a one-dimensional lattice, the dynamics of $\langle \Delta \varrho_i(t) \rangle$ are said to be diffusive if they obey a *discrete diffusion equation* of the form [180, 181]

$$\frac{\mathrm{d}}{\mathrm{d}t} \langle \Delta \varrho_i(t) \rangle = D_{\mathrm{diff}} \left[\langle \Delta \varrho_{i-1}(t) \rangle - 2 \langle \Delta \varrho_i(t) \rangle + \langle \Delta \varrho_{i+1}(t) \rangle \right] \,, \tag{4.16}$$

where D_{diff} is the time- and space-independent diffusion coefficient [81]. The lattice diffusion equation (4.16) is related to the continuous diffusion equation with the Laplace operator $\nabla^2 = \sum_i \partial^2/\partial x_i^2$ [81]. For instance, by applying a finite difference approximation to the Laplace operator, the lattice diffusion equation can be derived. Of course, by discretizing the Laplace operator, a lattice diffusion equation can be deduced for higher spatial dimensions $d > 1$. Nevertheless, the one-dimensional lattice diffusion equation is considered here. From a physical point of view, diffusion of a physical observable is a statistical relaxation process in which an initially nonequilibrium distribution spreads out through the system over time [81].

For the lattice diffusion equation (4.16), a specific solution for an initial local injection at lattice site j, provided by $\langle \Delta\varrho_{i=j}(0)\rangle \neq 0$ and $\langle \Delta\varrho_{i\neq j}(0)\rangle = 0$, is given by [81, 175]

$$\langle \Delta\varrho_i(t)\rangle = \exp\left(-2D_{\text{diff}}\, t\right)\, B_{(i-j)}(2D_{\text{diff}}\, t)\,, \tag{4.17}$$

where $B_{(i-j)}(t)$ denotes the modified Bessel function of first kind and of order $(i-j)$ [81]. The lattice solution (4.17) can be well approximated by the corresponding continuum solution [81]

$$\langle \Delta\varrho_i(t)\rangle = \frac{1}{\sqrt{2\pi}\Sigma(t)} \exp\left[-\frac{(i-j)^2}{2\Sigma^2(t)}\right]. \tag{4.18}$$

That is, for diffusive behavior, the initial density peak is broadens in time, while the Gaussian form is maintained over time. The width of the Gaussian in Eq. (4.18) corresponds to the spatial variance for some inhomogeneous density distribution that can be obtained by

$$\Sigma^2(t) = \sum_i i^2 \langle \Delta\varrho_i(t)\rangle - \left[\sum_i i\, \langle \Delta\varrho_i(t)\rangle\right]^2, \tag{4.19}$$

with the normalization condition $\sum_i \Delta\varrho_i(t) = 1$. As a first signature of diffusive transport, the temporal growth of the spatial variance $\Sigma^2(t)$ can be investigated [81, 182]. If the dynamics are diffusive for all times, the spatial variance (4.19) satisfies the following relation [179]:

$$\frac{\mathrm{d}}{\mathrm{d}t}\Sigma^2(t) = 2D_{\text{diff}}\,. \tag{4.20}$$

Finally, consider the specific initial state ρ in Eq. (4.13), with the coefficients $f_{i=j} \neq 0$ and $f_{i\neq j} = 0$. If λ is small, the expectation values can be written in terms of the Kubo correlation function as [81]

$$\langle \Delta\varrho_i(t)\rangle \propto \lambda\beta \mathcal{K}_{\Delta\varrho_j \Delta\varrho_i}(t)\,, \tag{4.21}$$

where D_{diff} again denotes a time- and space-independent diffusion coefficient as given in Eq. (4.16). For this thesis the most important quantity is the correlation function of local densities at formally infinite temperature (see Sec. 2.4), given by

$$C_{i,j}(t) = \langle \varrho_i(t)\, \varrho_j\rangle\,, \tag{4.22}$$

which turns into the equal-site correlation function $C(t) = C_{i,i}(t)$ due to the choice of periodic boundary conditions. In this context, the emergence of hydrodynamics reflects itself in terms of a power-law tail [81], that is,

$$C(t) \propto t^{-\alpha} \,. \tag{4.23}$$

In particular, in the case of normal diffusive transport on one-dimensional lattices, combining Eqs. (4.18) and (4.20) leads to a distinct power-law decay,

$$C(t) \propto t^{-1/2} \,. \tag{4.24}$$

To address higher lattice dimensions $d > 1$ (see Fig. 3.1), the exponent becomes explicitly dimension-dependent, that is, $\alpha \to \alpha(d)$. In this context, while $\alpha = d/2$ corresponds to normal diffusive transport, which is caused by an extension of Eq. (4.18) to d dimensions, two other cases are given by an exponent $\alpha < d/2$ (subdiffusion) and $\alpha > d/2$ (superdiffusion). Moreover, ballistic transport is indicated by $\alpha = d$. Notably, equal-site correlation functions are discussed in greater detail in e.g., Pt. III, Sec. A - Sec. C.

Although it is not a central part of the present thesis, for the sake of completeness, diffusion in the space of lattice momenta is briefly discussed. To this end, the lattice Fourier transformation of $\langle \Delta\varrho_i(t) \rangle$ in one dimension leads to the representation in momentum space,

$$\langle \Delta\varrho_q(t) \rangle = \frac{1}{\sqrt{N}} \sum_i \mathrm{e}^{\imath q i} \, \langle \Delta\varrho_i(t) \rangle \,, \tag{4.25}$$

with the (discrete) lattice momenta $q = 2\pi k/N$, where k runs from $k = 0, \ldots, (N-1)$. Inserting the preceding equation into the lattice diffusion equation in real space [cf. Eq. (4.16)] leads to the diffusion equation in momentum space [81],

$$\frac{\mathrm{d}}{\mathrm{d}t} \langle \Delta\varrho_q(t) \rangle = -\tilde{q}^2 D_{\mathrm{diff}} \, \langle \Delta\varrho_q(t) \rangle \,, \tag{4.26}$$

with the abbreviation $\tilde{q}^2 = 2 - 2\cos(q)$. Notably, in the limit of sufficiently small values of q, the approximation $\tilde{q}^2 \approx q^2$ holds. The solution of the diffusion equation in momentum space yields

$$\langle \Delta\varrho_q(t) \rangle \propto \exp\left(-\tilde{q}^2 D_{\mathrm{diff}} \, t \right) \,. \tag{4.27}$$

A further Fourier transformation from the time domain to the frequency domain,

$$\langle \Delta\varrho_q(\omega) \rangle = \int_0^\infty \mathrm{e}^{\imath\omega t} \, \langle \Delta\varrho_q(t) \rangle \, \mathrm{d}t \,, \tag{4.28}$$

provides information about the structure factors, which are not explicated here. Further information can be found in Ref. [81].

4.4. Remarks on the Kubo Formula

Returning to the variance $\Sigma^2(t)$ given in Eq. (4.19), its scaling behavior provides information about the overall width of the density profile discussed above. In particular, with a scaling according to $\Sigma(t) \propto t^\alpha$, the following cases can be distinguished: (*i*) *ballistic* transport

corresponds to $\alpha = 1$, (*ii*) $1/2 < \alpha < 1$ indicates *superdiffusive* transport, (*iii*) $\alpha = 1/2$ is called *diffusive*, (*iv*) $0 < \alpha < 1/2$ *subdiffusive*, and (*v*) $\alpha = 0$ is related to *insulating*.

Within the framework of LRT, the spatial variance $\Sigma^2(t)$ can be related to autocorrelation functions of currents. The relation can be deduced if the initial state ρ is "close enough" to the equilibrium state ρ_{eq} (see Sec. 4.1). Following Sec. 4.1, and considering the initial state given in Eq. (4.13), the spatial width is described by [179, 183, 184]

$$\frac{\mathrm{d}}{\mathrm{d}t}\Sigma^2(t) = 2\, D_{\text{diff}}(t)\,, \tag{4.29}$$

where the diffusion coefficient becomes time dependent (in contrast to Eq. (4.20), where the diffusion coefficient is time independent). The time-dependent diffusion coefficient $D_{\text{diff}}(t)$ is related to the Kubo correlation function [cf. Eq. (4.8)] according to [81]

$$D_{\text{diff}}(t) = \frac{\beta}{\chi}\int_0^t \mathcal{K}_{\mathcal{J}^{(\mathcal{Q})}\mathcal{J}^{(\mathcal{Q})}}(t')\,\mathrm{d}t'\,. \tag{4.30}$$

Considering the limit of formally infinite temperature, the preceding equation reduces to

$$D_{\text{diff}}(t) = \frac{\beta}{\chi\, N}\int_0^t \langle \mathcal{J}^{(\mathcal{Q})}(t')\mathcal{J}^{(\mathcal{Q})}\rangle\,\mathrm{d}t'\,, \tag{4.31}$$

where χ again denotes the static susceptibility, N is the system size and $\langle \mathcal{J}^{(\mathcal{Q})}(t)\mathcal{J}^{(\mathcal{Q})}\rangle$ represents a current-current correlation function [179] for the total current $\mathcal{J}^{(\mathcal{Q})}(t)$ of some conserved quantity $\mathcal{Q}$. The total current is defined as the sum of local currents $j_i^{(\mathcal{Q})}(t)$, that is,

$$\mathcal{J}^{(\mathcal{Q})}(t) = \sum_i j_i^{(\mathcal{Q})}(t)\,, \tag{4.32}$$

at lattice sites i. Thus, within the framework of LRT [5], nonequilibrium properties of some physical system are explicitly related to correlation functions, evaluated in equilibrium. In this context, transport coefficients can be obtained in terms of such correlation functions, via the so-called *Kubo formula* [5, 81].

Although it is not a central part of this thesis, it is worth noting that the definition of the local current $j_i^{(\mathcal{Q})}$ follows from the requirement that such local currents fulfil a *lattice continuity equation* [78]. By combining the continuity equation with Heisenberg's equation of motion (see Sec. 2.3.1), an explicit form of the local (and total) currents can be deduced. For detailed information on currents, see, e.g., Ref. [81]. Instead of dealing with the scaling behavior of the variance $\Sigma^2(t)$, one can consider the time-dependent diffusion coefficient $D_{\text{diff}}(t)$ to gain insights into different types of transport and, moreover, into the respective time scales [81].

5. Disordered Systems

This section is dedicated to disordered systems. In particular, as a paradigmatic model, the disordered one-dimensional Heisenberg spin model is presented in Sec. 5.1. Moreover, Sec. 5.2 remarks on both equilibration and thermalization. In this context, the eigenstate thermalization hypothesis, which essentially describes a microscopic mechanism of thermalization in quantum systems, is discussed. Finally, Sec. 5.3 discusses the temporal behavior of the correlation function.

5.1. Paradigmatic Model for Many-Body Localization

The one-dimensional anisotropic Heisenberg model, which has been presented in Sec. 3.1.2, is extended by an additional parameter that gives rise to *disorder* in the model. The Hamiltonian of this model reads

$$\mathcal{H}_{\mathrm{W}} = J \sum_i \left(S_i^x S_{i+1}^x + S_i^y S_{i+1}^y + \Delta S_i^z S_{i+1}^z \right) + \sum_i h_i S_i^z \,, \tag{5.1}$$

where h_i denotes *on-site* magnetic fields, which are randomly drawn from a uniform distribution, $h_i \in [-W, W]$, where $W \geq 0$ sets the overall magnitude of disorder. Importantly, for the special case of $S = 1/2$, through a Jordan-Wigner transformation (see Sec. 3.1.4), the Hamiltonian from (5.1) can be mapped onto a one-dimensional model of interacting spinless fermions in a random on-site potential μ_i. The Hamiltonian then reads

$$\mathcal{H}_{\mathrm{JW}} = J \sum_i \left[\frac{1}{2} \left(c_i^\dagger c_{i+1} + c_{i+1}^\dagger c_i \right) + V \sum_i \left(n_i - \frac{1}{2} \right) \left(n_{i+1} - \frac{1}{2} \right) \right] + \sum_i \mu_i \left(n_i - \frac{1}{2} \right) , \tag{5.2}$$

where n_i represents the occupation number operator, given by $n_i = c_i^\dagger c_i$, in full analogy to Sec. 3.1.4. For the special case of vanishing disorder ($W = 0$) the model is integrable in terms of Bethe ansatz methods (see Sec. 3.3), while for $W \neq 0$, the model is nonintegrable. Comparing (5.1) to (5.2), it becomes apparent that the parameter Δ has been substituted by $V = \Delta$ and denotes, in the context of Hamiltonian (5.2), the strength of particle-particle interactions between neighboring sites. Moreover, the on-site potentials $\mu_i = h_i$ are also drawn randomly from a uniform distribution in the interval $\mu_i \in [-W, W]$. The conservation of total magnetization with respect to the spin Hamiltonian (5.1) corresponds to the conservation of the total number of particles in the model (5.2).

While the most commonly studied distribution of disorder is the one considered here, it is worth noting that a frequently investigated distribution is the quasi-periodic distribution, given by $h_i = |W| \cos(2\pi p i)$, where p denotes an irrational number. Such a distribution provides the study of the so-called Aubry-André model [185].
Returning to the Hamiltonian (5.2), for vanishing interaction strength $V = 0$, the model

turns into a model of noninteracting fermions in a random potential, which essentially leads to the *Anderson localization* [47, 119]. In what follows, the issue of Anderson localization in one-dimensional systems is considered briefly. For the limiting case of vanishing disorder ($W \to 0$), the Hamiltonian (5.2) features lattice solutions in terms of Bloch states (plane waves) [186]. In contrast, for a nonvanishing magnitude of disorder $W \neq 0$, wave functions become localized around a region i' and decay exponentially away from that region, such that the overall shape of the wave function scales as $\propto \exp\left(-|i - i'|/\xi_{\mathrm{loc}}\right)$, where ξ_{loc} denotes the localization length. As becomes apparent, the eigenstates are not distributed over the entire space but, instead, are exponentially bounded to individual areas of the system.

A natural extension of the topic of Anderson localization is the subject of *many-body localization* (MBL) (for reviews, see Refs. [48, 50, 187]). Like Anderson localization, the phenomenon of many-body localization is based on the presence of disorder in the model but with an additional nonzero interaction term. In this context, the model described by the Hamiltonian (5.1) with $\Delta = 1$ and $S = 1/2$ (or its Jordan-Wigner transformed version (5.2)) has become an archetypal model to study MBL [123, 126, 188–193]. This model is believed to undergo a transition from an ergodic (thermal) phase at small to intermediate disorder ($W < W_*$) into a nonergodic (localized) phase at strong disorder ($W > W_*$) at a critical disorder strength $W_* \approx 3.5$ (see, e.g., Refs. [123, 126]). Notably, larger values have also been found [194, 195].

At sufficiently low disorder, the eigenstates satisfy the eigenstate thermalization hypothesis (ETH). In contrast, the localized phase is characterized, for example, by a breakdown of the ETH, therefore, thermalization does not occur [38, 187]. The situation is schematically illustrated in Fig. 5.1. Moreover, the phenomenology of the localized phase can be understood in terms of an emergent set of local integrals of motion [49, 120, 121, 196].

Although many-body localization is a subject of exhaustive theoretical [46, 123, 126, 197–199] and experimental [13, 200, 201] investigations, several aspects of a putative MBL phase transition are not yet fully understood or are still under discussion [202]. Moreover, the existence of genuine MBL has been questioned [203, 204].

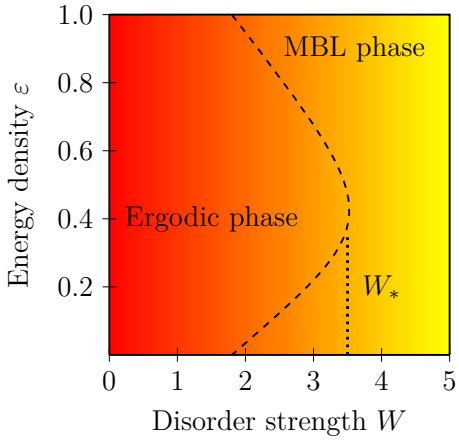

Figure 5.1.: Schematic illustration of the phase diagram of the disordered Heisenberg chain, that is, Hamiltonian (5.1) with $\Delta = 1$. The ergodic phase is separated from the localized phase. The horizontal axis represents the total magnitude of the disorder strength W while, vertically, some energy density ε is shown. The illustration is based on [126].

A common method used to distinguish the ergodic from the localized phase is based on *spectral statistics* (see Sec. 3.3). It has been found that in the ergodic phase, the probability distribution $P(s)$ of adjacent level spacings s follows a Wigner-Dyson distribution $P_{\mathrm{WD}}(s)$. In contrast, the localized phase is characterized by level statistics following a Poissonian distribution $P_{\mathrm{P}}(s)$. In this context, it is instructive to consider the ratio of consecutive level spacings [122, 123]. The average $\langle r \rangle$ changes from an ergodic phase ($\langle r \rangle_{\mathrm{WD}} \approx 0.54$ [123]) to a localized phase ($\langle r \rangle_{\mathrm{P}} \approx 0.39$ [123]). Therefore, the value of $\langle r \rangle$ provides one way to distinguish the ergodic from the localized phase.

5.2. Remarks on Equilibration and Thermalization

5.2.1. Equilibration

The process of *equilibration* refers the question of whether and how an isolated system, which has been initially prepared at a nonequilibrium expectation value of some observable and subsequently evolves unitarily in time, reaches a (stable) value [205] and remains close to this value for almost all times [39, 206]. Whether a system reaches a stable value for long times depends on the precise details of the underlying model (for instance, initial state properties or the respective Hamiltonian).

To describe equilibration in quantum many-body systems, consider an isolated system, described by a Hamiltonian $\mathcal{H}$. Initially, the quantum system is assumed to be prepared in a pure state $|\psi(0)\rangle$. Following Sec. 2.1.2, the initial state $|\psi(0)\rangle$ can be evolved in time by applying the unitary time-evolution operator $\mathcal{U}(t)$ according to the Schrödinger representation,

$$|\psi(t)\rangle = \mathrm{e}^{-\imath \mathcal{H} t} \, |\psi(0)\rangle = \sum_n c_n \, \mathrm{e}^{-\imath E_n t} \, |n\rangle \ , \tag{5.3}$$

where, again, $\{|n\rangle\}$ denotes a set of energy eigenstates of $\mathcal{H}$ with the associated eigenvalues $\{E_n\}$, and the complex expansion coefficients are given by $c_n = \langle n|\psi(0)\rangle$. Recall that the probability w_n of finding the quantum system in a given quantum eigenstate $|n\rangle$, given by $w_n = |c_n|^2$, is entirely determined by the initial states. Moreover, the initial state $|\psi(0)\rangle$ has an average energy $\bar{E} = \langle \psi(0)|\mathcal{H}|\psi(0)\rangle = \sum_n |c_n|^2 \, E_n$, with the eigenvalues $\{E_n\}$ and *energy fluctuations* δE

$$\delta E = \sqrt{\langle \psi(0)|\mathcal{H}^2|\psi(0)\rangle - \langle \psi(0)|\mathcal{H}|\psi(0)\rangle} = \sqrt{\langle \psi(0)|\mathcal{H}^2|\psi(0)\rangle - \bar{E}^2} \, . \tag{5.4}$$

Following Sec. 2.1.2, the expectation value $\langle \mathcal{O}(t)\rangle$ for some given observable $\mathcal{O}$ can be written in terms of energy eigenstates $\{|n\rangle\}$,

$$\langle \mathcal{O}(t)\rangle = \sum_n |c_n|^2 \, \mathcal{O}_{nn} + \sum_{m \neq n} c_m^* c_n \, \mathrm{e}^{\imath (E_m - E_n) t} \, \mathcal{O}_{mn} \, , \tag{5.5}$$

with the matrix elements $\mathcal{O}_{mn} = \langle m|\mathcal{O}|n\rangle$ in the eigenbasis of $\mathcal{H}$. In the context of the equilibration process, one conceptually determines the *long-time average* $\overline{\mathcal{O}}$ of the expectation value [39, 207],

$$\overline{\mathcal{O}} \equiv \lim_{\tau \to \infty} \frac{1}{\tau} \int_0^\tau \langle \mathcal{O}(t)\rangle \, \mathrm{d}t = \lim_{\tau \to \infty} \frac{1}{\tau} \int_0^\tau \langle \psi(t)|\mathcal{O}|\psi(t)\rangle \, \mathrm{d}t \, , \tag{5.6}$$

where the average is determined over the interval $[0, \tau]$, followed by a subsequent normalization to the length of the interval. Inserting Eq. (5.5) into Eq. (5.6) leads to

$$\overline{\mathcal{O}} = \lim_{\tau\to\infty} \frac{1}{\tau} \int_0^\tau \left(\sum_n |c_n|^2 \, \mathcal{O}_{nn} + \sum_{m\neq n} c_m^* c_n \, \mathrm{e}^{\imath(E_m - E_n)t} \, \mathcal{O}_{mn} \right) \mathrm{d}t \,. \tag{5.7}$$

By performing this integral explicitly and taking the limit of long times, $\tau \to \infty$, it becomes apparent that the off-diagonal matrix elements $\mathcal{O}_{mn}$ average out over time due to oscillations with different frequencies (assuming the absence of degeneracies in the energy spectrum). The diagonal part remains time independent by integrating over t. As a result, the long-time average of the expectation value finally becomes

$$\overline{\mathcal{O}} = \sum_n |c_n|^2 \, \mathcal{O}_{nn} = \mathrm{tr}\left[\rho_{\mathrm{diag}} \, \mathcal{O}\right] = \langle \mathcal{O} \rangle_{\mathrm{diag}} \,, \tag{5.8}$$

where ρ_{diag} denotes the density matrix of the so-called *diagonal ensemble* [44]. In other words, the density matrix is diagonal in the energy eigenbasis. This density matrix is explicitly given by

$$\rho_{\mathrm{diag}} = \sum_n |c_n|^2 \, |n\rangle \, \langle n| \,. \tag{5.9}$$

Thus, ρ_{diag} contains information on the initial state in terms of $|c_n|^2$. If the expectation value of $\mathcal{O}$ stays close to its long-time average, the observable $\mathcal{O}$ is said to *equilibrate*.

5.2.2. Thermalization

From a perspective of classical mechanics, the concept of *thermalization* is related to the *ergodicity hypothesis* [54, 55], which essentially states that trajectories can get arbitrarily close to any point of the phase space for long times [45, 118]. Such a notion of thermalization cannot straightforwardly be transferred to the quantum domain because the description of quantum systems is based on Hilbert spaces, where the dynamics is unitary in terms of the Schrödinger equation. Thus, the notion of trajectories in phase space is "meaningless" in a sense [38].

To describe thermalization processes at the level of (individual) eigenstates of quantum systems, a revealing framework is based on the *eigenstate thermalization hypothesis* (ETH) [38, 42–44, 48]. This hypothesis implies that the expectation values of local observables in isolated quantum systems converge to time-independent values, represented in terms of textbook statistical mechanics ensembles [44]. With regard to Eqs. (5.7) and (5.8), it becomes apparent that the initial state is distinctly defined by $|c_n|^2$. To ensure that a thermal expectation value is reached by a local observable, the long-time value $\overline{\mathcal{O}}$ in Eq. (5.9) has to coincide with the expectation value of the observables in the microcanonical ensemble $\mathcal{O}_{\mathrm{mc}}$ at the corresponding energy density,

$$\mathcal{O}_{\mathrm{mc}} = \frac{1}{\mathcal{N}_{\bar{E}}} \sum_m \mathcal{O}_{mm} \,, \tag{5.10}$$

where the normalization factor $\mathcal{N}_{\bar{E}}$ is the number of eigenstates $|m\rangle$ within the energy window $\left[\bar{E} - \delta E, \bar{E} + \delta E\right]$. If the system *thermalizes*, the long-time average (value) $\overline{\mathcal{O}}$ has to coincide with the expectation value of the microcanonical ensemble $\mathcal{O}_{\mathrm{mc}}$ [cf. Eq. (5.10)].

The ETH can be formulated for the matrix elements $\mathcal{O}_{mn} = \langle m|\mathcal{O}|n\rangle$ of a local observable $\mathcal{O}$ in the energy eigenbasis of $\mathcal{H}$ according to the ansatz [207, 208]

$$\mathcal{O}_{mn} = g_{\mathcal{O}}(\bar{E})\,\delta_{mn} + \mathrm{e}^{-S(\bar{E})/2}\, f_{\mathcal{O}}(\bar{E},\omega)\, R_{mn}\,, \tag{5.11}$$

where $|n\rangle$ and $|m\rangle$ are again eigenstates of the Hamiltonian $\mathcal{H}$, the average value of the energy is denoted by $\bar{E} = (E_m + E_n)/2$ and $\omega = E_m - E_n$ represents the energy difference. Moreover, $S(\bar{E})$ denotes the thermodynamic entropy, evaluated at energy $\bar{E}$. The functions $g_{\mathcal{O}}(\bar{E})$ and $f_{\mathcal{O}}(\bar{E},\omega)$ are smooth functions of their arguments [209, 210] and especially the function $g_{\mathcal{O}}(\bar{E})$ coincides with the expectation value of the microcanonical ensemble at energy $\bar{E}$, that is, $\mathcal{O}_{\mathrm{mc}}(\bar{E})$ [38, 211, 212]. The second term in Eq. (5.11) implies that the off-diagonal matrix elements are exponentially small in system size (since the entropy is an extensive quantity). The generally complex random numbers $R_{mn}(= R^*_{nm})$ are drawn from a Gaussian distribution with zero mean and unit variance, that is, $\overline{R^2_{mn}} = 1$ for real-valued random numbers and $\overline{|R_{mn}|^2} = 1$ for complex numbers.

Moreover, since the diagonal matrix elements are smooth functions of their arguments, the term $\mathcal{O}_{mm}$ in Eq. (5.8) can be written in front of the sum, implying $\overline{\mathcal{O}} = \mathcal{O}_{\mathrm{mc}}$, provided by the normalization condition $\sum_n |c_n|^2 = 1$ [38].

Finally, by exploiting the ETH ansatz (5.11), the fluctuations $\sigma^2_{\mathcal{O}}$ of the dynamics of $\langle\mathcal{O}(t)\rangle$ around the long-time average can be obtained as [38]

$$\begin{aligned}
\sigma^2_{\mathcal{O}} &= \lim_{\tau\to\infty}\frac{1}{\tau}\int_0^\tau \left[\langle\mathcal{O}(t)\rangle^2 - \overline{\mathcal{O}}^2\right]\mathrm{d}t \\
&= \lim_{\tau\to\infty}\frac{1}{\tau}\int_0^\tau \mathrm{d}t \sum_{m\neq n}\sum_{p\neq q}\left[\mathcal{O}_{mn}\mathcal{O}_{pq}c^*_m c_n c^*_p c_q\ \mathrm{e}^{\imath[(E_m-E_n)-(E_q-E_p)]t} - \overline{\mathcal{O}}^2\right] \\
&= \sum_{m,n\neq m}|c_m|^2\,|c_n|^2\,|\mathcal{O}_{mn}|^2 \leq \max|\mathcal{O}_{mn}|^2\sum_{m,n}|c_m|^2\,|c_n|^2 = \max|\mathcal{O}_{mn}|^2 \propto \mathrm{e}^{-S(\bar{E})}\,,
\end{aligned} \tag{5.12}$$

which essentially implies that the fluctuations of the expectation value $\langle\mathcal{O}(t)\rangle$ are exponentially small in system size, since $\exp(-S(\bar{E}))$ typically increases exponentially in system size.

While it has been demonstrated that an ansatz as given in Eq. (5.11) is sufficient to guarantee the occurrence of thermalization [207], it remains unknown whether this ansatz is also a necessary condition for thermalization to occur [38]. It is worth noting that although a rigorous mathematical proof for ETH is currently missing, ETH has been verified numerically in many nonintegrable quantum models [36, 38, 44, 166, 209, 213–217].

A class of systems that fails to thermalize and, therefore, does not fulfil the ETH ansatz (5.11) are *integrable* systems, which possess an extensive set of nontrivial conserved quantities. This is caused by the fact that under unitary time evolution, integrable systems do not lose their memory of the initial states for all times [218, 219]. Therefore, such conserved quantities can prevent the system from thermalizing [36, 214, 220, 221], which has been observed experimentally as well (see, e.g., Ref. [8]). Another class of systems that violate the ETH are *disordered systems*, which are believed to exhibit a transition between a thermal (ergodic) phase for low to intermediate disorder to a many-body localized (nonergodic) phase for strong disorder (see Sec. 5.1). While the ETH holds in the thermal phase, it breaks down in the many-body localized phase [48, 50, 222].

5.3. Transport of Densities

To study the transport of local densities in the presence of disorder, the "bare" equal-site correlation function considered in Sec. 4.2 has to be modified, since the results depend on the individual configuration of the randomly drawn magnetic fields h_i. In this context, the central quantity of interest is the *disorder-averaged* correlation function $\overline{C(t)}$ evaluated at formally infinite temperature ($\beta \to 0$),

$$\overline{C(t)} = \frac{1}{M_h} \sum_{h=1}^{M_h} C(t)\,, \tag{5.13}$$

where the "bare" correlation function $C(t)$ is calculated for different configurations of the randomly drawn magnetic fields h_i, and M_h represents a large number of independent realizations. The correlation function $\overline{C(t)}$ is expected to exhibit a power-law decay,

$$\overline{C(t)} \propto t^{-\alpha}\,, \tag{5.14}$$

where the exponent α enables the identification of different types of transport (see Sec. 4.3). In the ergodic phase, the correlation function (5.13) is expected to show slower hydrodynamic behavior, which manifests itself in a power-law decay with $\alpha < 1/2$. In one-dimensional systems, an exponent of $\alpha = 1/2$ in Eq. (5.14) refers to conventional diffusive transport. In particular, for the disordered one-dimensional Heisenberg spin model with $S = 1/2$, there is some numerical evidence for the occurrence of subdiffusive transport in the regime of low to intermediate disorder below the localization transition [129, 223–230]. The subdiffusive regime is reflected by an anomalously slow relaxation of the correlation function $\overline{C(t)}$ with an exponent of $\alpha < 1/2$. While subdiffusive transport is suggested even at very small disorder [227, 230], a transition to normal diffusion is stated in Ref. [223, 224] at moderate disorder. For much longer times, the correlation function will approach a constant saturation value which scales as $\propto 1/N$ [231], where N denotes the system size.

In contrast, the decay of the correlation function is significantly slower in the localized phase compared to the ergodic regime. At long times, the correlation function $\overline{C(t)}$ reaches a nonzero value [193, 232] (or for a *finite* system $> 1/N$). Such a saturation value at long times indicates that the system retains information about the initial conditions [226]. In that sense, the correlation function $\overline{C(t)}$ can be used as a probe for the many-body localized phase transition [233]. Moreover, in the case of classical spins, strong disorder has been demonstrated to cause a drastic reduction of transport coefficients and anomalously slow relaxation [104, 131]. Nevertheless, for classical spin models, the occurrence of genuine MBL is not expected [104, 234].

Additionally, in the context of disordered models, a frequently considered quantity is the *self-averaging* property [235, 236] of a disordered system. The self-averaging property refers to the fact that by increasing the system size N, increasingly fewer disorder realizations are needed to correctly represent the ensemble. With respect to the correlation function, the system is called self-averaging [236] if the ratio between the variance and square of mean value vanishes as the system size increases. The relative variance $R(t)$ of sample-to-sample

fluctuations is given by [236, 237]

$$R(t) = \frac{\overline{C(t)^2} - \overline{C(t)}^2}{\overline{C(t)}^2} \,. \tag{5.15}$$

To test whether the correlation function is self-averaging, not only in equilibrium but over the entire time evolution of $C(t)$, the relative variance is time dependent. In general, to capture various types of self-averaging, the asymptotic dependence of the relative variance $R(t)$, displayed by [235]

$$R(t) \propto N^{-\nu} \,, \tag{5.16}$$

is considered. In this context, a system is said to be (i) nonself-averaging if $R(t)$ becomes constant ($\nu = 0$) in the limit $N \to \infty$ and (ii) self-averaging if $R(t)$ decays to zero for $N \to \infty$ [235]. Beyond this distinction, self-averaging systems are further categorized into weak and strong self-averaging systems. While the latter case is associated with an exponent $\nu = 1$, weak self-averaging goes along with a slower power-law decay ($0 < \nu < 1$).

The issues discussed in this section are continued in Pt. (III), where Eqs. (5.15) and (5.16) become crucial in studying the self-averaging property of the disordered Heisenberg model from Sec. 5.1.

6. Numerical Approaches to Quantum Many-Body Systems

Sec. 6 is dedicated to present numerical approaches to the study of quantum many-body systems. To this end, Sec. 6.1 deals with exact diagonalization, while the ensuing section presents the Lanczos method. Following the concept of typicality, Sec. 6.2 outlines the numerical approach of dynamical quantum typicality. In that context, the propagation of pure states is presented in Sec. 6.3 by means of (*i*) the fourth-order Runge-Kutta method, (*ii*) the Suzuki-Trotter decomposition and (*iii*) Chebyshev polynomials. To conclude, Sec. 6.4 deals with the numerical linked cluster expansion.

It is worth mentioning that the numerical approaches presented within this section are not all-encompassing by any means. There exist significantly more numerical methods to study quantum many-body systems, for example, density matrix renormalization group techniques and relatives [134, 135]. These are not considered in this thesis.

6.1. Exact Diagonalization

Numerical approaches that aim to solve (at least partially) eigenvalue equations (eigenvalue problems) up to machine accuracy refer to so-called *exact diagonalization* (ED) methods. In this context, the most intuitive and at the same time most memory- and time-consuming approach is known as *full diagonalization*. Moreover, for cases where merely the properties of ground states (low-lying eigenstates) of the physical system are of interest, *iterative* diagonalization approaches provide results with almost machine precision in many cases.

6.1.1. Full Diagonalization

The numerical method of *full diagonalization* [132, 157, 238] is presumably the most intuitive approach to tackle quantum many-body systems numerically. The basic idea of full diagonalization is to represent the system's Hamiltonian $\mathcal{H}$ as a matrix, which has subsequently to be diagonalized. The full diagonalization of $\mathcal{H}$ provides the knowledge of the entire (energy) spectrum $\{E_n\}$ and the corresponding set of eigenstates $\{|n\rangle\}$. This enables, in principle, the calculation of all static and dynamic properties of a quantum many-body system.

Usual full diagonalization routines determine the (energy) eigenvalues and eigenstates explicitly by calculating the roots of the characteristic polynomial $\mathcal{P}(E_n)$ of degree D, and subsequently obtaining the corresponding eigenstates by solving the resulting system of linear equations numerically. Due to the potentially huge complexity of the characteristic polynomial for large matrices (notably, there exists no exact solution for $D > 4$ [239]), most full diagonalization routines use the approach of generating iteratively a unitary transformation U that diagonalizes the Hamiltonian matrix by

$$\mathcal{H} \to U^\dagger \, \mathcal{H} \, U \, . \tag{6.1}$$

More general, the strategy is to construct the matrix U iteratively by

$$\mathcal{H} \to U_1^\dagger \, \mathcal{H} \, U_1 \to U_2^\dagger \, U_1^\dagger \, \mathcal{H} \, U_1 \, U_2 \to \cdots \,, \tag{6.2}$$

until the matrix takes on a diagonal form, where the columns of the matrix $U = U_1 \, U_2 \, U_3 \, \cdots$ contain the eigenstates of the Hamiltonian $\mathcal{H}$.

In practice, the method of full diagonalization is restricted to rather small system sizes, due to the exponential growth of the Hilbert-space dimension $\mathcal{D}$. For example, for a spin-1/2 system the Hilbert-space dimension is $\mathcal{D} = 2^N$ for N lattice sites. Thus, the associated Hamiltonian matrix is $(2^N \times 2^N)$-dimensional, which has to be diagonalized numerically. This fact poses a major problem for full diagonalization routines due to the huge computational effort and memory requirements. Even for not too large system sizes, the memory requirements eventually become prohibitive. To reduce memory requirements, model-dependent symmetries can be exploited to transform the Hamiltonian matrix into a block-diagonal form (see, e.g., Ref. [157]). The resulting blocks belong to (spin) states with different conserved quantum numbers which are associated with the symmetries (see Sec. 3.1.3). As becomes apparent, the advantage of exploiting symmetries is that each of the blocks can be diagonalized separately, leading to a substantial reduction of the computational effort.

For the sake of illustration, consider the numerical calculation of density-density-correlation functions (i.e. $\langle \varrho_i(t) \varrho_i \rangle$). To apply full diagonalization, the main idea is to expand the correlation function in terms of the Hamiltonian's eigenstates $\{|n\rangle\}$ and the corresponding eigenvalues $\{E_n\}$ [cf. Eq. (2.47)],

$$\langle \varrho_i(t) \varrho_i \rangle = \frac{\mathrm{tr}\left[\mathrm{e}^{-\beta\mathcal{H}} \varrho_i(t) \varrho_i\right]}{\mathcal{Z}_\beta} = \sum_{n,m} \frac{\mathrm{e}^{-\beta E_n}}{\mathcal{Z}_\beta} \, |\langle n|\varrho_i|m\rangle|^2 \, \mathrm{e}^{\imath(E_n - E_m)t} \,, \tag{6.3}$$

where the partition function $\mathcal{Z}_\beta$ is written as $\mathcal{Z}_\beta = \sum_n \exp(-\beta E_n)$. It is worth pointing out that in particular for disordered systems (see Sec. 5), exact (full) diagonalization becomes rather costly already for $N \approx 14$ lattice sites [231]. This is essentially based on two arguments: (*i*) the translational invariance is broken due to the presence of disorder-perturbing terms and (*ii*) it has to be averaged over a large number of instances of random potentials [231]. Because only systems with rather small lattice sizes can be treated, it is difficult to describe physical quantities correctly in the thermodynamics limit (i.e. $N \to \infty$).

Nevertheless, despite the computational limitations, exact diagonalization routines are not useless by any means, at least for checking results calculated by alternative sophisticated numerical techniques. It is worth commenting briefly on some system sizes which have been reached by exact (full) diagonalization for the one-dimensional Heisenberg spin-1/2 model. By exploiting translational invariance (see Sec. 3.1.3), the one-dimensional Heisenberg spin-1/2 Hamiltonian has been numerically diagonalized for a system size of $N \approx 20$ lattice sites [157]. A previous study [240] has accessed $N \approx 24$ lattice sites by using exact diagonalization for the same spin model.

6.1.2. Lanczos Method

The *Lanczos method* [241] is essentially an iterative diagonalization method and is commonly used to study quantum many-body systems. This method is particularly appropriate if only the system's ground states and low-lying excited states are of interest. The central

idea of the Lanczos method is to construct a special basis, in which the Hamiltonian $\mathcal{H}$ has tridiagonal structure. Once having generated this matrix representation of $\mathcal{H}$, the ground state can be computed by standard numerical recipes. The corresponding tridiagonal matrix is determined iteratively. For this purpose, consider an arbitrary normalized vector, say $|u_0\rangle$ with $||u_0|| = 1$, which is represented in the many-body basis $|n\rangle$ of the system. The only condition imposed on this vector is that it is not orthogonal to the ground state of the Hamiltonian. That means that the overlap of the actual system's ground state $|\psi_0\rangle$ and the initially chosen vector $|u_0\rangle$ has to be nonzero. This condition is most likely fulfilled if the entries of the initial vector $|u_0\rangle$ are drawn at random.

Next, the vector $|u_1\rangle$ is constructed. This vector is determined by applying the Hamiltonian $\mathcal{H}$ to the initial state $|u_0\rangle$ and subtracting the projection onto the initial vector, which results in

$$|u_1\rangle = \mathcal{H}\,|u_0\rangle - \frac{\langle u_0|\mathcal{H}|u_0\rangle}{\langle u_0|u_0\rangle}\,|u_0\rangle\ , \tag{6.4}$$

and obeys the orthogonality condition, $\langle u_0|u_1\rangle = 0$. Moreover, another vector is constructed according to

$$|u_2\rangle = \mathcal{H}\,|u_1\rangle - \frac{\langle u_1|\mathcal{H}|u_1\rangle}{\langle u_1|u_1\rangle}\,|u_1\rangle - \frac{\langle u_1|u_1\rangle}{\langle u_0|u_0\rangle}\,|u_0\rangle\ , \tag{6.5}$$

which also satisfies the orthogonality condition, that is, $\langle u_1|u_2\rangle = \langle u_0|u_2\rangle = 0$. A generalization of this scheme can be achieved by defining an orthogonal basis recursively,

$$|u_{n+1}\rangle = \mathcal{H}\,|u_n\rangle - a_n\,|u_n\rangle - b_n^2\,|u_{n-1}\rangle\ , \tag{6.6}$$

where the coefficients a_n and b_n are explicitly given by

$$a_n = \frac{\langle u_n|\mathcal{H}|u_n\rangle}{\langle u_n|u_n\rangle} \quad \text{and} \quad b_n^2 = \frac{\langle u_n|u_n\rangle}{\langle u_{n-1}|u_{n-1}\rangle}\,, \tag{6.7}$$

with $b_0 = 0$ and $|u_{-1}\rangle = 0$. The Hamiltonian matrix $\mathcal{H}$ can subsequently be written in the following tridiagonal matrix [157]

$$\mathcal{H}'_n = \begin{pmatrix} a_0 & b_1 & 0 & 0 & \dots & 0 \\ b_1 & a_1 & b_2 & 0 & \dots & 0 \\ 0 & b_2 & a_2 & b_3 & 0 & 0 \\ 0 & 0 & \ddots & \ddots & \ddots & \vdots \\ \vdots & \vdots & \vdots & \ddots & \ddots & b_n \\ 0 & \dots & \dots & 0 & b_n & a_n \end{pmatrix}\,, \tag{6.8}$$

which can be diagonalized by standard numerical methods [242]. The diagonalization of $\mathcal{H}'_n$ provides the eigenvalues $\{E_0, E_1, \dots, E_n\}$ and eigenstates $\{|\psi_0\rangle, |\psi_1\rangle, \dots, |\psi_n\rangle\}$, formulated in the basis of Lanczos basis vectors $|u_n\rangle$. Upon increasing the recursion number, the eigenvalues of the matrix $\mathcal{H}'_n$ converge to those of the genuine Hamiltonian matrix $\mathcal{H}$ and its eigenstates are eventually expanded in terms of the Lanczos basis vectors $|u_n\rangle$. To acquire the desired eigenstates in the genuine many-body basis $|n\rangle$, a basis

transformation can be performed as follows

$$|\psi_m\rangle = \sum_{n,j} c_j \langle n|u_j\rangle \, |n\rangle = \sum_j c_j \, |u_j\rangle \ . \tag{6.9}$$

The main advantage of the Lanczos method relies on the fact that the matrix $\mathcal{H}'_n$ can be generated by a rather small number of iterations, particularly if the matrix is given as a sparse matrix and merely the non-zero matrix elements have to be examined. Especially, in situations when one is dealing with large matrices it is also advantageous that only three vectors $(|u_n\rangle\,, |u_{n-1}\rangle\,, |u_{n+1}\rangle)$ need to be stored at once [157].

6.2. Dynamical Quantum Typicality

The concept of *quantum typicality* [138, 139, 243] states that even a single pure quantum state, drawn at random from a high-dimensional Hilbert space, is sufficient to imitate the entire statistical ensemble. To be more precise, expectation values of typical pure states are close to the expectation value of the statistical ensemble [136–140, 244–247]. A detailed presentation of the concept of static and dynamical quantum typicality can be found in Refs. [137, 247]. For pragmatic purposes and as a numerical tool, the concept of dynamical quantum typicality essentially relies on replacing the trace over the entire many-body basis by a scalar product, which only contains a single (typical) pure state.

As a central quantity in this thesis, consider the density-density correlation function $C^{\beta}_{i,j}(t)$. The expectation value $\langle \varrho_i(t)\varrho_j\rangle$, encoded in the correlation function $C^{\beta}_{i,j}(t)$, can be rewritten by exploiting the the concept of typicality as [245, 248]

$$C^{\beta}_{i,j}(t) = \frac{\operatorname{tr}\left[\rho_\beta \, \varrho_i(t) \, \varrho_j\right]}{\mathcal{Z}_\beta} = \frac{\langle \psi_\beta(t)|\varrho_i|\varphi_\beta(t)\rangle}{\langle \psi_\beta(0)|\psi_\beta(0)\rangle} + \epsilon(|\psi\rangle)\,, \tag{6.10}$$

where the *auxiliary states*, $|\varphi_\beta(t)\rangle$ and $|\psi_\beta(t)\rangle$, can be time- and temperature-dependent. Explicitly, these states are given by

$$|\varphi_\beta(t)\rangle = \mathrm{e}^{-\imath\mathcal{H}t} \, \varrho_j \, \mathrm{e}^{-\beta\mathcal{H}/2} \, |\psi\rangle \ , \quad |\psi_\beta(t)\rangle = \mathrm{e}^{-\imath\mathcal{H}t} \, \mathrm{e}^{-\beta\mathcal{H}/2} \, |\psi\rangle \ , \tag{6.11}$$

for some Hamiltonian $\mathcal{H}$. The (reference) random pure state $|\psi\rangle$ from Eq. (6.10) is drawn from the unitarily invariant Haar measure [244],

$$|\psi\rangle = \sum_k c_k \, |k\rangle = \sum_k (a_k + \imath b_k) \, |k\rangle \ . \tag{6.12}$$

The coefficients a_k and b_k both are drawn randomly from a Gaussian probability distribution with zero mean and unit variance. In fact, other types of probability distributions have also been discussed [249, 250]. Moreover, the states $|k\rangle$ denote a complete set of orthogonal basis states spanning the Hilbert space $\mathscr{H}$ with dimension $\mathcal{D} = \dim(\mathscr{H})$. It is worth noting that these basis states can be any orthogonal basis, for example, the common eigenbasis of symmetries [81]. While the statistical error $\epsilon(|\psi\rangle)$ within the typicality approximation (6.10) depends on the specific realization of the random (pure) state $|\psi\rangle$, the standard deviation $\sigma(\epsilon)$ of the statistical error scales as $\sigma(\epsilon) \propto 1/\sqrt{\mathcal{D}_{\text{eff}}}$, with $\mathcal{D}_{\text{eff}}$ being the effective dimension $\mathcal{D}_{\text{eff}} = \operatorname{tr}\left[\exp\left(-\beta(\mathcal{H} - E_0)\right)\right]$ and E_0 denotes the ground-state energy of the Hamiltonian $\mathcal{H}$ [141, 251]. Importantly, in the limiting case of formally infinite temperature ($\beta \to 0$), the effective dimension $\mathcal{D}_{\text{eff}}$ converges to the Hilbert-space

dimension $\mathcal{D}$. As a consequence, increasing the number of degrees of freedom (e.g. the number of lattice sites N) of a certain quantum many-body system, leads to an exponential improvement of the accuracy and in the thermodynamic limit $N \to \infty$ the formal expression in Eq. (6.10) becomes exact.

A simplification is possible at the limit of formally infinite temperature ($\beta \to 0$). In this case the density-density correlation function $C_{i,j}(t)$ can be evaluated by means of just *one* auxiliary state $|\widetilde{\psi}(t)\rangle$ [252–255]. As a result, the density-density correlation function $C_{i,j}(t)$ can be rewritten in terms of $|\widetilde{\psi}(t)\rangle$ as,

$$C_{i,j}(t) = \langle \widetilde{\psi}(t) | \varrho_i | \widetilde{\psi}(t) \rangle + \epsilon(|\psi\rangle) \,, \tag{6.13}$$

where $|\psi\rangle$ denotes a (reference) random pure state as stated in Eq. (6.12) and it has been used that the trace of ϱ_i vanishes (i.e. $\mathrm{tr}\,[\varrho_i] = 0$) [92]. The initial state $|\widetilde{\psi}(0)\rangle$ is given by

$$|\widetilde{\psi}(0)\rangle = \frac{\sqrt{\varrho_j + \lambda}}{\sqrt{\langle \psi | \psi \rangle}} \, |\psi\rangle \;, \tag{6.14}$$

where the constant λ is chosen such that the term $(\varrho_j + \lambda)$ has nonnegative eigenvalues and the full time-dependent state is $|\widetilde{\psi}(t)\rangle = \exp\left(-\imath \mathcal{H} t\right) |\widetilde{\psi}(0)\rangle$. It is crucial, that the square root of the operator in Eq. (6.13) can be carried out. In the case of local magnetization (local S_i^z operators), the Ising basis can be chosen, where the basis states are depicted as follows $\{|\uparrow_1 \downarrow_2 \downarrow_3 \cdots\rangle \,, \, |\downarrow_1 \uparrow_2 \downarrow_3 \cdots\rangle \,, \, |\downarrow_1 \downarrow_2 \uparrow_3 \cdots\rangle \,, \cdots\}$. In the case of local energy, the task is feasible and requires a local basis transformation, involving a few lattice sites.

To conclude this section, the spatio-temporal correlation functions for both (local) spin and (local) energy densities have been determined for a quasi-one-dimensional two-leg ladder (with $S = 1/2$), for a total system size of up to $N = 20 \times 2$ lattice sites [90]. Moreover, in Ref. [R1] further (selected) applications of the concept of dynamical quantum typicality can be found. The reader is referred to Pt. III, Sec. A.

6.3. Pure-State Propagation

From a numerical point of view, the central advantage of the typicality-based approximations in Eqs. (6.10) and (6.13) relies on the fact that one can work with pure states instead of dealing with the full density matrices. The action of the matrix exponential can be effectively obtained without having to resort to exact diagonalization methods (see Sec. 6.1). This fact leads to a substantial reduction of the required computational resources, due to the possibility to generate time and temperature dependencies of pure states efficiently. The full time (and temperature) dependence emerges as a property of pure states and can therefore be evaluated by iteratively solving the Schrödinger equation in real and imaginary time, respectively [81, 247].

Apart from that, dynamical quantum typicality can be implemented rather memory efficiently, which ensures to study dynamical properties of quantum many-body systems with Hilbert-space dimensions significantly larger compared to standard exact diagonalization. Moreover, there are no conceptual limitations on the reachable time scales.

In particular, the full time evolution of the state $|\psi_\beta(0)\rangle$ given in Eq. (6.11) is generated

by the action of the matrix exponential on the initial state,

$$|\psi_\beta(t)\rangle = \mathrm{e}^{-\imath\mathcal{H}t}\,|\psi_\beta(0)\rangle\ . \tag{6.15}$$

The time evolution can be subdivided into a product of consecutive discrete time steps $\delta t = t/M$:

$$|\psi_\beta(t)\rangle = \mathrm{e}^{-\imath\mathcal{H}t}\,|\psi_\beta(0)\rangle = \left(\mathrm{e}^{-\imath\mathcal{H}\delta t}\right)^M |\psi_\beta(0)\rangle\ , \tag{6.16}$$

where the discrete time step δt is chosen sufficiently small. There exists a variety of numerical methods to accurately approximate the action of the matrix exponential $\exp\left(-\imath\mathcal{H}\delta t\right)$ without the necessity of exact diagonalization routines.

6.3.1. Fourth-Order Runge-Kutta Method

A rather straightforward numerical method is given by the *fourth-order Runge-Kutta* (RK4) *method* [256, 257]. According to the RK4 method, the time-evolution operator is approximated as [245, 258]

$$|\psi_\beta(t+\delta t)\rangle \approx |\psi_\beta(t)\rangle + \sum_n |k_n\rangle\ , \tag{6.17}$$

where the auxiliary states $|k_n\rangle$ are constructed as follows [245, 258]

$$|k_n\rangle = \frac{-\imath\mathcal{H}\delta t}{n}\,|k_{n-1}\rangle\ , \tag{6.18}$$

with $|k_0\rangle = |\psi_\beta(t)\rangle$ and the error of the approximation (6.17) scales as $\mathcal{O}(\delta t^5)$. Notably, the RK4 scheme in Eqs. (6.17) and (6.18) is equivalent to a Taylor expansion of the exponential $\exp\left(-\imath\mathcal{H}t\right)$ up to fourth order. Moreover, although it is not needed for the purposes of this thesis, in complete analogy to the (pure) state propagation in real time, a potential temperature dependence of the state $|\psi_\beta(t)\rangle$ can be generated by a time evolution in small imaginary time steps ($\imath\delta\beta$).

It is worth emphasizing that the RK4 method, has additionally been used to solve the classical (nonlinear) Hamilton's equations of motion for classical spin variables (see, Refs. [R2, R3]).

6.3.2. Suzuki-Trotter Decomposition

The *Suzuki-Trotter decomposition* is based on the decomposition of the (unitary) exponential operator, to generate unitary approximations to the matrix exponential [259]. To this end, consider the unitary time-evolution operator $\mathcal{U}(t,t_0) = \exp\left(-\imath\mathcal{H}(t-t_0)\right)$. For the sake of simplicity, t_0 is set to zero. Thus, by using Suzuki-Trotter product formula [260, 261], the time evolution-operator is essentially decomposed as

$$\mathcal{U}(t) = \mathrm{e}^{-\imath\mathcal{H}t} = \mathrm{e}^{-\imath(\mathcal{H}_1+\mathcal{H}_2+\ldots+\mathcal{H}_m)t} = \lim_{n\to\infty}\left(\prod_i \mathrm{e}^{\frac{-\imath t\mathcal{H}_i}{n}}\right)^n\ , \tag{6.19}$$

where the (total) Hamiltonian $\mathcal{H}$ is subdivided into a sum of "sub-Hamiltonians" $\mathcal{H}_i$, by $\mathcal{H} = \sum_i \mathcal{H}_i$. In practice, the right hand side of Eq. (6.19) is determined for a finite value

of n. In particular, the second-order approximation $\widetilde{\mathcal{U}}_2(\delta t)$ [262, 263] is given by

$$\widetilde{\mathcal{U}}_2(\delta t) = \mathrm{e}^{-\imath\delta t\mathcal{H}_i/2}\ldots\mathrm{e}^{-\imath\delta t\mathcal{H}_1/2}\mathrm{e}^{-\imath\delta t\mathcal{H}_1/2}\ldots\mathrm{e}^{-\imath\delta t\mathcal{H}_i/2}\,. \tag{6.20}$$

This approximation is bounded from above by [263]

$$\left\|\mathcal{U}(\delta t) - \widetilde{\mathcal{U}}_2(\delta t)\right\| \ll c\,\delta t^3\,, \tag{6.21}$$

where c is a positive constant. Another approximation that is useful in practice is the fourth- order approximation [262],

$$\mathcal{U}_4(\delta t) = \mathcal{U}_2(a\,\delta t)\,\mathcal{U}_2(a\,\delta t)\,\mathcal{U}_2((1-4a)\delta t)\,\mathcal{U}_2(a\,\delta t)\,\mathcal{U}_2(a\,\delta t)\,, \tag{6.22}$$

with the constant $a = 1/(4-4^{1/3})$ [263]. Similar to the bound of the second order approximation in Eq. (6.21), this approximation is bounded by

$$\left\|\mathcal{U}(\delta t) - \widetilde{\mathcal{U}}_4(\delta t)\right\| \ll c'\,\delta t^4\,, \tag{6.23}$$

with the constant $c' > 0$. For practical purposes and in the context of the one-dimensional Heisenberg spin-1/2 model (see Sec. 3.1.2), the Hamiltonian can be decomposed according to the so-called XYZ decomposition, where the Hamiltonian is subdivided into its spatial components x, y and z of the spin operators, this is,

$$\mathcal{H} = \sum_n \mathcal{H}^n = \mathcal{H}^x + \mathcal{H}^y + \mathcal{H}^z\,, \tag{6.24}$$

where the terms $\mathcal{H}^{x,y}$ and $\mathcal{H}^z$ are explicitly given by

$$\mathcal{H}^{x,y} = J\sum_i S_i^{x,y}S_{i+1}^{x,y} \quad \text{and} \quad \mathcal{H}^z = J\Delta\sum_i S_i^z S_{i+1}^z\,. \tag{6.25}$$

When choosing the eigenstates of S^z as the computational basis, the matrix representation of $\exp(-\imath\delta t\mathcal{H}^z)$ is diagonal. This leads to a phase shift when applying to a basis state. By choosing an efficient basis rotation (rotation matrix) into the eigenstates of the $S^{x,y}$ operators, the operators $\exp(-\imath\delta t\mathcal{H}^x)$ and $\exp(-\imath\delta t\mathcal{H}^y)$, respectively, act in the same way as $\exp(-\imath\delta t\mathcal{H}^z)$ [175, 263].

6.3.3. Chebyshev Polynomials

The *Chebyshev polynomial approach* is based on the numerical approximation of the matrix exponential by Chebyshev polynomials [259, 264–266]. Before considering explicitly the Chebyshev polynomials as a numerical approach, it is worth pointing out some remarks on the general scheme for expanding arbitrary functions in orthogonal polynomials.

To this end, consider two (integrable) real-valued functions $h(x)$ and $g(x)$. A scalar product on a finite interval $[a_1, a_2]$ is defined by

$$\langle h(x)|g(x)\rangle = \int_{a_1}^{a_2} h(x)\,g(x)\,w(x)\,\mathrm{d}x\,, \tag{6.26}$$

with $w(x)$ being the so-called weight function. There exists a complete set of some

polynomials $p_k(x)$ satisfying an orthogonality relation, namely

$$\langle p_k(x)|p_m(x)\rangle = \delta_{km}\,. \tag{6.27}$$

This fact implies that a given smooth and continuous function $h(x)$ can be expressed in a series of the polynomials $p_k(x)$ by

$$h(x) = \sum_k c_k\, p_k(x)\,, \tag{6.28}$$

where the expansion coefficients c_k are determined by $c_k = \langle p_k|h\rangle$. While in principle every class of orthogonal polynomials can be used for such an expansion, it turns out that especially the Chebyshev polynomials are very good for the vast majority of (physical) applications. The advantage of using Chebyshev polynomials relies on the fact that the associated series displays excellent convergence properties. To be more precise, the Chebyshev polynomials T_n of first kind are defined by the following recursion relation [267]

$$T_{n+1}(x) = 2xT_n(x) - T_{n-1}(x)\,, \tag{6.29}$$

supplemented by $T_0(x) = 1$ and $T_1(x) = x$. Following Eq. (6.26), on a closed interval $I = [-1, 1]$ the Chebyshev polynomials are orthogonal with respect to the following scalar product

$$\langle T_k(x)|T_l(x)\rangle = \frac{1}{\pi}\int_{-1}^{1} T_k(x)\,\cdot\, T_l(x)\,\frac{1}{\sqrt{1-x^2}}\,\mathrm{d}x = \frac{\delta_{kl}(1+\delta_{n0})}{2}\,. \tag{6.30}$$

A given function $r(x)$ on this interval can be expanded according to the Chebyshev polynomials as follows

$$r(x) = \left[\mu_0 + 2\sum_m \mu_m\, T_m(x)\right], \tag{6.31}$$

where the series has to be understood as an infinite series and the expansion coefficients (moments) μ_m are given by the integral

$$\mu_m = \int_{-1}^{1} r(x)\, T_m(x)\,\mathrm{d}x\,. \tag{6.32}$$

The method of Chebyshev polynomial expansion is essentially based on the Eqs. (6.31) and (6.32). While the Chebyshev polynomials are defined on a finite interval $I = [-1, 1]$, the physical quantities of interest are given in terms of eigenvalues E_n of a matrix, associated to a Hamiltonian $\mathcal{H}$. To adapt the (eigenvalue) spectrum to the interval I, a linear transformation (rescaling) is performed according to [267, 268]

$$\widetilde{\mathcal{H}} = \frac{1}{a}\left(\mathcal{H} - b\mathbb{1}\right)\,, \tag{6.33}$$

where the parameters a and b are given by

$$a = \frac{E_{\max} - E_{\min}}{2-\varepsilon}\,, \quad b = \frac{E_{\max} + E_{\min}}{2}\,, \tag{6.34}$$

with $E_{\min}$ ($E_{\max}$) representing the smallest (largest) energy eigenvalue of $\mathcal{H}$ and the factor

ε can be fixed [268]. Notably, E_{min} and E_{max} can be evaluated by means of Lanczos techniques (see Sec. 6.1.2).

As a result, the time evolution of a state $|\psi(t)\rangle$ (or more precisely, the time-evolution operator $\mathcal{U}(t)$) can be approximated in terms of Chebyshev polynomials by

$$\mathcal{U}(t) = \mathrm{e}^{-\imath(a\widetilde{\mathcal{H}}+b)t} = \mathrm{e}^{-\imath bt}\left[c_0 + 2\sum_k c_k\, T_k(\widetilde{\mathcal{H}})\right], \tag{6.35}$$

by using the rescaled Hamiltonian in Eq. (6.33). Moreover, the expansion coefficients c_k are evaluated by means of Eq. (6.32)

$$c_k = \frac{1}{\pi}\int_{-1}^{1} \frac{\mathrm{e}^{-\imath axt}\, T_k(x)}{\sqrt{1-x^2}}\,\mathrm{d}x = (-\imath)^k\, J_k(at)\,, \tag{6.36}$$

where $J_k(at)$ denotes the first kind Bessel function of order k [267], evaluated at (at). For practical purposes, the sum in Eq. (6.35) is truncated after a finite sequence of terms, such that an approximation for the time-evolution operator $\mathcal{U}(t)$ in k-th order reads as follows

$$\mathcal{U}(t)\,|\psi(0)\rangle \approx \mathcal{U}_k(t)\,|\psi(0)\rangle = c_0\,|w_0\rangle + 2\sum_k c_k\,|w_k(\widetilde{\mathcal{H}})\rangle\ . \tag{6.37}$$

The vectors $|w_k(\widetilde{\mathcal{H}})\rangle$ are given recursively by applying the rescaled Hamiltonian. By identifying the vector $|w_0\rangle$ with the initial state $|\psi(0)\rangle$ (i.e. $|w_0\rangle = |\psi(0)\rangle$), and $|w_1\rangle = \widetilde{\mathcal{H}}\,|w_0\rangle$, respectively, the other vectors are generated by a recursion relation

$$|w_{k+1}\rangle = 2\widetilde{\mathcal{H}}\,|w_k\rangle - |w_{k-1}\rangle\ , \tag{6.38}$$

for $k \geq 1$. In essence, the time evolution of the pure state $|\psi(t)\rangle$ is based on the evaluation of matrix-vector products, provided by Eqs. (6.37) and (6.38).

To conclude, it is worth noting that both Trotter decompositions (see Sec. 6.3.2) and Chebyshev polynomial expansions (see Sec. 6.3.3) are used in the massively parallelized simulations on the supercomputer "JUWELS" (at Forschungszentrum Jülich, Institute for Advanced Simulation (IAS), Jülich Supercomputing Centre (JSC)) in the context of Ref. [R2].

6.4. Numerical Linked Cluster Expansion

The main idea of *numerical linked cluster expansion* (NLCE) [142, 143, 269] is that the *per-site* value of an extensive quantity on an infinite lattice can be expanded in terms of respective weights on all linked (sub-)lattices that can be embedded in the entire lattice [270].

Here, particular emphasis is given to the physical applications of NLCE in the context of correlation functions in one-dimensional quantum systems. To this end, a NLCE scheme is essentially given by the following expression

$$\frac{\langle \mathcal{O}(t)\mathcal{O}\rangle}{N} = \sum_c \mathcal{L}_c W_c(t)\,, \tag{6.39}$$

where W_c denotes the weight of a cluster c with multiplicity $\mathcal{L}_c$. Moreover, the general operators $\mathcal{O}(t)$ can, for example, be chosen as the current operator [90]. To avoid redundant

computations, the multiplicity factor, which is divided by the total number of lattice sites, accounts for all clusters, which are symmetrically or topologically related to one representative cluster and, therefore, yield the same weight. The weight of each cluster is evaluated by the so-called *inclusion-exclusion principle*

$$W_c(t) = \langle \mathcal{O}(t)\mathcal{O} \rangle^{(c)} - \sum_{s \subset c} W_s(t)\,, \tag{6.40}$$

where the weights of all embedded clusters s are subtracted from $\langle \mathcal{O}(t)\mathcal{O} \rangle^{(c)}$ evaluated on the cluster c. Since the maximum treatable cluster size is limited by the available computational resources, the sum in Eq. (6.39) has to be truncated to a maximum size $C \equiv c_{\max}$. For one-dimensional models, this truncated sum reduces to the difference of the correlation functions of the two largest open-boundary chains with lengths C and $(C-1)$. The latter implies,

$$\sum_{c=2}^{C} W_c(t) = \langle \mathcal{O}(t)\mathcal{O} \rangle^{(C)} - \langle \mathcal{O}(t)\mathcal{O} \rangle^{(C-1)}\,. \tag{6.41}$$

As shown in Ref. [90], this rather simple formula can have a better convergence towards the thermodynamic limit than a standard finite-size scaling at effectively equal computational cost. For the one-dimensional Heisenberg spin-1/2 model the current-current autocorrelation function in the thermodynamic limit has been studied [90]. When studying thermodynamic quantities, using larger cluster sizes similarly improves the convergence of the expansion down to lower temperatures [143, 271]. The numerical method of NLCE is part of Ref. [R1], but will not be revisited again in Pt. III.

Part III.

Guide to Publications

7. Publications

The main purpose of Pt. III and Sec. 7 is to give an overview of the publications given in Refs. [R1–R3], and to outline the central results. To this end, Sec. A deals with several applications of the concept of dynamical quantum typicality to quantum many-body systems. Moreover, in Sec. B quantum and classical spin dynamics on various low-dimensional lattice geometries are presented and finally Sec. C deals with the question of the dynamics of quantum and classical spin chains subjected to random potentials (disorder).

A. Selected Applications of Typicality to Real-Time Dynamics of Quantum Many-Body Systems

Ref. [R1] is a review and deals with the versatility of a numerical approach, based on *dynamical quantum typicality* (DQT) (see Sec. 6.2). More precisely, in Ref. [R1] various applications of the concept of quantum typicality in the context of investigating the dynamics of quantum many-body systems are discussed.

In particular, in Ref. [R1] it is described how (*i*) pure states in combination with a forward propagation in real time can be used to determine the (local) density of states of some Hamiltonian $\mathcal{H}$ with eigenvalues E_n [141, 272], (*ii*) DQT provides an efficient means to obtain time-dependent equilibrium correlation functions for comparatively large Hilbert-space dimensions and long time scales and (*iii*) quantum typicality can be applied to study far-from-equilibrium dynamics. Moreover, DQT is discussed in combination with other (numerical) approaches, either (*iv*) to improve the convergence of the method of numerical linked cluster expansion (NLCE) (see Sec. 6.4) or (*v*) to obtain so-called memory kernels, which play a major role in the context of projection operator techniques [151, 273–275]. Because of the variety of applications given in Ref. [R1], a detailed description of the topics (*i*) and (*v*) is omitted here. Instead, this section focusses on the issues *(ii)* and *(iii)* in greater detail. Notably, the method of NLCE has already been described in Pt. II, Sec. 6.4.

To begin with, recall the central idea of the concept of quantum typicality (see Sec. 6.2). For practical applications, the notion of typicality states that the trace over the (many-body) basis can be replaced by a scalar product with respect to a single pure quantum state. This pure state can imitate the full statistical (quantum) ensemble. First, quantum typicality is considered in the context of time-dependent (equilibrium) correlation functions, which can occur within LRT. Such equilibrium correlation functions (see Sec. 2) are given by

$$C^{\beta}_{\mathcal{O}\mathcal{O}'}(t) = \langle \mathcal{O}(t)\mathcal{O}' \rangle = \mathrm{tr}\left[\rho_\beta\, \mathcal{O}(t)\, \mathcal{O}'\right] , \tag{7.1}$$

for operators $\mathcal{O}$ and $\mathcal{O}'$, where the time-dependent operator $\mathcal{O}(t)$ has to be understood with respect to the Heisenberg representation. The (canonical) density matrix at equilibrium is denoted by $\rho_\beta = \exp\left(-\beta\mathcal{H}\right)/\mathcal{Z}_\beta$ and the partition function $\mathcal{Z}_\beta$ is represented by

$\mathcal{Z}_\beta = \mathrm{tr}\left[\exp\left(-\beta\mathcal{H}\right)\right]$. Exploiting the concept of (quantum) typicality (see Sec. 6.2), it is demonstrated that Eq. (7.1) can be rewritten as

$$\langle\mathcal{O}(t)\mathcal{O}'\rangle = \frac{\langle\psi_\beta(t)|\mathcal{O}|\varphi_\beta(t)\rangle}{\langle\psi_\beta(0)|\psi_\beta(0)\rangle} + \epsilon(|\psi\rangle)\,, \tag{7.2}$$

where the trace $\mathrm{tr}\left[\bullet\right]$ from Eq. (7.1) is replaced by a scalar product $\langle\psi|\bullet|\psi\rangle$ of a pure quantum state $|\psi\rangle$. The reference pure state $|\psi\rangle$ is drawn from the unitarily invariant Haar measure and is given by

$$|\psi\rangle = \sum_k c_k\,|k\rangle = \sum_k (a_k + \imath b_k)\,|k\rangle\ , \tag{7.3}$$

where $|k\rangle$ denotes a set of orthogonal basis states of the $\mathcal{D}$-dimensional Hilbert space. The coefficients a_k and b_k are drawn from a Gaussian distribution with zero mean and unit variance and the standard deviation of the statistical error $\epsilon(|\psi\rangle)$ scales as $\sigma \propto 1/\sqrt{\mathcal{D}_{\mathrm{eff}}}$ with $\mathcal{D}_{\mathrm{eff}}$ being the effective Hilbert-space dimension (see Sec. 6.2). Moreover, the auxiliary states $|\varphi_\beta(t)\rangle$ and $|\psi_\beta(t)\rangle$ in Eq. (7.2) are explicitly represented by

$$|\varphi_\beta(t)\rangle = \mathrm{e}^{-\imath\mathcal{H}t}\,\mathcal{O}'\,\sqrt{\rho_\beta}\,|\psi\rangle \quad \text{and} \quad |\psi_\beta(t)\rangle = \mathrm{e}^{-\imath\mathcal{H}t}\sqrt{\rho_\beta}\,|\psi\rangle\ . \tag{7.4}$$

A main advantage of the typicality-based approach (7.2) relies on the fact that the operators $\mathcal{O}$ and $\mathcal{O}'$ do not longer carry any time (and temperature) dependence. Instead, the full time (and temperature) dependence emerges as a property of pure states and can be evaluated by iteratively solving the Schrödinger equation in real and imaginary time, respectively [81, 247]. From a numerical point of view, this is provided by several iterator schemes (see Sec. 6.3). As a result, on the one hand the potentially demanding numerical method of exact diagonalization (see Sec. 6.1) can be circumvented. On the other hand there is no need to store full matrices leading to substantially reduced computational requirements.

As a central quantity of interest in Ref. [R1] (and this thesis), time-dependent density-density correlation functions $C^\beta_{i,j}(t) = \langle\varrho_i(t)\varrho_j\rangle$ for some local density ϱ_i and ϱ_j, respectively, are discussed in the context of quantum typicality. The calculation of such correlation functions,

$$C^\beta_{i,j}(t) = \langle\varrho_i(t)\varrho_j\rangle = \mathrm{tr}\left[\rho_\beta\,\varrho_i(t)\varrho_j\right]\ , \tag{7.5}$$

substantially simplifies when considering the limit of formally infinite temperature (i.e. $\beta \to 0$). In this specific case the correlation function can be rewritten as,

$$C_{i,j}(t) = \langle\widetilde{\psi}(t)|\varrho_i|\widetilde{\psi}(t)\rangle + \epsilon(|\psi\rangle)\,, \tag{7.6}$$

where an initial pure state $|\widetilde{\psi}(t=0)\rangle = |\widetilde{\psi}(0)\rangle$ is given by

$$|\widetilde{\psi}(0)\rangle = \frac{\sqrt{\varrho_j + \lambda}}{\sqrt{\langle\psi|\psi\rangle}}\,|\psi\rangle\ , \tag{7.7}$$

with $|\psi\rangle$ being, again, drawn randomly and λ represents a constant, such that $(\varrho_j + \lambda)$ has nonnegative eigenvalues. As becomes apparent, it is possible to evaluate the density-density correlation function (7.6) just from *one* auxiliary state, while a calculation according to

Eq. (7.2) would include two auxiliary states that have to be evolved in time. As a special case of Eq. (7.6), the equal-site spin-spin correlation function,

$$C(t) = C_{i,i}(t) = \langle S_i^z(t) S_i^z \rangle \,, \tag{7.8}$$

at lattice site $i = N/2$ for the spin-1/2 XXZ chain is discussed in Ref. [R1]. Bear in mind that in this thesis the one-dimensional XXZ model has $N = L_x \times 1$ lattice sites in total (see Sec. 3).

In particular, the correlation function in (7.8) is considered for two different lengths, namely $N = 14$ and $N = 28$ (see Fig. 7.1). In this context, for two independently drawn pure states $|\psi_1\rangle$ and $|\psi_2\rangle$, the accuracy of the DQT approximation is demonstrated. With regard to Fig. 7.1, while the DQT data closely follows the results obtained from exact diagonalization at $N = 14$, the residual statistical fluctuations almost disappear completely for a system size of $N = 28$ lattice sites. While in Ref. [R1] it is only reported on the accuracy of the quantum typicality approach in the context of the equal-site correlation function for the XXZ chain, additional comparisons between data extracted from a DQT approach and exact ensemble averages are available (see, e.g., Refs. [217, 245]).

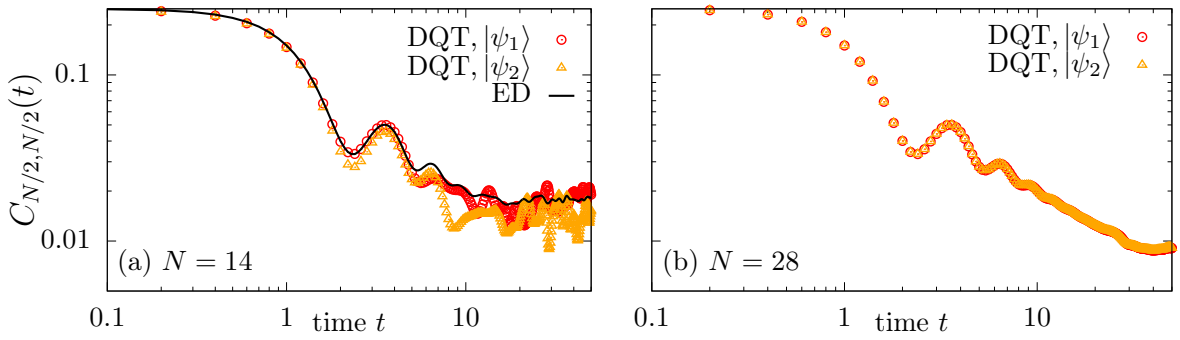

Figure 7.1.: Equal-site spin-spin correlation function $C_{N/2,N/2}(t)$ for the one-dimensional $S = 1/2$ XXZ chain for $\Delta = 1$ and with either (a) $N = 14$ and (b) $N = 28$ lattice sites in total. Full diagonalization data are compared to DQT data for two different random states $|\psi_1\rangle$ and $|\psi_2\rangle$ in (a). While full diagonalization becomes unfeasible for $N = 28$, the statistical fluctuations of the typicality approach become negligible for this system size. Data is adapted from Ref. [247].

In addition to the equal-site spin-spin correlation function (7.8), the full time-space profile $C_{i,j}(t) = \langle S_i^z(t) S_j^z \rangle$ at $j = N/2$ for a spin-1/2 chain with next-nearest neighbor interactions of length $N = 36$ is considered [175]. Especially for the local density of magnetization, and in the limit of formally infinite temperature ($\beta \to 0$) different lattice sites are initially ($t = 0$) uncorrelated and correlations start to built up for longer times $t > 0$. Thus, the initially realized δ peak spreads over the whole system. This is illustrated by the numerical results shown in Fig. 7.2 (a), see below.

Similar to the XXZ spin-1/2 chain, the quasi-one-dimensional two-leg ladder (see Sec. 3) is discussed, where the coupling constants, $J_{||}$ and $J_\perp$, represent either the coupling on the legs ($J_{||}$) or on the rungs ($J_\perp$). Notably, Ref. [R1] is focussed on $J_{||} = J_\perp = 1$ and $N = 20 \times 2 = 40$ lattice sites in total [252]. For this model, particularly the full time-space profile $C_{i,j}(t)$ with $j = N/2$, for local spin (see Fig. 7.2 (b)) are considered, which

has been calculated by means of DQT. As becomes apparent from Fig. 7.2, the profile of the spin density is described by Gaussians. Such a Gaussian-shaped density profile can be interpreted as a clear signature of spin diffusion in the limit of formally infinite temperature (see Sec. 4.3) in this and other models [86, 175, 182, 231, 276].

Moreover, Ref. [R1] reports that DQT has been used to study density-density correlation functions in other models. In particular, clean Gaussian profiles have been found in various parameter regimes, even for integrable models such as the spin-1/2 chain [182] or the Fermi-Hubbard model [276]. Beside those models, other classes of (nonintegrable) models such as the spin-1 XXZ chain [92] and disordered models [R3] are listed.

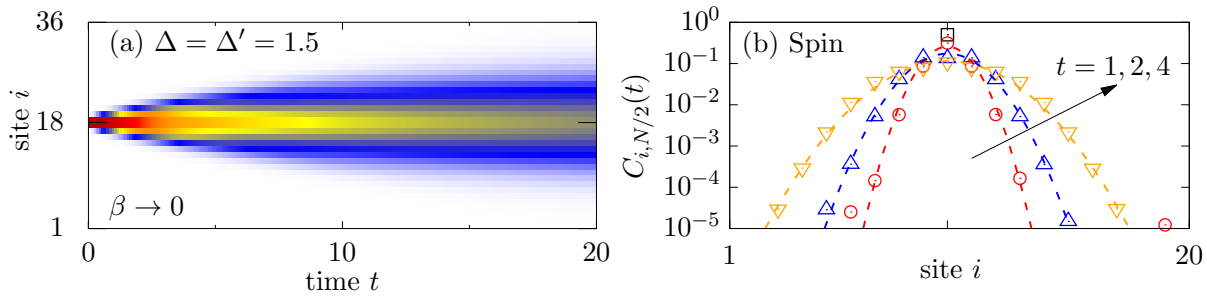

Figure 7.2.: (a) Time-space density plot of the spin-spin correlation function $C_{i,N/2}(t)$ in the limit of formally infinite temperature $\beta \to 0$ for the XXZ spin-1/2 chain of $N = 36$ lattice sites and nearest neighbor $\Delta = 1.5$ and next-nearest neighbor $\Delta' = 1.5$ coupling. (b) $C_{i,N/2}(t)$ at fixed times $t = 0$ (δ peak) $t = 1, 2, 4$ (arrow), for a spin-1/2 quasi-one-dimensional two-leg ladder of total size of $N = 20 \times 2 = 40$ in the limit of formally infinite temperatures. The dashed lines indicate Gaussian fits to the data. Data is adapted from [252].

As another application of quantum typicality, a *nonequilibrium scenario* in isolated quantum systems is described in Ref. [R1]. A common nonequilibrium setup is given as follows. Consider a quantum system that is initially prepared in a so-called *Gibbs state* with respect to some initial Hamiltonian $\mathcal{H}_0$, imposed by an initial density matrix $\rho(t = 0) = \rho(0)$,

$$\rho(0) = \frac{\mathrm{e}^{-\beta \mathcal{H}_0}}{\mathcal{Z}_0}\,, \tag{7.9}$$

where $\mathcal{Z}_0 = \mathrm{tr}\,[\exp(-\beta \mathcal{H}_0)]$ denotes the partition function with respect to the initial Hamiltonian $\mathcal{H}_0$. Subsequently, a so-called *quantum quench* [277] is considered, where the initial Hamiltonian $\mathcal{H}_0$ is changed to some other Hamiltonian, say $\mathcal{H}_1$. The scenario is illustrated in Fig. 7.3, see below. Then, the system is in a nonequilibrium state and the system evolves unitarily in time according to the Hamiltonian $\mathcal{H}_1$ with respect to the von-Neumann equation [cf. Eq. (2.23)],

$$\rho(t) = \mathrm{e}^{-\imath \mathcal{H}_1 t}\, \rho(0)\, \mathrm{e}^{\imath \mathcal{H}_1 t}\,. \tag{7.10}$$

The Hamiltonian $\mathcal{H}_1$ can for instance be generated by adding (or removing) some (weak or strong) static force of strength η to the (initial) Hamiltonian $\mathcal{H}_0$ (see Sec. 4). As a consequence, the total Hamiltonian $\mathcal{H}_1$ reads

$$\mathcal{H}_1 = \mathcal{H}_0 \pm \eta\, \mathcal{O}\,, \tag{7.11}$$

with $\mathcal{O}$ being a operator, conjugated to the static force [231, 253, 253, 278]. The resulting dynamics of the expectation value of the operator $\mathcal{O}$ is denoted by

$$\langle \mathcal{O}(t) \rangle = \mathrm{tr}\left[\rho(t)\,\mathcal{O}\right] . \tag{7.12}$$

In principle, the evaluation of this expression requires exact (full) diagonalization of both Hamiltonians $\mathcal{H}_0$ and $\mathcal{H}_1$. By preparing a typical pure state with the randomly chosen reference state $|\psi\rangle$,

$$|\psi(0)\rangle = \frac{\mathrm{e}^{-\beta\mathcal{H}_0/2}\,|\psi\rangle}{\sqrt{\langle\psi|\mathrm{e}^{-\beta\mathcal{H}_0}|\psi\rangle}} , \tag{7.13}$$

the density matrix $\rho(0)$ from above can be imitated and exact diagonalization can be circumvented. Thus, by using the typicality-approach, both the imaginary-time evolution with respect to the Hamiltonian $\mathcal{H}_0$ and the real-time evolution with respect to $\mathcal{H}_1$ can be performed by exploiting the techniques of pure-state propagation (see Sec. 6.3). Finally, this leads to the time dependent expectation value $\langle \mathcal{O}(t) \rangle$, which can be rewritten as

$$\langle \mathcal{O}(t) \rangle = \langle \psi(t)|\mathcal{O}|\psi(t)\rangle + \epsilon(|\psi\rangle) , \tag{7.14}$$

with the pure state $|\psi(t)\rangle = \exp\left(-\imath\mathcal{H}_0 t\right)|\psi(0)\rangle$ and the initial state given in (7.13). It is worth pointing out that the protocol above can be modified by additional changes of the Hamiltonian in time. A static force (see Sec. 4.1) switched on at time $t = 0$ can, for instance, be removed again at some later time $t > 0$. Even for such protocols, the additional efforts of the DQT approximation are minor compared to full diagonalization.

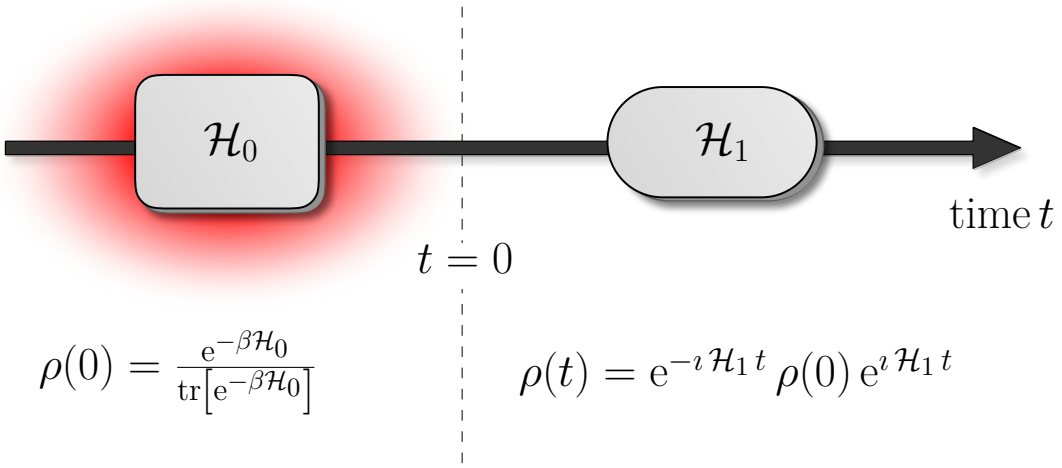

Figure 7.3.: Sketch of the nonequilibrium scenario. The system starts in a Gibbs state $\rho(0)$ with respect to some initial Hamiltonian $\mathcal{H}_0$. For times $t > 0$, the system evolves unitarily according to some other Hamiltonian $\mathcal{H}_1$ and to $\rho(t)$.

B. Quantum versus Classical Dynamics in Spin Models: Chains, Ladders, and Square Lattices

In Ref. [R2] a qualitative and quantitative comparison between quantum and classical spin models is presented. While it seems likely quantum and classical systems become akin to each other as the spin quantum number S increases from $S = 1/2, 1, \ldots$ towards the classical limit $S \to \infty$, it remains a generally nontrivial question whether and to which level the dynamics of quantum and classical spins coincide with each other for small quantum spin numbers S.

This question is tackled by considering the anisotropic Heisenberg model on three different lattice geometries, namely (*i*) the one-dimensional chain, (*ii*) the quasi-one-dimensional two-leg ladder and (*iii*) the two-dimensional square lattice (see Fig. 3.1). Each of these lattices is equipped with periodic boundary conditions. Recall, that the Hamiltonian (see Sec. 3) reads,

$$\mathcal{H}_{\mathrm{XXZ}} = J \sum_{\langle \boldsymbol{r},\boldsymbol{r}'\rangle} h_{\boldsymbol{r},\boldsymbol{r}'} \,, \tag{7.15}$$

where the sum runs over all bonds of nearest-neighboring lattice sites $\boldsymbol{r}$ and $\boldsymbol{r}'$ and the model's parameter as well as the local terms $h_{\boldsymbol{r},\boldsymbol{r}'}$ have been presented in Sec. 3.1.

The one-dimensional spin-1/2 Heisenberg model is integrable by means of Bethe ansatz methods for any anisotropy value Δ (see Sec. 3.3.2). By contrast, even the one-dimensional classical spin Heisenberg model is nonintegrable with respect to the Liouville-Arnold theorem and behaves chaotic (see Sec. 3.3.1). More generally, the integrability is broken for each model with either $S > 1/2$ or $d > 1$, where d denotes the (spatial) lattice dimension.

As the physical quantity of interest the dynamics of a local density $\varrho_{\boldsymbol{r}}(t)$ of either magnetization or energy is studied (see Sec. 3.1.1). Each of the quantities correspond to a globally conserved quantity, that is, the total magnetization or the total energy. From a quantum mechanical point of view, this fact is reflected by the vanishing of the commutation relations (see Sec. 3.1.3), while classically the commutation relations have to be replaced by the Poisson bracket (see Sec. 3.2). The time-dependent equal-site (density-density) correlation functions $C(t) = C_{\boldsymbol{r},\boldsymbol{r}'=\boldsymbol{r}}(t)$ for the lattice geometries (*i*) - (*iii*) are investigated in the limit of formally infinite temperatures ($\beta \to 0$). In this limiting case, the equal-site correlation function is given by (see Sec. 2.4.1),

$$C(t) = \langle \varrho_{\boldsymbol{r}}(t)\varrho_{\boldsymbol{r}}(0)\rangle = \begin{cases} \mathrm{tr}\left[\varrho_{\boldsymbol{r}}(t)\varrho_{\boldsymbol{r}}(0)\right]/\mathcal{D} & \text{for } S = 1/2 \\ 1/R \sum_r \left[\varrho_{\boldsymbol{r}}(t)\varrho_{\boldsymbol{r}}(0)\right] & \text{for } S \to \infty \end{cases} . \tag{7.16}$$

On the one hand, in the quantum case ($S = 1/2$), the equal-site correlation function is given by the trace of the local densities divided by the Hilbert-space dimension $\mathcal{D}$ (see Sec. 3.1). On the other hand, in the classical case ($S = \infty$), the correlation function is given as an average over a large number (i.e. $R \gg 1$) of trajectories in phase space, where the initial configurations $\varrho_{\boldsymbol{r}}(0)$ are drawn randomly for each realization r (see Sec. 3.2).

To ensure a fair comparison between the dynamics of a quantum and classical spin model, the time axis is rescaled $t \to t\tilde{S}$, to account for the different length of quantum

and classical spins,

$$\tilde{S} = \begin{cases} \sqrt{S(S+1)} & \text{for quantum spin } S \\ 1 & \text{for classical spin } S \end{cases} , \tag{7.17}$$

where the actual value of $\tilde{S}$ depends on the spin quantum number S. This rescaling plays a more important role in Ref. [R3], while Ref. [R2] is exclusively restricted to $S = 1/2$.

With regard to the time-dependent correlation function $C(t)$, it has been reported about solving the equations of motion to determine the time evolution. Quantum mechanically, the time evolution is governed by the linear Schrödinger equation (see Sec. 2.1), whereas the classical spin variables evolve in time according to the nonlinear Hamilton's equations of motion (see Sec. 3.2). Hamilton's equations of motion have been solved numerically by means of a RK4 scheme with a small time step δt (see Sec. 6). With regard to Eq. (7.16), an average over many samples $R \gg 1$ has been used in order to reduce statistical fluctuations. In contrast to the quantum case, the memory requirements for the classical spins do not scale exponentially, but only linearly in system size N. This fact enabled the possibility to reach much larger system sizes (for example $N = 1024$ lattice sites in total) and long times, compared to the quantum spin model. Since in Ref. [R2] the limiting case of formally infinite temperature has been considered, the quantum equal-site correlation function enables applying dynamical quantum typicality on the basis of just *one* auxiliary state (see Sec. 6.2 and Ref. [R1]),

$$C(t) = \langle \widetilde{\psi}(t) | \varrho_{\boldsymbol{r}} | \widetilde{\psi}(t) \rangle + \epsilon(|\psi\rangle) \, , \tag{7.18}$$

where $|\psi\rangle$ is again a random (pure) state [cf. Eq. (6.12)] and the initial state $|\widetilde{\psi}(0)\rangle$ is given by

$$|\widetilde{\psi}(0)\rangle = \frac{\sqrt{\varrho_{\boldsymbol{r}} + \lambda}\, |\psi\rangle}{\sqrt{\langle \psi | \psi \rangle}} \, , \tag{7.19}$$

where λ denotes again a constant such that $(\varrho_{\boldsymbol{r}} + \lambda)$ has nonnegative eigenvalues. The central Tadvantage of the typicality approximation Eq. (7.18) relies on the fact that the time dependence appears as a property of (pure) states. As a consequence, only one state has to be evolved in time by using an iterative forward propagation in real time (see Sec. 6.3),

$$|\widetilde{\psi}(t + \delta t)\rangle = \mathrm{e}^{-\imath \mathcal{H}_{\mathrm{XXZ}} \delta t} \, |\widetilde{\psi}(t)\rangle \, , \tag{7.20}$$

with a small discrete time step $\delta t \ll J$. To perform the action of the matrix exponential in Eq. (7.20), (*i*) Trotter decompositions methods and (*ii*) Chebyshev-polynomial expansions (see Sec. 6.3.3 and Sec. 6.3.2) have been used. The fact that the matrix-vector multiplications, required in these methods, can be carried out efficiently with respect to memory, gives access to treat quantum systems with up to $N = 36$ lattice sites in total. In fact, this is beyond the range of exact diagonalization. To ensure a fair comparison with the quantum case, also classical spin systems with fewer lattice sites $N \leq 36$ have been studied in Ref. [R2].

In both the classical and the quantum case, the time evolution of the equal-site correlation function $C(t)$ follows from the underlying microscopic equations of motion, and depends

on the specific model and its parameters. Due to the conservation of total energy and magnetization, it is generally expected that the dynamics of local densities acquire a hydrodynamic behavior at long time scales. With regard to the equal-site correlation function, the emergence of hydrodynamics is reflected in terms of a power-law decay,

$$C(t) \propto t^{-\alpha}\,, \tag{7.21}$$

where $\alpha = \alpha(d)$ depends on the spatial lattice dimension d. As described in Sec. 4.3, a dimensionality-dependent exponent $\alpha = \alpha(d) = d/2$ corresponds to normal diffusive transport, that is, $\alpha = 1/2$ in one-dimensional or quasi-one-dimensional systems, and $\alpha = 1$ for the two-dimensional square lattice. Moreover, anomalous superdiffusion and subdiffusion go along with an exponent $\alpha > d/2$ and $\alpha < d/2$, respectively, while ballistic transport is indicated by $\alpha = d$. In any finite system, caused by the saturation value $C(t \to \infty) > 0$, diffusion breaks down for long time scales. To illustrate the situation, Fig. 7.4 from Ref. [R2] shows a hydrodynamic power-law tail at intermediate times with an exponent $\alpha = 2/3$, which suggests superdiffusive transport.

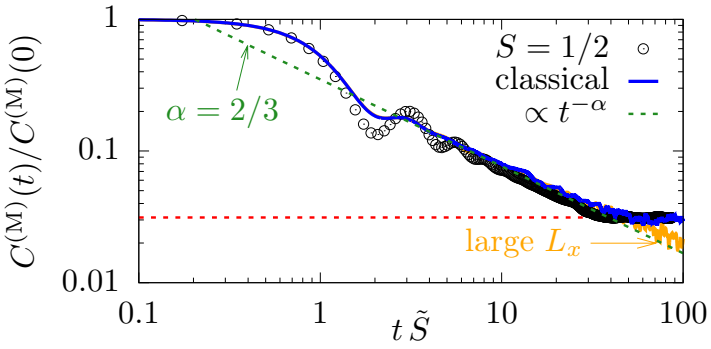

Figure 7.4.: Decay of the equal-site correlation function $C^{(\mathrm{M})}(t)$ in the quantum ($S = 1/2$) and classical case ($S = \infty$) at the isotropic point ($\Delta = 1$) shown in a log.-log. plot. The expected long-time value $C^{(\mathrm{M})}(t \to \infty) = 1/L_x$ as well as the power-law decay $\propto t^{-\alpha}$ with $\alpha = 2/3$ is shown. Classical data for a much larger $L_x = 1024$ lattice sites are depicted.

The results presented in Ref. [R2] show that the dynamics of local magnetization in the infinite-temperature limit in the one-dimensional chain ($L_x = 32$) for both quantum and classical spins coincide to a high degree of accuracy (on small and large time scales) for both the isotropic point $\Delta = 1$ and $\Delta = 1.5$. In particular, superdiffusive behavior ($\alpha = 2/3$) at the isotropic point is found (see Fig. 7.4). This is well established in the quantum realm, see for example Ref. [279], and is consistent with previous studies which report that the dynamics of local magnetization is described by the Kardar-Parisi-Zhang universality class [88, 89, 91, 94]. In the classical case, spin transport is quite controversial [96, 97].

For $\Delta = 1.5$, it is shown that the exponent changes to $\alpha = 1/2$, which indicates a diffusive decay. This is well-known to occur in the regime $\Delta > 1$, even in the integrable quantum model. While for the latter cases the dynamics coincided very well, for $\Delta = 0.5$ the overall agreement between the quantum and classical dynamics is worse. On the one hand it is demonstrated that the classical dynamics is diffusive ($\alpha = 1/2$), while on the other hand quantum dynamics have to be ballistic, which is indicated by $\alpha = 1$ in the thermodynamic limit and has been proven rigorously using quasi-local conserved charges [280, 281]. Thus, in such cases, where the quantum dynamics is dominated by

the extensive set of conservation laws, the correspondence between quantum and classical dynamics necessarily has to break down.

By considering spatially higher dimensional lattices with $d > 1$ (see cases (*ii*) and (*iii*) above), the model's integrability is broken. This nonintegrable situation is certainly more generic and might be seen as a fair test bed for the comparison between the dynamics in models with $S = 1/2$ and classical spins. In particular, for the quasi-one-dimensional two-leg ladder, it is pointed out that the dynamics of the quantum $S = 1/2$ spins are well captured by the dynamics of the classical spins for all anisotropies ($\Delta = 0.5\,, 1.0\,, 1.5$), not only on a qualitative, but even on a quantitative level to high accuracy. As expected, the equal-site correlation function exhibits diffusive behavior, with $\alpha = 1/2$. For the square lattice, a good agreement between the dynamics of quantum and classical spins has been found. As expected the dimensionality-dependent exponent is given by $\alpha = 1$.

To ensure that the agreement of quantum and classical dynamics is not only restricted to one observable (local magnetization), in addition, the equal-site correlation function for local energies is studied in Ref. [R2]. This case is exclusively focussed on a fixed anisotropy parameter ($\Delta = 1$) and the impact of different lattice geometries has been studied. Especially for the quasi-one-dimensional two-leg ladder and the two-dimensional square lattice the dynamics of the quantum spin-1/2 are well captured by the dynamics of the classical spins. However, substantial differences have been identified for the one-dimensional model. These differences are rather natural, since energy dynamics is ballistic ($\alpha = 1$) for the quantum spin-1/2 model, caused by integrability.

The classical spin chain exhibits diffusive ($\alpha = 1/2$) energy transport instead. However, this disagreement constitutes a counterexample to our typical observation that the decay of quantum and classical density-density correlations agree both qualitatively and quantitatively.

Therefore, based on the findings in Ref. [R2], it has been concluded that classical or semiclassical (hybrid) simulations might provide a meaningful strategy to investigate the quantum dynamics of strongly interacting quantum spin models, even if S is small and far away from the classical limit.

C. Decay of Spin-Spin Correlations in Disordered Quantum and Classical Spin Chains

This section gives an overview of Ref. [R3], where a comparison between the real-time dynamics of equal-site correlation functions for quantum and classical disordered spin models is presented. In contrast to Ref. [R2] (see Sec. B), Ref. [R3] is focussed on studying the disordered one-dimensional Heisenberg model (see Sec. 5.1). While Ref. [R2] deals with the specific spin quantum number $S = 1/2$, in Ref. [R3] additionally small spin quantum numbers ($S \geq 1/2$) are considered and compared to classical spins ($S \to \infty$). As before, the question is addressed whether and to which degree the dynamics of the quantum and classical Heisenberg model coincide, qualitatively and quantitatively, but contrarily to Ref. [R2], here in the presence of *disorder*.

In addition, the question to what extent the phenomenon of many-body localization occurs in the considered model, upon increasing the spin quantum number S towards the classical limit $S \to \infty$ is discussed. While it is believed that many-body localization is a purely quantum phenomenon, the quantum spins become increasingly akin to their classical counterparts with increasing S (see Sec. 3.2). Moreover, on the one hand, the spin-1/2 model is believed to undergo a transition from an ergodic to a many-body localized regime above a critical disorder strength $W_* \approx 3.5$ (see Sec. 5.1). On the other hand, the occurrence of many-body localization is not expected in classical spin systems, although strong disorder has been shown to cause anomalously slow relaxation.

Recall from Sec. 5.1 that the Hamiltonian of the disordered one-dimensional Heisenberg spin model reads,

$$\mathcal{H}_{\mathrm{W}} = J \sum_i \left(S_i^x S_{i+1}^x + S_i^y S_{i+1}^y + S_i^z S_{i+1}^z \right) + \sum_i h_i S_i^z \,, \tag{7.22}$$

where h_i denotes *on-site* magnetic fields, which are randomly drawn from a uniform distribution, that is, $h_i \in [-W, W]$, where $W \geq 0$ sets the overall magnitude of disorder. Regarding integrability, for vanishing disorder $W = 0$ and $S = 1/2$ the model is integrable in terms of the Bethe ansatz (see Sec. 3.3.2). In contrast, in presence of disorder $W \neq 0$, or for $S > 1/2$ the integrability is broken. As pointed out before in Sec. B, integrability as such does not necessarily rule out that quantum and classical transport properties can agree with each other. For instance, as previously discussed in Ref. [R2], both the quantum and classical chain exhibit diffusive spin transport above the isotropic point ($\Delta > 1$).

As the main quantity of interest, in Ref. [R3] the disorder-averaged equal-site correlation function $\overline{C(t)}$ is studied in the limit of formally infinite temperature (i.e. $\beta \to 0$). Recall that this correlation function is given by (see Sec. 5.3)

$$\overline{C(t)} = \frac{1}{M_h} \sum_{h=1}^{M_h} C(t) \,, \tag{7.23}$$

where the "bare" equal-site correlation function $C(t)$ is defined as previously defined (see, e.g., Sec. B). Notably, as a standard approach in the context of disordered models, $C(t)$ is averaged over M_h different random configurations of the magnetic fields h_i. As opposed to Sec. B (Ref. [R2]), here, exclusively the local density of magnetization is considered, while, as previously stated [cf. Eq. (7.17)], the time axis is rescaled by $\tilde{S}$ to take the length of the different quantum and classical spins into account (see Sec. B). Furthermore, an effective

disorder W_{eff} is introduced according to

$$W_{\text{eff}} = \begin{cases} W/\sqrt{S(S+1)} & \text{for quantum spin } S \\ W & \text{for classical spin } S \end{cases} . \tag{7.24}$$

Concerning the dynamics of the classical spins, the nonlinear classical Hamilton's equations of motion (see Sec. 3.2) are solved by employing a RK4 scheme with a small time step δt. While calculations in Ref. [R3] for the classical spin chain have been limited to $N \leq 200$ and $t \leq 1000$, following the arguments given in Sec. B, compared to the quantum case, classical spin chains can be treated for comparatively huge systems and long times with significantly less computational resources.

As also described in Sec. A (Ref. [R1]) and Sec. B (Ref. [R2]), the numerical calculations for the quantum case have been performed by using the concept of dynamical quantum typicality (see Sec. 6.2). Taking again advantage of the infinite-temperature limit leads to a similar expression for the equal-site correlation function as stated in Eq. (7.18), that is,

$$C(t) = \langle \widetilde{\psi}(0) | S_i^z | \widetilde{\psi}(0) \rangle + \epsilon(|\psi\rangle) \, . \tag{7.25}$$

The initial state $|\widetilde{\psi}(0)\rangle$ can be prepared similar to Eq. (7.19) with the substitutions $\varrho_{\boldsymbol{r}} \to S_i^z$ and $\lambda \to S$, with $S = 1/2,\, 1,\, 3/2$. The time evolution of the pure state $|\widetilde{\psi}(t)\rangle$ can again be efficiently generated by iteratively solving the real-time Schrödinger equation with the methods stated previously in Sec. A and Sec. B. As a result, system sizes beyond the range of standard exact diagonalization have been reached (see Sec. 6.1). In particular, in Ref. [R3] systems sizes up to $N = 14$ for $S = 3/2$ have been treated.

It is worth mentioning, that the typicality approach in Eq. (7.25) is independent of the validity of the ETH (see Sec. 5.2.2) and solely relies on the largeness of the Hilbert space. The DQT approach, therefore, enables accurate calculations in strongly disordered models which undergo a many-body localization transition [192], where the ETH fails (see Sec. 5.3).

Independent of the typicality relation in Eq. (7.25), each side of this relation can be interpreted as a certain type of imperfect "echo protocol" [282]. In this context the right-hand side of Eq. (7.2) can be rewritten as

$$\langle \widetilde{\psi}(0) | \mathrm{e}^{\imath \mathcal{H}_{\mathrm{W}} t} \, S_i^z \, \mathrm{e}^{-\imath \mathcal{H}_{\mathrm{W}} t} \widetilde{\psi}(0) \rangle \, , \tag{7.26}$$

which means that after evolving the out-of-equilibrium initial state $|\widetilde{\psi}(0)\rangle$ for some time t, a "perturbation" is applied in form of the operator S_i^z. Subsequently, the perturbed state is evaluated backward in time and the overlap between the the initial state $|\widetilde{\psi}(0)\rangle$ and the resulting state $\exp(\imath \mathcal{H}_{\mathrm{W}} t)\, S_i^z \exp(-\imath \mathcal{H}_{\mathrm{W}} t)\, |\widetilde{\psi}(0)\rangle$ is measured.

Concerning the dynamics of the disorder-averaged equal-site correlation function, $\overline{C(t)}$ is expected to exhibit a slower hydrodynamic behavior (compared to the disorder-free model) in the ergodic phase (see Sec. 5.3). This fact is reflected by a power-law decay of $\overline{C(t)}$ according to,

$$\overline{C(t)} \propto t^{-\alpha} \, , \quad \text{with} \quad \alpha < 1/2 \, . \tag{7.27}$$

There exists numerical evidence for the existence of a subdiffusive phase in the regime of low to intermediate disorder below the localization transition [129, 223–225]. This

subdiffusive regime is reflected by an exponent $\alpha < 1/2$. Since a finite spin chain of length N is assumed, for longer times the initially prepared spin excitation spreads out to the whole system. The equal-site correlation function $\overline{C(t)}$ saturates to a constant nonzero long-time value (i.e. $\overline{C(t)} \propto 1/N$) for long times [231]. Conversely, the localized regime is characterized by a significantly slower decay of the equal-site correlation function and, for long times, the correlation function $\overline{C(t)}$ saturates to a value $> 1/N$ in a finite system.

Ref. [R3] is focussed on different values of effective disorder (i.e. $W_{\text{eff}} \approx 0.58$, 1.15, 2.31 and $W_{\text{eff}} \approx 5.77$). First, regarding the comparison between the dynamics of $\overline{C(t)}$ for the quantum and classical model, on the one hand it is found that for vanishing and small values of (effective) disorder ($W_{\text{eff}} = 0$, $W_{\text{eff}} \lesssim 1.15$), the dynamics of $\overline{C(t)}$ is almost independent of the spin quantum number S and agrees with the classical case $S \to \infty$, evaluated at the same effective disorder W_{eff}. On the other hand, for stronger values of the (effective) disorder ($W_{\text{eff}} \lesssim 5.77$), the findings show that this agreement at least partially breaks down (see Fig. 7.5). Especially, the dynamics of $S = 1/2$ deviates from the dynamics of $S \geq 1$ and the classical case and, exhibit distinctly slower dynamics, which is consistent with subdiffusive transport in this parameter regime. In particular, a very good agreement between the quantum $S = 3/2$ and classical spin dynamics, even in the case of strong (effective) disorder ($W_{\text{eff}} = 5.77$), is shown. The situation for all cases of effective disorder is illustrated in Fig. 7.5.

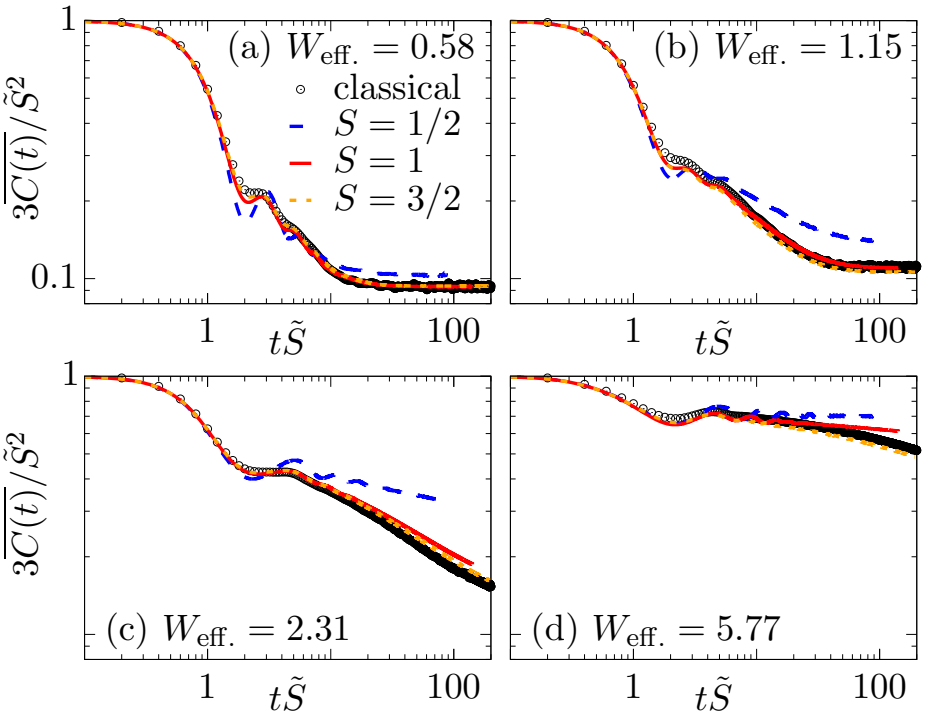

Figure 7.5.: Equal-site correlation function $3\overline{C(t)}/\tilde{S}^2$ versus the rescaled time $t\tilde{S}$ for different spin quantum numbers $S = 1/2$, 1, 3/2 and the classical spins $S = \infty$. Data is shown for different values of effective disorder (a) $W_{\text{eff}} \approx 0.58$, (b) $W_{\text{eff}} \approx 1.15$, (c) $W_{\text{eff}} \approx 2.31$ and (d) $W_{\text{eff}} \approx 5.77$. In all cases the system size is $L_x = 12$.

Apart from that, it is demonstrated that the spin-1/2 model appears to be localized at strong disorder ($W_{\text{eff}} \approx 5.77$), while for $S \geq 1$ as well as the classical spins, this does no seem to be the case, since they have a nonzero slope and continue to decay at long times.

Furthermore, the findings for the dynamics of $\overline{C(t)}$ are consistent with the behavior of the analysis of the mean ratio $\langle r \rangle$ of adjacent level spacings (see Sec. 3.3.3). Recall that this quantity is given by

$$\langle r \rangle = \left\langle \frac{\min\{s_m, s_{m+1}\}}{\max\{s_m, s_{m+1}\}} \right\rangle , \tag{7.28}$$

with $s_m = |E_{m+1} - E_m|$ being the energy-ordered eigenvalues of the disordered Hamiltonian $\mathcal{H}_{\mathrm{W}}$ [cf. (7.22)]. The brackets denote both averaging over energy levels and additionally over different realizations of disorder. In particular, it is found that the transition of $\langle r \rangle$ from Wigner-Dyson ($\langle r \rangle_{\mathrm{WD}} \approx 0.53$) towards Poissonian level statistics ($\langle r \rangle_{\mathrm{P}} \approx 0.39$) appears at increased disorder values upon increasing the spin quantum number S (see Fig. 7.6). Combining the results from the comparison of the dynamics of the quantum and classical spins and as well by analyzing the statistics of energy-level spacings, it is speculated that many-body localization eventually occurs also in models with $S = 1$ and $S = 3/2$.

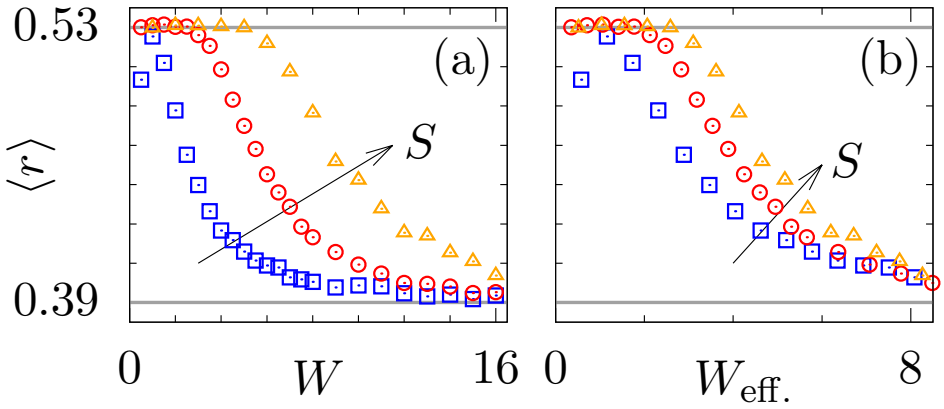

Figure 7.6.: Mean ratio $\langle r \rangle$ of adjacent level spacings for the model (7.22) with $S = 1/2, 1, 3/2$ (arrow) as a function of (a) "bare" disorder strength W and (b) effective disorder $W_{\mathrm{eff}} = W/\tilde{S}$. The green lines indicate the value for Wigner-Dyson ($\langle r \rangle_{\mathrm{WD}} \approx 0.53$) and Poisson distribution ($\langle r \rangle_{\mathrm{P}} \approx 0.39$). In all cases the system size is $L_x = 8$.

Apart from the results mentioned above, the self-averaging property of the correlation function $C(t)$ (see Sec. 5.3) is analyzed. Recall that a physical quantity of a disordered system is called *self-averaging* if its relative variance $R(t)$, that is, the ratio between its variance for disordered realizations and the square of its mean, decreases upon increasing the system size N (see Sec. 5.3). For the case that self-averaging holds with increasing system size, the number of samples can be reduced. To this end, the relative variance $R(t)$ of sample-to-sample fluctuations specifically for $S = 1/2$ is analyzed. It is outlined that the expectation, i.e. for vanishing disorder the relative variance $R(t)$ is strictly zero (due to the absence of disorder), could not have been confirmed. This can be traced back to the numerical calculations by means of typicality in Ref. [R3]. The nonzero data of $R(t)$, therefore, can be interpreted as the accuracy of the used typicality approximation. Thus, in the context of Eq. (5.15) in Sec. 5.3, the "super"-self-averaging property of the equal-site correlation function $C(t)$ is pointed out [236]. For finite values of disorder, it is shown that $R(t)$ decreases exponentially with N for short times, while for longer times

this scaling breaks down. While for short times the correlation function is shown to be self-averaging which is consistent with recent results, for longer times, this self-averaging is much weaker, or breaks down (see Fig. 7.7). A power-law scaling according to $R(t) \propto N^{-\nu}$, with $\nu \in (0, 1]$ has not been ruled out in [R3].

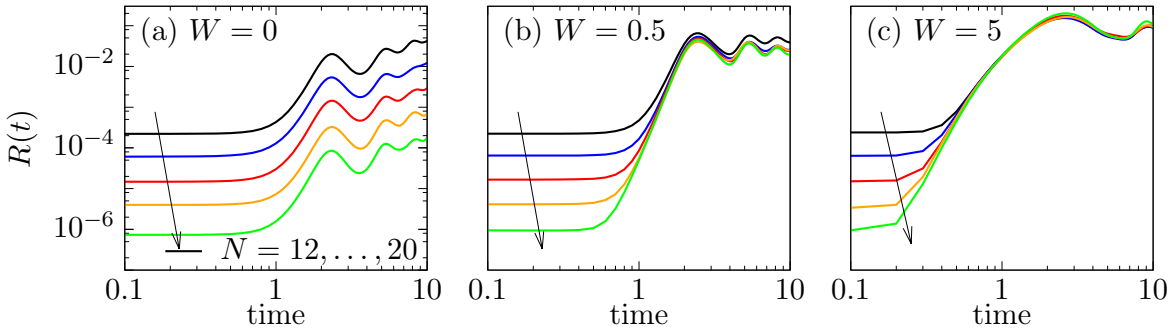

Figure 7.7.: Relative variance $R(t)$ of sample-to-sample fluctuations [cf. Eq. (5.15)] in a logarithmic plot for $S = 1/2$ chains with different system sizes $N = 12, \ldots, 20$ (arrows) and disorder strengths (a) $W = 0$, (b) $W = 0.5$ and (c) $W = 5$.

Part IV.

Conclusion

8. Summary and Outlook

The present dissertation has addressed the dynamics of interacting quantum and classical spin models based on the publications [R1–R3]. Particular attention has been paid to the question of whether and to which degree the dynamics of these models agree with each other.

To this end, XXZ models have been studied on different lattice geometries of finite size, ranging from one-dimensional chains and quasi-one-dimensional ladders towards two-dimensional square lattices. Particular emphasis has been placed on the analysis of time-dependent autocorrelation functions of local densities for both the local density of magnetization (spin) and energy in the limit of formally infinite temperature. Due to the conservation of total energy and total magnetization, the dynamics of such densities are expected to exhibit hydrodynamic behavior for long times, which manifests itself in a power-law tail of the autocorrelation function in time. From a quantum mechanical perspective, the calculation of these autocorrelation functions required solving the linear Schrödinger equation, while, from a classical point of view, Hamilton's equations of motion were solved. Based on the concept of typicality, an efficient numerical pure-state approach enabled to circumvent the costly numerical method of exact diagonalization and to treat quantum autocorrelation functions with up to $N = 36$ lattice sites in total.

While, in full generality, a quantitative agreement between quantum and classical dynamics could not have been expected, contrarily, based on the results of large-scale numerical simulations, it was demonstrated that the dynamics of the quantum $S = 1/2$ and classical spin models coincided, not only qualitatively but even quantitatively, to a remarkably high level of accuracy for all considered lattice geometries. In particular, in the case of nonintegrable quantum models, that is, the quasi-one-dimensional ladder and two-dimensional lattice, the agreement was found to be best. Nevertheless, also in integrable models, the agreement remained satisfactory, at least in cases where transport was not ballistic due to the extensive set of conservation laws. Additionally, it was noted that, for the spin chain, such an agreement of the dynamics held even in the presence of small values of disorder, while, at strong disorder, the agreement was most pronounced for high spin quantum numbers.

Finally, this research has demonstrated that a putative many-body localization transition within the one-dimensional spin chain shifts to stronger values of disorder with increasing spin quantum number. This leads to the conclusion that classical or semi-classical simulations could offer a meaningful strategy to investigate the quantum dynamics of strongly interacting quantum spin models, even if the spin quantum number is small and far from the classical limit.

The findings of this dissertation raise a variety of intriguing questions which provide the basis for future work. The scope of the results of this dissertation is limited by the fact that the focus was solely on the comparison between quantum and classical spin dynamics for the observables of local magnetization and energy. For this reason, further studies could aim to extend the current findings by examining the question of whether a similar agreement between the dynamics of quantum and classical spins can be

observed for observables beyond local densities or other out-of-equilibrium quantities apart from the (equal-site) correlation functions $C(t)$. For instance, examining the full space profiles at fixed times $C_{i,j}(t) = \langle \varrho_i(t)\varrho_j \rangle$ for $i \neq j$ with $j \to N/2$ would be interesting for future research. Some progress is currently being made towards investigating such profiles regarding a correspondence between classical spin models and the (extended) Fermi-Hubbard model, which can be mapped to a quantum spin-1/2 ladder model (see Sec. 3) via Jordan-Wigner transformation (see Sec. 3.1.4). Initial results are displayed in Fig. 8.1. Further numerical and analytical efforts in future research are required.

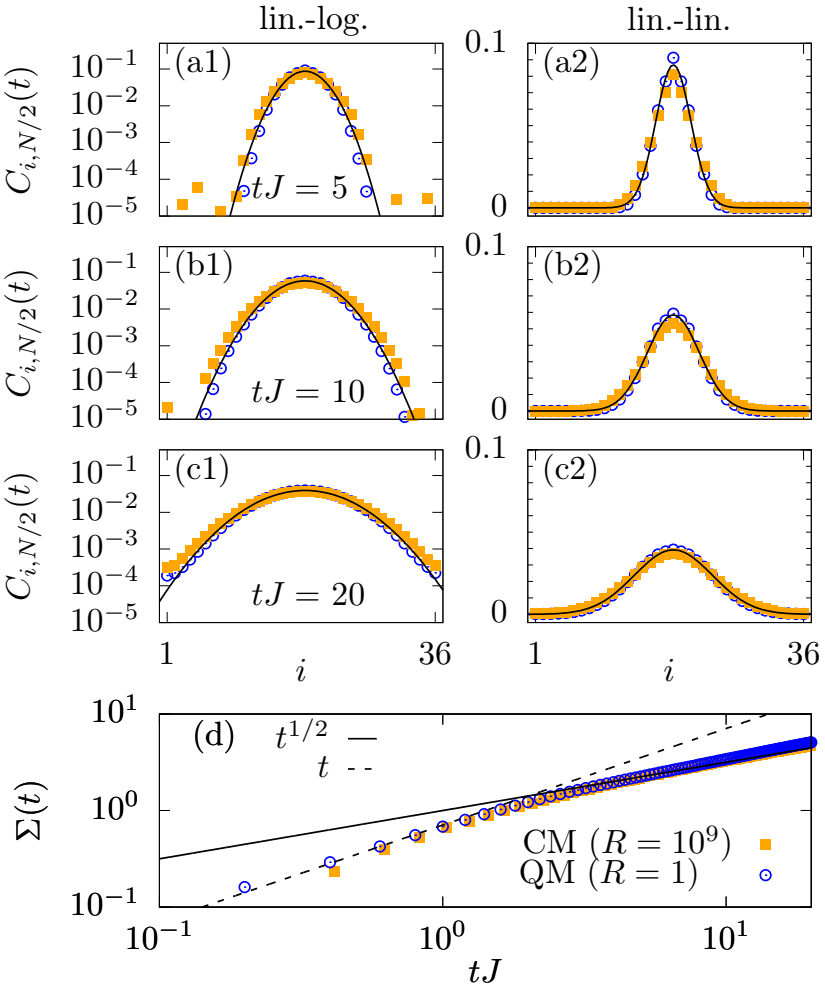

Figure 8.1.: (a1)-(c2) Magnetization profiles in the XXZ spin chain with anisotropy $\Delta = 1.5$ and $L_x = 36$, sampled over R initial states. (d) Time-dependent spatial width $\Sigma(t)$ as obtained by Eq. (4.19). Dashed and solid lines indicate scaling t^α for $\alpha = 1$ and $1/2$.

Another aspect of this research is worth highlighting: Although the results are promising and support a correspondence of the dynamics of quantum and classical spin models, the calculations within this dissertation were performed in the limit of formally infinite temperature, where quantum effects are less pronounced. A natural next step would be to elucidate whether and how far an agreement between the dynamics of quantum and classical spins can be validated by passing over to finite temperatures, i.e. $\beta > 0$, or very low temperatures, i.e. $\beta \to \infty$, where quantum effects are significantly more pronounced. Nevertheless, it is clear that there should be some energy scale, where the

specific excitations of a given quantum model become (more) relevant and likely cause large differences from the classical counterpart. In this context, an additional interesting question is whether the observed signatures of diffusion even persist at lower (finite) temperature.

Following the research according to Ref. [R3], future studies should explore the dynamics of quantum and classical spins in the presence of disorder for higher spatial lattice geometries $d > 1$. While it is widely accepted that especially the one-dimensional quantum model undergoes a many-body localization transition, the situation for higher dimensional lattices is far less clear today [200, 283–285]. In terms of future studies on those disordered models, it is necessary to extend the current results of this dissertation by clarifying the occurrence of a potential many-body localization transition and evaluating the exact value of critical disorder W_* in models with $d > 1$. This could be an interesting avenue of future analytical and numerical research.

Acknowledgements

It is my pleasure to thank and acknowledge many people who have crucially influenced contributed to the completion of the dissertation. Certainly, this thesis would not have been possible without the support of these people.

First of all, I would like to express my sincere gratitude to my supervisor Prof. Dr. Robin Steinigeweg for giving me the opportunity to join his research group in Osnabrück. Thank you for providing invaluable guidance, feedback and encouragement throughout the last years and this thesis. Without your persistent support, this thesis would not have been possible.

I am very thankful to Prof. Dr. Jochen Gemmer, who agreed to write the second report on this thesis. I would also thank Dr. Monika Wesner and Prof. Dr. Joachim Wollschläger, who have thankfully agreed to be on the Ph.D. committee. In particular, I would like to thank Dr. Monika Wesner for the consistently good and fruitful cooperation. I have always enjoyed being a tutor under your management for several semesters.
I would also extend my gratitude to all coauthors and colleagues. This dissertation would not have been possible without them. Especially, I would like to thank Prof. Dr. Kristel Michielsen, Dr. Fengping Jin (both from Institute for Advanced Simulation, Jülich Supercomputing Centre) and Prof. Dr. Hans de Raedt (Zernike Institute for Advanced Materials University of Groningen) for their fruitful cooperation. Moreover, I would like to offer my special thanks to Dr. Jonas Richter (University College London) for his constantly valuable advices.

Furthermore, I gratefully thank Dr. Christian Bartsch for being permanently available for questions, helpful suggestions, discussions and for proofreading this thesis. I would like to thank all the theory group members in Osnabrück, in particular Tjark Heitmann and Robin Heveling for proofreading this thesis and exciting discussions during the lunch break and for sharing the apartment at visits to conferences, as well as Mats Lamann and Dr. Jiaozi Wang. I am glad for having met you during my time in Osnabrück and wish each of you all the best on your future path. I would also like to thank the secretary of our research group, Lana-Maria Stork-Bohmann for always taken great care of dealing with administrative routines. She has contributed with her friendly manner decisively to the good atmosphere in the group.

I am grateful for my parents for their constant support throughout my studies for providing guidance and stability as well as my brother Niklas whom I wish all the best for his own academic career.

Finally, I owe my deepest gratitude to my love Samy, who keeps me grounded and always reminds me of what is important in life (apart from physics). I am forever thankful for your unconditional love, your unwavering support and profound belief in me throughout the entire time of completing this thesis and far-far beyond that. Thank you for all from the bottom of my heart. I look forward to the future with you, I love you!

Bibliography

[R1] T. Heitmann, J. Richter, D. Schubert, and R. Steinigeweg, Z. Naturforsch. A **75**, 421 (2020).

[R2] D. Schubert, J. Richter, F. Jin, K. Michielsen, H. De Raedt, and R. Steinigeweg, Phys. Rev. B **104**, 054415 (2021).

[R3] J. Richter, D. Schubert, and R. Steinigeweg, Phys. Rev. Research **2**, 013130 (2020).

[4] M. Toda, R. Kubo, and N. Saito, *Statistical Physics I - Equilibrium Statistical Mechanics*, 1st ed., Solid-State Sciences (Springer, Berlin, 1983).

[5] R. Kubo, M. Toda, and N. Hashitsume, *Statistical Physics II - Nonequilibrium Statistical Mechanics*, 2nd ed., Solid-State Sciences (Springer, Berlin, 1991).

[6] I. Bloch, J. Dalibard, and S. Nascimbène, Nat. Phys. **8**, 267 (2012).

[7] I. Bloch, Nat. Phys. **1**, 23 (2005).

[8] T. Kinoshita, T. Wenger, and D. S. Weiss, Nature **440**, 900 (2006).

[9] M. Lewenstein, A. Sanpera, V. Ahufinger, B. Damski, A. Sen De, and U. Sen, Adv. Phys. **56**, 243 (2007).

[10] I. Bloch, J. Dalibard, and W. Zwerger, Rev. Mod. Phys. **80**, 885 (2008).

[11] M. Greiner, O. Mandel, T. W. Hänsch, and I. Bloch, Nature **419**, 51 (2002).

[12] T. Langen, R. Geiger, and J. Schmiedmayer, Annu. Rev. Condens. Matter Phys. **6**, 201 (2015).

[13] M. Schreiber, S. S. Hodgman, P. Bordia, H. P. Lüschen, M. H. Fischer, R. Vosk, E. Altman, U. Schneider, and I. Bloch, Science **349**, 842 (2015).

[14] C. Gross and I. Bloch, Science **357**, 995 (2017).

[15] R. Blatt and C. F. Roos, Nat. Phys. **8**, 277 (2012).

[16] A. Friedenauer, H. Schmitz, J. T. Glueckert, D. Porras, and T. Schaetz, Nat. Phys. **4**, 757 (2008).

[17] M. Schlosshauer, Rev. Mod. Phys. **76**, 1267 (2005).

[18] T. Fukuhara, A. Kantian, M. Endres, M. Cheneau, P. Schauß, S. Hild, D. Bellem, U. Schollwöck, T. Giamarchi, C. Gross, I. Bloch, and S. Kuhr, Nat. Phys. **9**, 235 (2013).

[19] S. Hild, T. Fukuhara, P. Schauß, J. Zeiher, M. Knap, E. Demler, I. Bloch, and C. Gross, Phys. Rev. Lett. **113**, 147205 (2014).

[20] P. N. Jepsen, J. Amato-Grill, I. Dimitrova, W. W. Ho, E. Demler, and W. Ketterle, Nature **588**, 403 (2020).

[21] M. Cheneau, P. Barmettler, D. Poletti, M. Endres, P. Schauß, T. Fukuhara, C. Gross, I. Bloch, C. Kollath, and S. Kuhr, Nature **481**, 484 (2012).

[22] J. P. Ronzheimer, M. Schreiber, S. Braun, S. S. Hodgman, S. Langer, I. P. McCulloch, F. Heidrich-Meisner, I. Bloch, and U. Schneider, Phys. Rev. Lett. **110**, 205301 (2013).

[23] G. Salomon, J. Koepsell, J. Vijayan, T. A. Hilker, J. Nespolo, L. Pollet, I. Bloch, and C. Gross, Nature **565**, 56 (2019).

[24] N. Goldman, J. C. Budich, and P. Zoller, Nat. Phys. **12**, 639 (2016).

[25] D. C. Aveline, J. R. Williams, E. R. Elliott, C. Dutenhoffer, J. R. Kellogg, J. M. Kohel, N. E. Lay, K. Oudrhiri, R. F. Shotwell, N. Yu, and R. J. Thompson, Nature **582**, 193 (2020).

[26] H.-J. Mikeska and A. K. Kolezhuk, *One-dimensional magnetism*, 1st ed. (Springer, Berlin, 2004).

[27] N. Hlubek, P. Ribeiro, R. Saint-Martin, A. Revcolevschi, G. Roth, G. Behr, B. Büchner, and C. Hess, Phys. Rev. B **81**, 020405 (2010).

[28] T. Kawamata, N. Takahashi, T. Adachi, T. Noji, K. Kudo, N. Kobayashi, and Y. Koike, J. Phys. Soc. Jpn. **77**, 034607 (2008).

[29] N. Hlubek, X. Zotos, S. Singh, R. Saint-Martin, A. Revcolevschi, B. Büchner, and C. Hess, J. Stat. Mech. **2012**, P03006 (2012).

[30] N. Motoyama, H. Eisaki, and S. Uchida, Phys. Rev. Lett. **76**, 3212 (1996).

[31] A. V. Sologubenko, K. Giannó, H. R. Ott, U. Ammerahl, and A. Revcolevschi, Phys. Rev. Lett. **84**, 2714 (2000).

[32] J. van Kranendonk and J. H. van Vleck, Rev. Mod. Phys. **30**, 1 (1958).

[33] M. E. Lines, Phys. Rev. **135**, A1336 (1964).

[34] O. Ciftja, M. Luban, M. Auslender, and J. H. Luscombe, Phys. Rev. B **60**, 10122 (1999).

[35] E. H. Lieb, Commun. Math. Phys. **31**, 327 (1973).

[36] A. Polkovnikov, K. Sengupta, A. Silva, and M. Vengalattore, Rev. Mod. Phys. **83**, 863 (2011).

[37] J. Eisert, M. Cramer, and M. B. Plenio, Rev. Mod. Phys. **82**, 277 (2010).

[38] L. D'Alessio, Y. Kafri, A. Polkovnikov, and M. Rigol, Adv. Phys. **65**, 239 (2016).

[39] C. Gogolin and J. Eisert, Rep. Prog. Phys. **79**, 056001 (2016).

[40] P. Calabrese, F. H. L. Essler, and G. Mussardo, J. Stat. Mech. **2016**, 064001 (2016).

[41] F. Borgonovi, F. Izrailev, L. Santos, and V. Zelevinsky, Phys. Rep. **626**, 1 (2016).

[42] J. M. Deutsch, Phys. Rev. A **43**, 2046 (1991).

[43] M. Srednicki, Phys. Rev. E **50**, 888 (1994).

[44] M. Rigol, V. Dunjko, and M. Olshanii, Nature **452**, 854 (2008).

[45] J. M. Deutsch, Rep. Prog. Phys. **81**, 082001 (2018).

[46] E. Altman and R. Vosk, Annu. Rev. Condens. Matter Phys. **6**, 383 (2015).

[47] E. Abrahams, P. W. Anderson, D. C. Licciardello, and T. V. Ramakrishnan, Phys. Rev. Lett. **42**, 673 (1979).

[48] D. A. Abanin, E. Altman, I. Bloch, and M. Serbyn, Rev. Mod. Phys. **91**, 021001 (2019).

[49] D. A. Huse, R. Nandkishore, and V. Oganesyan, Phys. Rev. B **90**, 174202 (2014).

[50] R. Nandkishore and D. A. Huse, Annu. Rev. Condens. Matter Phys. **6**, 15 (2015).

[51] V. I. Arnold, *Mathematical Methods of Classical Mechanics*, 1st ed. (Springer, New York, 1978).

[52] J. V. José and E. J. Saletan, *Classical Dynamics: A Contemporary Approach*, 1st ed. (Cambridge University Press, Cambridge, 1998).

[53] A. Knauf, *Mathematical Physics: Classical Mechanics*, 1st ed., Vol. 109 (Springer, Berlin, 2018).

[54] C. C. Moore, Proc. Natl. Acad. Sci. **112**, 1907 (2015).

[55] I. E. Farquhar and R. J. Seeger, Am. J. Phys. **33**, 973 (1965).

[56] J.-S. Caux and J. Mossel, J. Stat. Mech. **2011**, P02023 (2011).

[57] H. G. Schuster and W. Just, *Deterministic Chaos*, 4th ed. (Wiley, Weinheim, 2005).

[58] M. C. Gutzwiller, *Chaos in Classical and Quantum Mechanics*, 1st ed. (Springer, New York, 1990).

[59] E. Ott, *Chaos in Dynamical Systems*, 2nd ed. (Cambridge University Press, Cambridge, 2002).

[60] J. Hietarinta, J. Math. Phys. **25**, 1833 (1984).

[61] H. Bethe, Z. Phys. **71**, 205 (1931).

[62] F. H. L. Essler, H. Frahm, F. Göhmann, A. Klümper, and V. E. Korepin, *The One-Dimensional Hubbard Model*, 1st ed. (Cambridge University Press, Cambridge, 2005).

[63] F. Franchini, *An Introduction to Integrable Techniques for One-Dimensional Quantum Systems*, 1st ed. (Springer, Cham, 2017).

[64] V. O. Tarasov, J. Math. Sci. **125**, 239 (2005).

[65] W. Hao, R. I. Nepomechie, and A. J. Sommese, Phys. Rev. E **88**, 052113 (2013).

[66] M. Takahashi, *Thermodynamics of One-Dimensional Solvable Models*, 1st ed. (Cambridge University Press, Cambridge, 1999).

[67] L. D. Faddeev, arXiv:9605187 .

[68] N. A. Slavnov, arXiv:1804.07350 .

[69] V. E. Korepin, N. M. Bogoliubov, and A. G. Izergin, *Quantum Inverse Scattering Method and Correlation Functions*, 1st ed. (Cambridge University Press, Cambridge, 1993).

[70] E. K. Sklyanin, arXiv:9211111 .

[71] C. N. Yang, Phys. Rev. **168**, 1920 (1968).

[72] R. J. Baxter, Phys. Rev. Lett. **26**, 832 (1971).

[73] D. A. Rabson, B. N. Narozhny, and A. J. Millis, Phys. Rev. B **69**, 054403 (2004).

[74] D. Poilblanc, T. Ziman, J. Bellissard, F. Mila, and G. Montambaux, Europhys. Lett. **22**, 537 (1993).

[75] F. H. L. Essler and M. Fagotti, J. Stat. Mech. **2016**, 64002 (2016).

[76] L. Vidmar and M. Rigol, J. Stat. Mech. **2016**, 064007 (2016).

[77] H. Castella, X. Zotos, and P. Prelovek, Phys. Rev. Lett. **74**, 972 (1995).

[78] X. Zotos, F. Naef, and P. Prelovsek, Phys. Rev. B **55**, 11029 (1997).

[79] T. Prosen and B. Žunkovič, Phys. Rev. Lett. **111**, 40602 (2013).

[80] F. Heidrich-Meisner, A. Honecker, and W. Brenig, Eur. Phys. J. Spec. Top. **151**, 135 (2007).

[81] B. Bertini, F. Heidrich-Meisner, C. Karrasch, T. Prosen, R. Steinigeweg, and M. Žnidarič, Rev. Mod. Phys. **93**, 025003 (2021).

[82] A. Klümper and K. Sakai, J. Phys. A. Math. Gen. **35**, 2173 (2002).

[83] S. Sachdev and K. Damle, Phys. Rev. Lett. **78**, 943 (1997).

[84] X. Zotos, Phys. Rev. Lett. **82**, 1764 (1999).

[85] M. Žnidarič, Phys. Rev. Lett. **106**, 220601 (2011).

[86] M. Ljubotina, M. Žnidari, and T. Prosen, Nat. Commun. **8**, 1 (2017).

[87] M. Kardar, G. Parisi, and Y.-C. Zhang, Phys. Rev. Lett. **56**, 889 (1986).

[88] M. Ljubotina, M. Žnidarič, and T. Prosen, Phys. Rev. Lett. **122**, 210602 (2019).

[89] S. Gopalakrishnan and R. Vasseur, Phys. Rev. Lett. **122**, 127202 (2019).

[90] J. Richter and R. Steinigeweg, Phys. Rev. B **99**, 094419 (2019).

[91] F. Weiner, P. Schmitteckert, S. Bera, and F. Evers, Phys. Rev. B **101**, 045115 (2020).

[92] J. Richter, N. Casper, W. Brenig, and R. Steinigeweg, Phys. Rev. B **100**, 144423 (2019).

[93] J. De Nardis, M. Medenjak, C. Karrasch, and E. Ilievski, Phys. Rev. Lett. **123**, 186601 (2019).

[94] M. Dupont and J. E. Moore, Phys. Rev. B **101**, 121106 (2020).

[95] G. Müller, Phys. Rev. Lett. **60**, 2785 (1988).

[96] R. W. Gerling and D. P. Landau, Phys. Rev. B **42**, 8214 (1990).

[97] O. F. de Alcantara Bonfim and G. Reiter, Phys. Rev. Lett. **69**, 367 (1992).

[98] D. Hone, C. Scherer, and F. Borsa, Phys. Rev. B **9**, 965 (1974).

[99] F. Borsa and M. Mali, Phys. Rev. B **9**, 2215 (1974).

[100] N. Srivastava, J.-M. Liu, V. S. Viswanath, and G. Müller, J. Appl. Phys. **75**, 6751 (1994).

[101] J. P. Boucher, M. A. Bakheit, M. Nechtschein, M. Villa, G. Bonera, and F. Borsa, Phys. Rev. B **13**, 4098 (1976).

[102] V. Constantoudis and N. Theodorakopoulos, Phys. Rev. E **55**, 7612 (1997).

[103] J. M. Liu, N. Srivastava, V. S. Viswanath, and G. Müller, J. Appl. Phys. **70**, 6181 (1991).

[104] V. Oganesyan, A. Pal, and D. A. Huse, Phys. Rev. B **80**, 115104 (2009).

[105] D. Bagchi, Phys. Rev. B **87**, 75133 (2013).

[106] P. Glorioso, L. Delacrétaz, X. Chen, R. Nandkishore, and A. Lucas, SciPost Phys. **10** (2021).

[107] O. F. de Alcantara Bonfim and G. Reiter, Phys. Rev. Lett. **70**, 249 (1993).

[108] J. De Nardis, M. Medenjak, C. Karrasch, and E. Ilievski, Phys. Rev. Lett. **124**, 210605 (2020).

[109] J. Kikuchi, N. Kurata, K. Motoya, T. Yamauchi, and Y. Ueda, J. Phys. Soc. Jpn. **70**, 2765 (2001).

[110] H. Kühne, H.-H. Klauss, S. Grossjohann, W. Brenig, F. J. Litterst, A. P. Reyes, P. L. Kuhns, M. M. Turnbull, and C. P. Landee, Phys. Rev. B **80**, 045110 (2009).

[111] K. R. Thurber, A. W. Hunt, T. Imai, and F. C. Chou, Phys. Rev. Lett. **87**, 247202 (2001).

[112] H. Maeter, A. A. Zvyagin, H. Luetkens, G. Pascua, Z. Shermadini, R. Saint-Martin, A. Revcolevschi, C. Hess, B. Büchner, and H.-H. Klauss, J. Phys. Condens. Matter **25**, 365601 (2013).

[113] A. Scheie, N. E. Sherman, M. Dupont, S. E. Nagler, M. B. Stone, G. E. Granroth, J. E. Moore, and D. A. Tennant, Nat. Phys. **17**, 726 (2021).

[114] C. Tang and J. S. Waugh, Phys. Rev. B **45**, 748 (1992).

[115] E. Fermi, P. Pasta, S. Ulam, and M. Tsingou, *Los Alamos Rep. LA-1940*, Tech. Rep. (published later in Collected Papers of Enrico Fermi, Chicago, 1955).

[116] T. Dauxois, Phys. Today **61**, 55 (2008).

[117] R. Steinigeweg, *Zur Dynamik von klassischen Heisenberg-Systemen: Klassen integrabler Systeme und symplektische Integratoren für nicht integrable Systeme*, Diplomarbeit, University of Osnabrück (2005).

[118] D. A. Abanin and Z. Papić, Ann. Phys. **529**, 1700169 (2017).

[119] P. W. Anderson, Phys. Rev. **109**, 1492 (1958).

[120] M. Serbyn, Z. Papić, and D. A. Abanin, Phys. Rev. Lett. **111**, 127201 (2013).

[121] V. Ros, M. Müller, and A. Scardicchio, Nucl. Phys. B **891**, 420 (2015).

[122] V. Oganesyan and D. A. Huse, Phys. Rev. B **75**, 155111 (2007).

[123] A. Pal and D. A. Huse, Phys. Rev. B **82**, 174411 (2010).

[124] J. Z. Imbrie, Phys. Rev. Lett. **117**, 027201 (2016).

[125] T. C. Berkelbach and D. R. Reichman, Phys. Rev. B **81**, 224429 (2010).

[126] D. J. Luitz, N. Laflorencie, and F. Alet, Phys. Rev. B **91**, 81103 (2015).

[127] J. A. Kjäll, J. H. Bardarson, and F. Pollmann, Phys. Rev. Lett. **113**, 107204 (2014).

[128] S. Bera, H. Schomerus, F. Heidrich-Meisner, and J. H. Bardarson, Phys. Rev. Lett. **115**, 046603 (2015).

[129] S. Gopalakrishnan, M. Müller, V. Khemani, M. Knap, E. Demler, and D. A. Huse, Phys. Rev. B **92**, 104202 (2015).

[130] S. Gopalakrishnan and S. A. Parameswaran, Phys. Rep. **862**, 1 (2020).

[131] B. Jenčič and P. Prelovšek, Phys. Rev. B **92**, 134305 (2015).

[132] A. Weiße and H. Fehske, in *Computational Many-Particle Physics*, edited by W. A. Fehske H., Schneider R. (Springer, Berlin, 2008) pp. 529–544.

[133] W. Kohn, Rev. Mod. Phys. **71**, 1253 (1999).

[134] S. R. White, Phys. Rev. Lett. **69**, 2863 (1992).

[135] U. Schollwöck, Ann. Phys. **326**, 96 (2011).

[136] S. Lloyd, *Pure state quantum statistical mechanics and black holes*, Ph.d. thesis, The Rockefeller University (1988), arXiv:1307.0378 .

[137] J. Gemmer, M. Michel, and G. Mahler, *Quantum Thermodynamics*, Lecture Notes in Physics, Vol. 657 (Springer, Berlin, 2004).

[138] S. Popescu, A. J. Short, and A. Winter, Nat. Phys. **2**, 754 (2006).

[139] S. Goldstein, J. L. Lebowitz, R. Tumulka, and N. Zanghì, Phys. Rev. Lett. **96**, 050403 (2006).

[140] P. Reimann, Phys. Rev. Lett. **99**, 160404 (2007).

[141] F. Jin, D. Willsch, M. Willsch, H. Lagemann, K. Michielsen, and H. De Raedt, J. Phys. Soc. Jpn. **90**, 012001 (2021).

[142] M. Rigol, T. Bryant, and R. R. P. Singh, Phys. Rev. Lett. **97**, 187202 (2006).

[143] B. Tang, E. Khatami, and M. Rigol, Comput. Phys. Commun. **184**, 557 (2013).

[144] N. Srivastava, C. Kaufman, G. Müller, R. Weber, and H. Thomas, Z. Phys. B **70**, 251 (1988).

[145] R. Steinigeweg, Europhys. Lett. **97**, 67001 (2012).

[146] O. Gamayun, Y. Miao, and E. Ilievski, Phys. Rev. B **99**, 140301 (2019).

[147] T. A. Elsayed and B. V. Fine, Phys. Rev. B **91**, 094424 (2015).

[148] G. A. Starkov and B. V. Fine, Phys. Rev. B **98**, 214421 (2018).

[149] G. A. Starkov and B. V. Fine, Phys. Rev. B **101**, 024428 (2020).

[150] T. Fließbach, *Quantenmechanik - Lehrbuch zur Theoretischen Physik III*, 6th ed. (Springer, Berlin, 2018).

[151] H.-P. Breuer and F. Petruccione, *The Theory of Open Quantum Systems* (Oxford University Press, New York, 2007).

[152] F. Schwabl, *Quantenmechanik*, 7th ed. (Springer, Berlin, 2007).

[153] P. Woit, *Quantum Theory, Groups and Representations*, 1st ed. (Springer, Cham, 2017).

[154] K. Joel, D. Kollmar, and L. F. Santos, Am. J. Phys. **81**, 450 (2013).

[155] E. Noether, Nachrichten von der Gesellschaft der Wissenschaften zu Göttingen, Math. Klasse **1918**, 235 (1918).

[156] A. Gubin and L. F. Santos, Am. J. Phys. **80**, 246 (2012).

[157] A. W. Sandvik, AIP Conference Proceedings **1297**, 135 (2010).

[158] P. Jordan and E. Wigner, Z. Phys. **47**, 631 (1928).

[159] T. Holstein and H. Primakoff, Phys. Rev. **58**, 1098 (1940).

[160] M. Månson, Phys. Rev. B **12**, 400 (1975).

[161] A. Bulgac and D. Kusnezov, Ann. Phys. **199**, 187 (1990).

[162] R. Steinigeweg and H.-J. Schmidt, Comput. Phys. Commun. **174**, 853 (2006).

[163] N. Srivastava, C. Kaufman, and G. Müller, Comput. Phys. **4**, 549 (1990).

[164] A. S. de Wijn, B. Hess, and B. V. Fine, Phys. Rev. Lett. **109**, 34101 (2012).

[165] R. Steinigeweg and H.-J. Schmidt, Math. Physics, Anal. Geom. **12**, 19 (2009).

[166] L. F. Santos and M. Rigol, Phys. Rev. E **82**, 031130 (2010).

[167] J. Sirker, R. G. Pereira, and I. Affleck, Phys. Rev. B **83**, 35115 (2011).

[168] M. Gaudin, *The Bethe Wavefunction*, 1st ed. (Cambridge University Press, Cambridge, 2014).

[169] F. Levkovich-Maslyuk, J. Phys. A Math. Theor. **49**, 323004 (2016).

[170] T. Aktosun, *Inverse Scattering Transform, KdV, and Solitons*, 1st ed. (Birkhäuser, Basel, 2004).

[171] L. D. Faddeev and L. A. Takhtajan, *Hamiltonian Methods in the Theory of Solitons*, 1st ed. (Springer, Berlin, 1987).

[172] F. Haake, S. Gnutzmann, and M. Kuś, *Quantum Signatures of Chaos*, 4th ed. (Springer, Cham, 2018).

[173] T. Guhr, A. Müller–Groeling, and H. A. Weidenmüller, Phys. Rep. **299**, 189 (1998).

[174] L. M. Mehta, *Random Matrices*, 3rd ed. (Academic Press, New York, 2004).

[175] J. Richter, F. Jin, H. De Raedt, K. Michielsen, J. Gemmer, and R. Steinigeweg, Phys. Rev. B **97**, 174430 (2018).

[176] N. Pottier, *Nonequilibrium Statistical Physics - Linear Irreversible Processes*, 1st ed. (Oxford University Press, Oxford, 2010).

[177] R. Zwanzig, *Nonequilibrium Statistical Mechanics*, 3rd ed. (Oxford University Press, Oxford, 2001).

[178] H. Mori, Prog. Theor. Phys. **33**, 423 (1965).

[179] R. Steinigeweg, H. Wichterich, and J. Gemmer, Europhys. Lett. **88**, 10004 (2009).

[180] M. Michel, G. Mahler, and J. Gemmer, Phys. Rev. Lett. **95**, 180602 (2005).

[181] R. Steinigeweg, H.-P. Breuer, and J. Gemmer, Phys. Rev. Lett. **99**, 150601 (2007).

[182] R. Steinigeweg, F. Jin, D. Schmidtke, H. De Raedt, K. Michielsen, and J. Gemmer, Phys. Rev. B **95**, 35155 (2017).

[183] Y. Yan, F. Jiang, and H. Zhao, Eur. Phys. J. B **88**, 11 (2015).

[184] M. Bohm and H. Leschke, J. Phys. A. Math. Gen. **25**, 1043 (1992).

[185] S. Aubry and G. André, Ann. Isr. Phys. Soc. **3**, 18 (1980).

[186] F. Bloch, Z. Phys. **52**, 555 (1929).

[187] F. Alet and N. Laflorencie, C. R. Phys. **19**, 498 (2018).

[188] M. Žnidarič, T. Prosen, and P. Prelovšek, Phys. Rev. B **77**, 64426 (2008).

[189] D. Schmidtke, R. Steinigeweg, J. Herbrych, and J. Gemmer, Phys. Rev. B **95**, 134201 (2017).

[190] B. Li, Phys. B Condens. Matter **502**, 82 (2016).

[191] E. J. Torres-Herrera and L. F. Santos, Phys. Rev. B **92**, 014208 (2015).

[192] R. Steinigeweg, J. Herbrych, F. Pollmann, and W. Brenig, Phys. Rev. B **94**, 180401 (2016).

[193] M. Mierzejewski, J. Herbrych, and P. Prelovšek, Phys. Rev. B **94**, 224207 (2016).

[194] T. Devakul and R. R. P. Singh, Phys. Rev. Lett. **115**, 187201 (2015).

[195] E. V. H. Doggen, F. Schindler, K. S. Tikhonov, A. D. Mirlin, T. Neupert, D. G. Polyakov, and I. V. Gornyi, Phys. Rev. B **98**, 174202 (2018).

[196] A. Chandran, I. H. Kim, G. Vidal, and D. A. Abanin, Phys. Rev. B **91**, 085425 (2015).

[197] R. Vosk, D. A. Huse, and E. Altman, Phys. Rev. X **5**, 31032 (2015).

[198] A. C. Potter, R. Vasseur, and S. A. Parameswaran, Phys. Rev. X **5**, 31033 (2015).

[199] M. Serbyn, Z. Papić, and D. A. Abanin, Phys. Rev. X **5**, 041047 (2015).

[200] J.-y. Choi, S. Hild, J. Zeiher, P. Schauß, A. Rubio-Abadal, T. Yefsah, V. Khemani, D. A. Huse, I. Bloch, and C. Gross, Science **352**, 1547 (2016).

[201] M. Rispoli, A. Lukin, R. Schittko, S. Kim, M. E. Tai, J. Léonard, and M. Greiner, Nature **573**, 385 (2019).

[202] B. Bertini, P. Kos, and T. Prosen, Phys. Rev. Lett. **121**, 264101 (2018).

[203] J. Šuntajs, J. Bonča, T. Prosen, and L. Vidmar, Phys. Rev. E **102**, 062144 (2020).

[204] D. Sels and A. Polkovnikov, Phys. Rev. E **104**, 054105 (2021).

[205] T. R. de Oliveira, C. Charalambous, D. Jonathan, M. Lewenstein, and A. Riera, New J. Phys. **20**, 033032 (2018).

[206] J. Eisert, M. Friesdorf, and C. Gogolin, Nat. Phys. **11**, 124 (2015).

[207] M. Srednicki, J. Phys. A. Math. Gen. **32**, 1163 (1999).

[208] M. Srednicki, J. Phys. A. Math. Gen. **29**, L75 (1996).

[209] R. Steinigeweg, J. Herbrych, and P. Prelovšek, Phys. Rev. E **87**, 012118 (2013).

[210] H. Kim, T. N. Ikeda, and D. A. Huse, Phys. Rev. E **90**, 052105 (2014).

[211] D. Jansen, J. Stolpp, L. Vidmar, and F. Heidrich-Meisner, Phys. Rev. B **99**, 155130 (2019).

[212] W. Beugeling, R. Moessner, and M. Haque, Phys. Rev. E **91**, 12144 (2015).

[213] M. Rigol and L. F. Santos, Phys. Rev. A **82**, 011604 (2010).

[214] M. Rigol, Phys. Rev. Lett. **103**, 100403 (2009).

[215] E. Khatami, G. Pupillo, M. Srednicki, and M. Rigol, Phys. Rev. Lett. **111**, 50403 (2013).

[216] W. Beugeling, R. Moessner, and M. Haque, Phys. Rev. E **89**, 042112 (2014).

[217] R. Steinigeweg, F. Heidrich-Meisner, J. Gemmer, K. Michielsen, and H. De Raedt, Phys. Rev. B **90**, 094417 (2014).

[218] M. Rigol and M. Srednicki, Phys. Rev. Lett. **108**, 110601 (2012).

[219] M. Rigol, Phys. Rev. Lett. **116**, 100601 (2016).

[220] J. Larson, J. Phys. B At. Mol. Opt. Phys. **46**, 224016 (2013).

[221] E. Canovi, D. Rossini, R. Fazio, G. E. Santoro, and A. Silva, Phys. Rev. B **83**, 094431 (2011).

[222] D. Basko, I. Aleiner, and B. Altshuler, Ann. Phys. **321**, 1126 (2006).

[223] K. Agarwal, S. Gopalakrishnan, M. Knap, M. Müller, and E. Demler, Phys. Rev. Lett. **114**, 160401 (2015).

[224] M. Žnidarič, A. Scardicchio, and V. K. Varma, Phys. Rev. Lett. **117**, 40601 (2016).

[225] D. J. Luitz and Y. B. Lev, Ann. Phys. **529**, 1600350 (2017).

[226] D. J. Luitz, N. Laflorencie, and F. Alet, Phys. Rev. B **93**, 060201 (2016).

[227] Y. Bar Lev, G. Cohen, and D. R. Reichman, Phys. Rev. Lett. **114**, 100601 (2015).

[228] V. K. Varma, A. Lerose, F. Pietracaprina, J. Goold, and A. Scardicchio, J. Stat. Mech. **2017**, 053101 (2017).

[229] O. S. Barišić, J. Kokalj, I. Balog, and P. Prelovšek, Phys. Rev. B **94**, 45126 (2016).

[230] I. Khait, S. Gazit, N. Y. Yao, and A. Auerbach, Phys. Rev. B **93**, 224205 (2016).

[231] J. Richter, J. Herbrych, and R. Steinigeweg, Phys. Rev. B **98**, 134302 (2018).

[232] P. Prelovšek, M. Mierzejewski, O. Barišić, and J. Herbrych, Ann. Phys. **529**, 1600362 (2017).

[233] D. J. Luitz and Y. Bar Lev, Phys. Rev. B **96**, 020406 (2017).

[234] D. M. Basko, Ann. Phys. **326**, 1577 (2011).

[235] S. Roy and S. M. Bhattacharjee, Phys. Lett. A **352**, 13 (2006).

[236] M. Schiulaz, E. J. Torres-Herrera, F. Pérez-Bernal, and L. F. Santos, Phys. Rev. B **101**, 174312 (2020).

[237] S. Wiseman and E. Domany, Phys. Rev. E **52**, 3469 (1995).

[238] H. Q. Lin, Phys. Rev. B **42**, 6561 (1990).

[239] W. H. Press, S. A. Teukolsky, W. T. Vetterling, and B. P. Flannery, *Numerical Recipes in C*, 2nd ed. (Cambridge University Press, Cambridge, 1992).

[240] F. Heidrich-Meisner, A. Honecker, and T. Vekua, Phys. Rev. B **74**, 20403 (2006).

[241] C. Lanczos, J. Res. Natl. Bur. Stand. B **45**, 255 (1950).

[242] A. Quarteroni, R. Sacco, and F. Saleri, *Numerical Mathematics*, 1st ed. (Springer, New York, 2007).

[243] J. Gemmer and G. Mahler, Eur. Phys. J. B **31**, 249 (2003).

[244] C. Bartsch and J. Gemmer, Phys. Rev. Lett. **102**, 110403 (2009).

[245] R. Steinigeweg, A. Khodja, H. Niemeyer, C. Gogolin, and J. Gemmer, Phys. Rev. Lett. **112**, 130403 (2014).

[246] T. Monnai and A. Sugita, J. Phys. Soc. Jpn. **83**, 94001 (2014).

[247] B. N. Balz, J. Richter, J. Gemmer, R. Steinigeweg, and P. Reimann, in *Thermodynamics in the Quantum Regime. Fundamental Aspects and New Directions* (Springer, Cham, 2018).

[248] T. Iitaka and T. Ebisuzaki, Phys. Rev. Lett. **90**, 047203 (2003).

[249] R. Alben, M. Blume, H. Krakauer, and L. Schwartz, Phys. Rev. B **12**, 4090 (1975).

[250] T. Iitaka and T. Ebisuzaki, Phys. Rev. E **69**, 057701 (2004).

[251] S. Sugiura and A. Shimizu, Phys. Rev. Lett. **108**, 240401 (2012).

[252] J. Richter, F. Jin, L. Knipschild, J. Herbrych, H. De Raedt, K. Michielsen, J. Gemmer, and R. Steinigeweg, Phys. Rev. B **99**, 144422 (2019).

[253] J. Richter and R. Steinigeweg, Phys. Rev. E **99**, 012114 (2019).

[254] J. Richter and A. Pal, Phys. Rev. Lett. **126**, 230501 (2021).

[255] C. Chiaracane, F. Pietracaprina, A. Purkayastha, and J. Goold, Phys. Rev. B **103**, 184205 (2021).

[256] C. Runge, Math. Ann. **46**, 167 (1895).

[257] W. Kutta, Zeit. Math. Phys. **46**, 435 (1901).

[258] T. A. Elsayed and B. V. Fine, Phys. Rev. Lett. **110**, 070404 (2013).

[259] H. De Raedt and K. Michielsen, in *Handbook of Theoretical and Computational Nanotechnology*, Vol. 2, edited by M. Rieth and W. Schommers (American Scientific Publishers, Los Angeles, 2006).

[260] H. F. Trotter, Proc. Am. Math. Soc. **10**, 545 (1959).

[261] M. Suzuki, S. Miyashita, and A. Kuroda, Prog. Theor. Phys. **58**, 1377 (1977).

[262] M. Suzuki, J. Math. Phys. **26**, 601 (1985).

[263] H. De Raedt and B. De Raedt, Phys. Rev. A **28**, 3575 (1983).

[264] A. Weiße, G. Wellein, A. Alvermann, and H. Fehske, Rev. Mod. Phys. **78**, 275 (2006).

[265] A. Holzner, A. Weichselbaum, I. P. McCulloch, U. Schollwöck, and J. von Delft, Phys. Rev. B **83**, 195115 (2011).

[266] V. V. Dobrovitski and H. A. De Raedt, Phys. Rev. E **67**, 056702 (2003).

[267] J. Mason and D. C. Handscomb, *Chebyshev Polynomials*, 1st ed. (Chapman and Hall/CRC, New York, 2002).

[268] H. Fehske, J. Schleede, G. Schubert, G. Wellein, V. S. Filinov, and A. R. Bishop, Phys. Lett. A **373**, 2182 (2009).

[269] E. Khatami and M. Rigol, J. Phys. Conf. Ser. **402**, 012018 (2012).

[270] J. Oitmaa, C. Hamer, and W. Zheng, *Series Expansion Methods for Strongly Interacting Lattice Models* (Cambridge University Press, Cambridge, 2006).

[271] K. Bhattaram and E. Khatami, Phys. Rev. E **100**, 013305 (2019).

[272] A. Hams and H. De Raedt, Phys. Rev. E **62**, 4365 (2000).

[273] J. Richter, F. Jin, L. Knipschild, H. De Raedt, K. Michielsen, J. Gemmer, and R. Steinigeweg, Phys. Rev. E **101**, 062133 (2020).

[274] S. Chaturvedi and F. Shibata, Z. Phys. B **35**, 297 (1979).

[275] R. Steinigeweg, Phys. Rev. E **84**, 011136 (2011).

[276] R. Steinigeweg, F. Jin, H. De Raedt, K. Michielsen, and J. Gemmer, Phys. Rev. E **96**, 1 (2017).

[277] A. Mitra, Annu. Rev. Condens. Matter Phys. **9**, 245 (2018).

[278] C. Bartsch and J. Gemmer, Europhys. Lett. **118**, 10006 (2017).

[279] V. B. Bulchandani, S. Gopalakrishnan, and E. Ilievski, J. Stat. Mech. **2021**, 084001 (2021).

[280] T. Prosen, Phys. Rev. Lett. **106**, 217206 (2011).

[281] E. Ilievski, M. Medenjak, T. Prosen, and L. Zadnik, J. Stat. Mech. **2016**, 064008 (2016).

[282] M. Schmitt and S. Kehrein, Phys. Rev. B **98**, 180301 (2018).

[283] E. Chertkov, B. Villalonga, and B. K. Clark, Phys. Rev. Lett. **126**, 180602 (2021).

[284] T. B. Wahl, A. Pal, and S. H. Simon, Nat. Phys. **15**, 164 (2019).

[285] K. S. C. Decker, D. M. Kennes, and C. Karrasch, arXiv:2106.12861 .

Erklärung über die Eigenständigkeit der erbrachten wissenschaftlichen Leistung

Ich erkläre hiermit, dass ich die vorliegende Arbeit ohne unzulässige Hilfe Dritter und ohne Benutzung anderer als der angegebenen Hilfsmittel angefertigt habe. Die aus anderen Quellen direkt oder indirekt übernommenen Daten und Konzepte sind unter Angabe der Quelle gekennzeichnet.

Bei der Auswahl und Auswertung folgenden Materials haben mir die nachstehend aufgeführten Personen in der jeweils beschriebenen Weise entgeltlich/unentgeltlich geholfen.

1. .....

   .....

2. .....

   .....

3. .....

   .....

Weitere Personen waren an der inhaltlichen materiellen Erstellung der vorliegenden Arbeit nicht beteiligt. Insbesondere habe ich hierfür nicht die entgeltliche Hilfe von Vermittlungs- bzw. Beratungsdiensten (Promotionsberater oder andere Personen) in Anspruch genommen. Niemand hat von mir unmittelbar oder mittelbar geldwerte Leistungen für Arbeiten erhalten, die im Zusammenhang mit dem Inhalt der vorgelegten Dissertation stehen.

Die Arbeit wurde bisher weder im In- noch im Ausland in gleicher oder ähnlicher Form einer anderen Prüfungsbehörde vorgelegt.

Osnabrück, den 13.04.2022 — Dennis Schubert